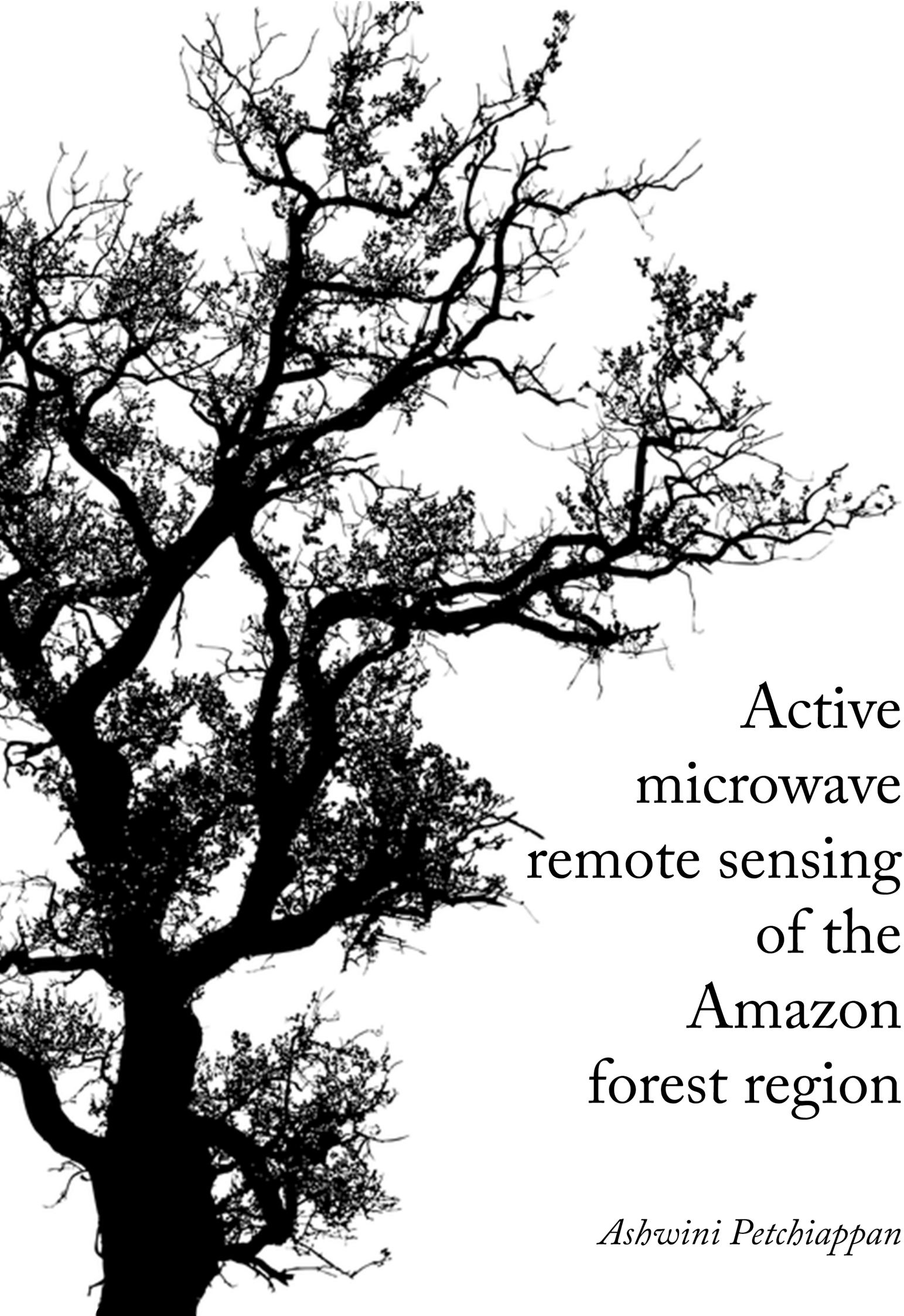

Active microwave remote sensing of the Amazon forest region

Ashwini Petchiappan

Active microwave remote sensing of the Amazon forest region

by

Ashwini Petchiappan

to obtain the degree of Master of Science (Environmental Engineering)

at the Delft University of Technology

Student number: 4738055

Assessment Committee:

Prof. Dr. ir. Susan Steele-Dunne	TU Delft
Dr.ir. Miriam Coenders	TU Delft
Dr. Phil Vardon	TU Delft
Dr. Mariette Vreugdenhil	TU Wien

ABSTRACT

The Amazon rainforest is among the most vital ecosystems on earth, holding about a quarter of the global terrestrial carbon sink. Since 2005, three 100-year return period droughts have occurred, the likes of which have the potential to turn the forest from a carbon sink to a source – meaning disastrous consequences for the planet. Monitoring of the Amazon is hence, indispensable. This study explored avenues for monitoring the canopy water dynamics in the region through ASCAT backscatter and dynamic vegetation parameters.

These dynamic vegetation parameters are slope and curvature - the first and second derivatives of a second-order Taylor polynomial describing the incidence angle dependence of ASCAT backscatter data. A 10-year length of data from 2007-16 was used to find spatial and temporal patterns in the backscatter, slope, and curvature over Amazonia, and related them to climatic variables such as radiation and precipitation to find the driving force behind the parameters.

The findings suggest that the spatial patterns of the ASCAT parameters match the distribution of major land cover types in the region, with significant differences between the major cover types. The evergreen forests have high mean backscatter and low mean curvature compared to other cover types, and weak seasonal variations. The savannas, on the other hand show much stronger amplitudes of seasonal changes. The wetlands, as well, have strong seasonality with especially high ranges in curvature. They also show a change in the backscatter-incidence angle relationship during flooding seasons, thus demonstrating potential for forest flood detection and monitoring.

Consistent diurnal differences were observed especially in the backscatter of all regions. These diurnal differences are shown to be an interaction between vegetation phenological activity and precipitation seasons. In the dry season, the morning values are generally higher as the vegetation transpires water through the day. Water stress and a consequent decrease in backscatter are also detected during the Amazon droughts of 2010 and 2015. The spatial distribution of these negative backscatter anomalies matched that of precipitation deficits during the droughts. The anomalies were also seen to be strongest during the peak drought months. These findings indicate that ASCAT backscatter can detect water stress and droughts in the Amazon vegetation.

Seasonal cycles in backscatter and dynamic vegetation parameters are visible in all regions. While backscatter follows the moisture availability in the canopy, the slope and curvature are related to variables of moisture demand (such as radiation and humidity) through a strong influence of vegetation phenology. In the radiation-limited Amazon vegetation, the slope peaks with the period of photosynthetic activity following the radiation maximum, while the curvature peak covers the leaf-flushing season. The ASCAT parameters show a relation to the vegetation water dynamics in all major cover types in the Amazon.

There is, thus, a solid prospect for the use of ASCAT backscatter and vegetation parameters for long-term monitoring of the Amazon with respect to canopy water dynamics in a variety of land cover types, as well as events such as droughts.

ACKNOWLEDGEMENTS

I was told by many that the thesis is a marathon and not a sprint, but to me it often felt like sprinting a marathon. I have deep gratitude for all those who kept me going through the journey.

First, my supervisor Susan Steele-Dunne. Your guidance, approachability, and sheer energy made the thesis a steep learning curve throughout and pushed many roadblocks off my way. In hard times, you reminded me of what I had managed to accomplished and eased my way to the finish line. Thank you.

Mariette Vreugdenhil, your inputs came at the right times and provided the spark to make new inroads possible. The excitement you showed for my results made me push harder. Thank you.

Phil Vardon and Miriam Coenders, for bearing with the long winding explanations of slope and curvature with multitudes of plots, and managing to give the critical inputs and suggestions to keep the work on track. Thank you.

Akshay Patil, for all the hours of help fixing Python codes and LaTeX templates, and for always always being around. Thank you.

Fabian, Manuel, Pooja, Alessandro, and all the others friends and family, in Delft and India, who kept me company, cribbed with me, and laughed with me, and made this journey something to remember.

Thank you!

...

CONTENTS

LIST OF FIGURES

LIST OF TABLES

ABBREVIATIONS

Table 1: List of abbreviations

Abbreviation	Full form
θ	Incidence angle
σ	Backscatter
σ°_{θ}	Backscatter at incidence angle, θ
σ'	Slope
σ''	Curvature
ASCAT	Advanced Scatterometer
DD	Diurnal difference
DOY	Day of year
ERS	European Remote Sensing
ESA	European Space Agency
EWT	Equivalent Water Thickness
GRACE	Gravity Recovery and Climate Experiment
KGCC	Köppen-Geiger Climate Classes
NASA	National Aeronautics and Space Administration
PD	Phase difference
WWF	World Wildlife Fund

1 INTRODUCTION

1.1 IMPORTANCE OF THE AMAZON REGION

The Amazon rainforest is among the most vital ecosystems on earth [Aragao et al., 2014]. It boasts one-tenth of the total biodiversity on the planet [Buainain et al., 2019]. With half of the present global rainforest cover, the forest absorbs 0.42-065 Pg C yr^{-1} annually - about a quarter of the global terrestrial carbon sink [Brienen et al., 2015].

The 21st century, however, has seen the region facing extreme droughts with mounting frequency [Zuleta et al., 2017]. The 100-year return period 2005 drought was followed by a similar event in 2010, and then a record-breaking drought in 2015 [Yang et al., 2018a]. Tree mortality can take a sharp upturn with these events, resulting from reduced canopy water and soil moisture deficits [Liu et al., 2018]. There are associated changes in forest structure, with slow recovery [Saatchi et al., 2013].

Notwithstanding the calamitous effect on the vegetation, and the resident fauna, the recurring droughts have a capacity to turn the Amazon from a carbon sink to source [Yang et al., 2018b]. During the 2005 drought, the forest was a source of 1.2-1.6 Pg C [Doughty et al., 2015]. With climate change, and rising sea temperatures, such droughts are projected to become more likely [Panisset et al., 2018].

The trouble is compounded by increasing forest fires, and deforestation at among the fastest rates seen worldwide [Morton et al., 2013]. Croplands, plantations, and cattle ranches are eating into the forest; this can have disastrous consequences for the global carbon and water budget [Bagley et al., 2014].

Monitoring Amazonia is, therefore, critical.

1.2 MICROWAVE REMOTE SENSING OF THE AMAZON

Space-borne remote sensing can be a convenient means for large-scale observations with a single instrument and methodology [Frolking et al., 2011]. This can be useful for monitoring places like the Amazon with accessibility limitations. Daily temporal resolutions can be achieved, making it possible to detect vegetation phenology [Frolking et al., 2011].

Passive optical satellites, however, are sensitive to atmospheric aerosol content, and cloud cover – a crucial factor in humid tropical regions such as Amazonia [Asner, 2001]. This limitation is overcome by microwave remote sensing, which also has the advantage of both day and night observations [Liu et al., 2018]. Active microwave backscatter has been found to be sensitive to vegetation cover, structure, and water content (through dielectric properties) [Frolking et al., 2017].

Active microwave observations can be from two types of radar sensors: scatterometers and synthetic aperture radar (SAR) [Scipal, 2002]. SAR sensors generally have higher spatial resolution compared to scatterometers. However, scatterometers have high temporal resolutions [Frison et al., 2016], enabling observations of

vegetation dynamics.

In the past, the Amazon has been considered as a standard target for calibrating space-borne scatterometers due to observed homogeneity in the backscatter response [Birrer et al., 1982]. In recent years, however, studies have detected spatial and temporal variations in the microwave backscatter over the Amazon forest, some of which have been mentioned below.

Frolking et al. [2011] saw strong seasonality in the Ku-band SeaWinds backscatter over Amazonia, with significantly more variation in the morning overpass, compared to the evening. The morning backscatter was found to be generally higher than the evening values due to the higher vegetation water content in the morning, with a possibility of dewdrops in the canopy. Diurnal variations in backscatter have also been seen in other studies in the Amazon (for instance, in Ku-band RapidScat backscatter by van Emmerik et al. [2017]) and on a global scale (for example, in ERS C-band backscatter by Friesen et al. [2012]), demonstrating a potential for measuring water stress in the canopy by combining the morning and evening values [Steele-Dunne et al., 2012].

During the Amazon drought of 2005, significant negative anomalies were observed in the SeaWinds Ku-band backscatter [Saatchi et al., 2013; Frolking et al., 2017]. Liu et al. [2018] spotted similar declines in the passive microwave-based backscatter over southwestern Amazonia through the 2010 drought. These anomalies were attributed to changes in the structure and water content of the forest upper canopy, and indicated water stress in the canopy [Saatchi et al., 2013]. Clearly, there is strong potential for application of microwave observations in the study of Amazon's vegetation health and dynamics.

Invaluable, for such studies, is a homogenous data record of sufficient length to produce a climatology [Stoffelen et al., 2017]. For C-band microwave, the combined data record from the ERS-1/2 satellites, the ASCAT instruments onboard Metop-A/B/C, and the Metop-SG SCA (to be launched in 2022) will extend for at least 40 years [Stoffelen et al., 2017]. This, in addition to the sensitivity of C-band microwave to vegetation properties [Stoffelen et al., 2017], provides a valuable opportunity for a long-term record and study of the Amazon vegetation. This study aims to see how this long and consistent dataset can be used for the monitoring of the forest.

1.2.1 ASCAT and dynamic vegetation parameters

The ASCAT instrument on-board the Metop satellites has three antennas on either side: oriented at 45° (fore), 90° (mid) and 135° (aft) to the satellite track. Each grid point is, thus, viewed with three incidence angles - called "backscatter triplets" [Hahn et al., 2017]. This enables the computation of an instantaneous incidence angle relationship for backscatter, resulting in two dynamic vegetation parameters: slope and curvature. They are the first and second derivatives of a second-order Taylor polynomial describing the incidence angle dependence of ASCAT backscatter data [Vreugdenhil et al., 2016].

Figure 1.1 illustrates the suitability of these parameters for the study of changes in vegetation properties. While a change in soil moisture (Figure 1.1a) manifests in a vertical offset of the curve, vegetation changes (Figure 1.1b) result in slope and curvature variation. Hence, while backscatter is sensitive to soil moisture, the slope and curvature can be considered to be factors of vegetation changes [Vreugdenhil et al., 2016]. This sensitivity to soil moisture decreases with increasing biomass [Scipal, 2002], the transmissivity of vegetation being related to the vegetation water content and height [Wagner et al., 1999]. Hence, in the Amazon forest with its tall dense vegetation with a closed canopy, the backscatter can be expected to be mainly sensitive to canopy moisture [Frolking et al., 2011].

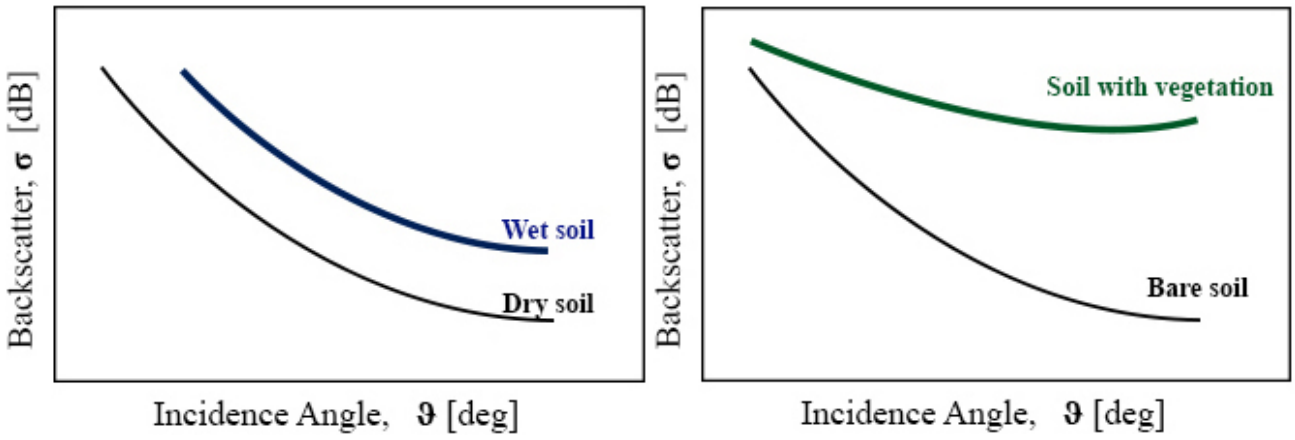

(a) Change in soil moisture

(b) Change in vegetation cover

Figure 1.1: Illustration for comparison of backscatter-incidence angle (σ-θ) dependence curves for different types of changes in land surface (*Source:* adapted from Vreugdenhil et al. [2016]).

The dynamic vegetation parameters (slope and curvature) were calculated from the ASCAT backscatter observations as per the methodology described by Hahn et al. [2017]. The simultaneous independent backscatter observations at different incidence angles are used to determine an instantaneous backscatter slope, also called the "local slope" using the equation:

$$\sigma^{'}(\frac{\theta_{mid}-\theta_{a/f}}{2}) = \frac{\sigma^{\circ}_{mid}(\theta_{mid}) - \sigma^{\circ}_{a/f}(\theta_{a/f})}{\theta_{mid} - (\theta_{a/f})} \qquad [dB/deg] \tag{1.1}$$

where the subscript "mid" refers to the mid beam antenna, and "a/f" means the for beam or aft beam antennas.

These local slope values are then used to compute the dynamic vegetation parameters using a Kernel Smoother (KS) approach (an Epanechnikov kernel with kernel width λ=21). Hence, local slope values within a 42-day window are used with more weights given to values at a closer temporal distance from a given day.

Once the slope and curvature are known, the backscatter values from different incidence angles can be normalized to a reference angle (θ_r) of 40° using the expression:

$$\sigma^{\circ}(\theta_r) = \sigma^{\circ}(\theta) - \sigma^{'}(\theta).(\theta-\theta_r) - \frac{1}{2}\sigma^{''}(\theta_r).(\theta-\theta_r)^2 \qquad [dB] \tag{1.2}$$

This relation is also used to calculate the backscatter values at 60°, once $\sigma^{\circ}(\theta_r)$ is known, by re-arranging as follows:

$$\sigma^{\circ}(\theta) = \sigma^{\circ}(\theta_r) + \sigma^{'}(\theta).(\theta-\theta_r) + \frac{1}{2}\sigma^{''}(\theta_r).(\theta-\theta_r)^2 \qquad [dB] \tag{1.3}$$

This equation was used for some types of analysis (such as for seeing drought effect) since the effect of vegetation is more prominent at bigger incidence angles.

The incidence angle relationship of backscatter is influenced by the relative importance of different scattering mechanism. This, in turn, is determined by factors such as canopy structure and water dynamics

Steele-Dunne et al. [2019]. The slope parameter is considered a measure of "vegetation density", and driven by the seasonal dynamics in the wet biomass of vegetation Vreugdenhil et al. [2016]. Steele-Dunne et al. [2019] examined the spatial and temporal variations of the vegetation parameters over different cover types in the North American Grasslands. They established that curvature contains "some information about vegetation independent of slope"; it was found to be influenced by the vegetation structure and phenology.

The study discovered seasonal cycles in the vegetation parameters concurring with the growth cycles of vegetation. Variations were seen across land cover types, with grasslands showing stronger seasonal trends than forested regions. Diurnal differences in the parameters, seen as the disparity between morning and evening values, were related to canopy water dynamics. Significant negative backscatter anomalies were also observed during drought events in 2011 and 2012.

Observation of changes in backscatter, slope, and curvature shows potential for applications such as detecting canopy water stress and drought monitoring.

1.3 RESEARCH AIM AND CONTRIBUTION

This study aims to contribute to existing knowledge about ASCAT backscatter and dynamic vegetation parameters, focussing on their potential for monitoring vegetation water dynamics and droughts in the Amazon region. Current literature suggests that slope is influenced by the dynamics of wet biomass, and curvature is related to the vegetation. This research will look to improve the understanding of these parameters and their driving factors.

The Amazon being an evergreen rainforest, the fluctuations in backscatter are low in magnitude when compared to grasslands. The research will look for variations and patterns in the parameters, and attempt to relate them climatic and vegetation factors. The goal is to establish what useful information about the Amazon vegetation can be gleaned from patterns in the ASCAT parameters.

The main research question to be answered by this study is the following:

"What spatial and temporal patterns can be observed in the ASCAT backscatter and dynamic vegetation parameters over the Amazon forest region?"

In order to answer the research question, the following sub-questions will be investigated:

1. Are there spatial differences in the mean and range of the parameters (backscatter, slope, and curvature)?
2. What seasonal trends are visible in the parameters?
3. Is there a diurnal cycle for the parameters, seen through a difference in morning and evening values of the parameters?
4. Is the effect of droughts visible through a change in the parameters?

The analysis will cover ASCAT backscatter and vegetation parameters for the length of 10 years from 2007-16 for the following coordinate extent:

- *Latitudes:* 9°N – 19°S
- *Longitudes:* 44°W – 80°W

The study area extends beyond the forest to include features such as montane forests over the Andes, and mangroves near the coast. The analysis in this study will be focussed on the Amazon biome and the Cerrado.

1.4 OUTLINE OF THE THESIS

The next chapter describes the study area, regions of interest, and the datasets used. The methodology used for the data analysis is included: the procedure followed for generating climatologies of vegetation and climatic parameters, calculating diurnal differences, phase lags between seasonal cycles, and cross-correlation analyses.

The third chapter presents the results for each research question. First, the spatial patterns in the ASCAT backscatter, slope, and curvature are mentioned and analysed for the different land cover types. Second, the seasonality of the parameters is discussed, along with their relation to climatic parameters including radiation and precipitation. Third, the diurnal differences (mainly in backscatter) have been studied in relation to the interplay of moisture demand and availability in the region. Fourth, anomalies in the parameters during the Amazon droughts of 2010 and 2015 are considered.

The last chapter gives the conclusions garnered from the research, and recommendations for future research with the scope of applying ASCAT backscatter and dynamic vegetation parameters to monitoring drought and canopy moisture dynamics in the Amazon region.

2 METHODS

2.1 STUDY AREA

The coordinates of the study area are as follows:

- *Latitudes:* 9°N – 19°S
- *Longitudes:* 44°W – 80°W

Figure 2.1 is a map of the land cover types in the study area. The Amazon rainforest, spread over an area of around 5.3 million km^2 [Soares et al., 2006], covers a major portion of the region. The riverine portions contain várzeas or seasonally flooded forests. The next prominent cover type are savannas. The Cerrado, a savanna region located to the southeast of the Amazon, is the second most extensive biome in South America. It covers an area of almost 2 million km^2 [Oliveira et al., 2005]. Within Amazonia, there are two major savanna regions: Beni savanna and Guianan savanna.

As seen in Figure 2.1, the study area extends beyond the forest to include covers such as montane forests over the Andes, and mangroves near the coast. The analysis in this study will be focussed on the Amazon biome and the Cerrado.

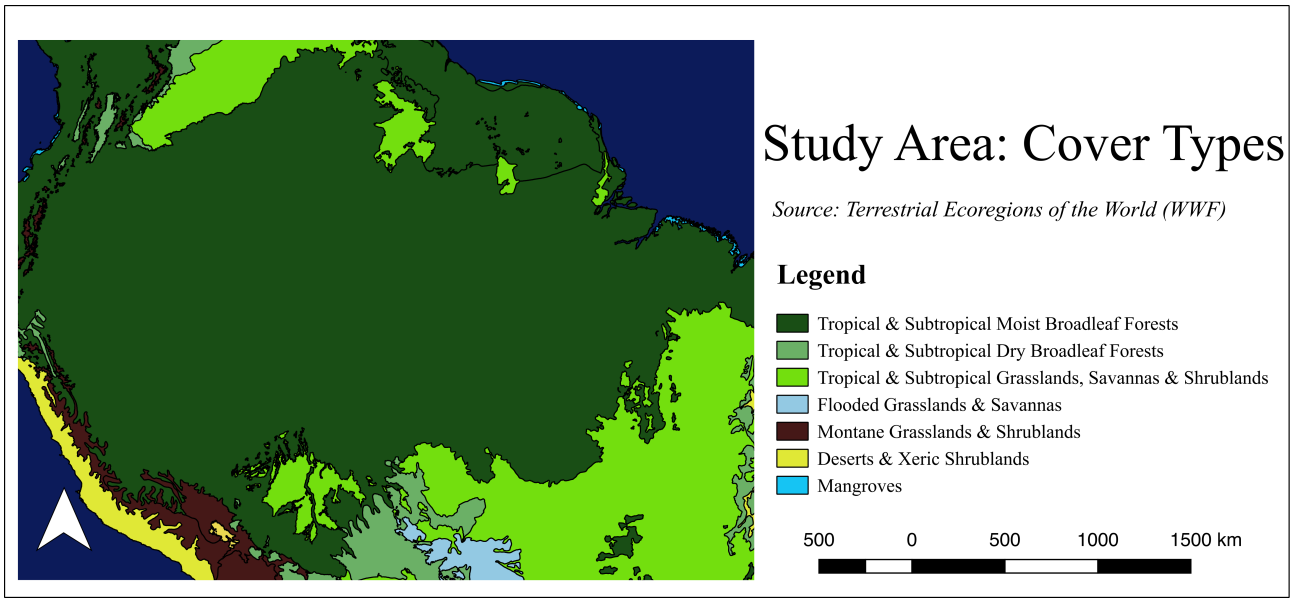

Figure 2.1: Map of land cover types in the study area (Source: Olson et al. [2001]).

2.1.1 Climate

Figure 2.2 shows the Köppen-Geiger Climate Classes (KGCC) in the study area. Three classes cover most of the region: the evergreen forest regions are classified Af (tropical fully humid) or Am (tropical monsoonal); the savanna regions have Aw (tropical winter dry) climate [Bradley et al., 2011].

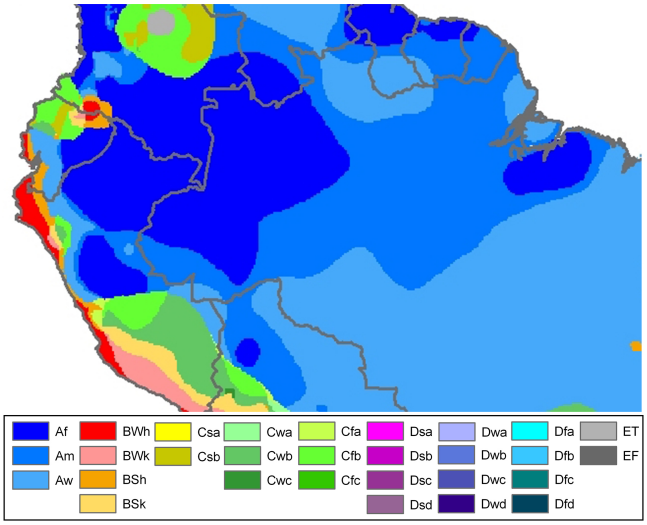

Figure 2.2: Köppen-Geiger climate zones in the study area (Source: Peel et al. [2007]). A list of KGCC symbols and the defining criteria has been provided in Appendix C.

The annual precipitation in the forests can exceed 2000-3000 mm, with less than 100 mm rainfall for up to three months in the year. The savannas have a wet season extending for 5-8 months, with the annual total being about 1000-2000 mm [Bradley et al., 2011]. The net radiation, however, peaks in the winter months, due to less cloud cover in the dry season [Liu et al., 2018].

2.1.2 Droughts

With the dawn of the 21st century, the Amazon Basin has been affected by severe droughts with increasing frequency [Marengo et al., 2011]. The drought of 2005 was considered to be a "once-in-a-century" event [Liu et al., 2018]. Since then, there have been two droughts of even higher severity: in 2010 and 2015. These last two droughts occur within the study period, and will be a focus of the study in section 3.4.

There are two main mechanisms that trigger droughts in the Amazon [Panisset et al., 2018]:

1. Tropical North Atlantic sea surface temperature (TNA-SST) anomalies
2. El Niño – Southern Oscillation (ENSO)

The 2010 drought saw the occurrence of both an El Niño event, and strong positive TNA-SST anomalies. While the drought started with the El Niño event early in the year, it intensified due to increasing TNA-SSTs. The maximum precipitation-deficit was observed between June-September [Panisset et al., 2018], with the worst affected regions being southern and western Amazonia [Liu et al., 2018].

The 2015-16 El Niño event was said to be one of the strongest observed [Yang et al., 2018a]. It developed late in 2014, and was strongest in November 2015, the peak being between October 2015 and January 2016.

The precipitation deficit during this event was larger than in 2005 and 2010, as was the area affected [Panisset et al., 2018]. The strongest anomalies were observed in eastern Amazonia [Jiménez-Muñoz et al., 2016].

2.1.3 Regions of interest

Nine regions of interest were selected for the study (shown in Figure 2.3). These are based on terrestrial ecoregion boundaries set by Olson et al. [2001]. Ecoregions are geographical units representing distinct biotas, and were designed to enable conservation action [Olson et al., 2001] . The regions of interest selected are from three different land cover types:

1. Evergreen forest
2. Seasonally flooded forest
3. Savanna

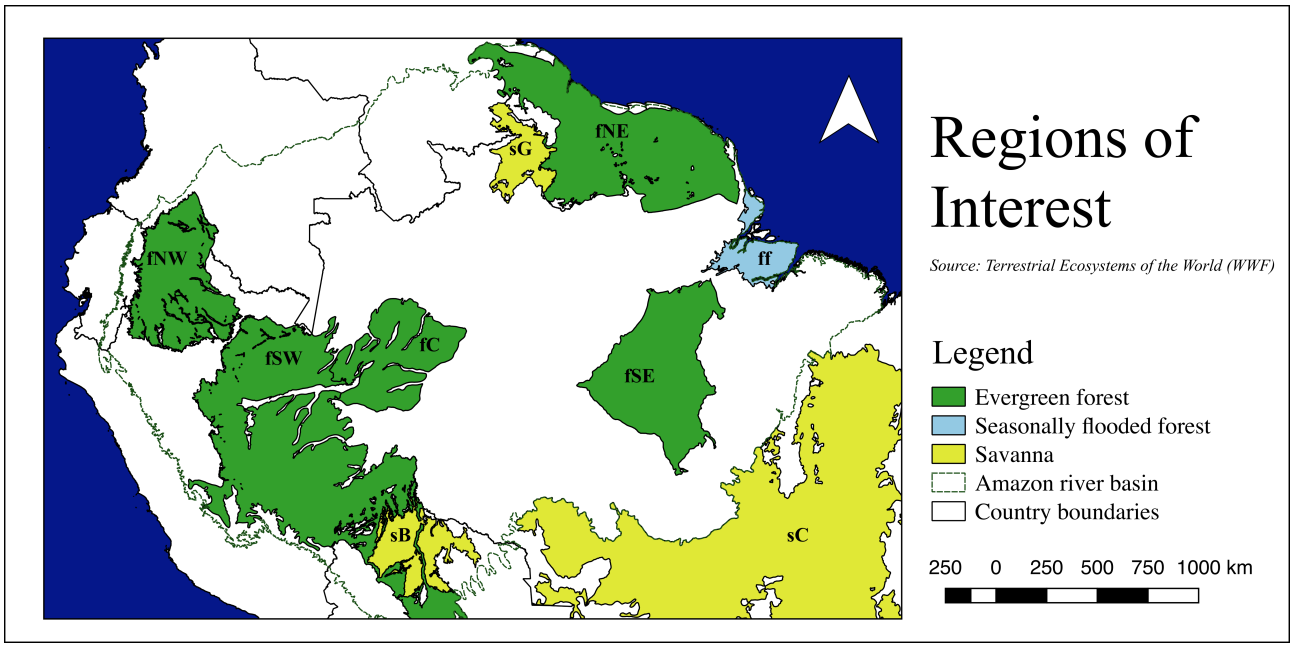

Figure 2.3: Map of regions of interest of the study. Names of the regions have been listed in Table 2.1

Table 2.1: Regions of interest for the study

Symbol	Name	Cover Type
fNW	Napo moist forests	Evergreen forest
fNE	Guianan moist forests	Evergreen forest
fSW	Southwest Amazon moist forests	Evergreen forest
fSE	Tapajós-Xingu moist forests	Evergreen forest
fC	Juruá-Perez moist forests	Evergreen forest
ff	Marajó várzea	Seasonally flooded forest
sC	Cerrado	Savanna
sG	Guianan savanna	Savanna
sB	Beni savanna	Savanna

The regions of interest have been listed in Table 2.1. Details about the regions of interest, grouped by cover type, are given in subsequent sub-sections.

Evergreen forest

Five evergreen forest ecoregions were picked from different geographical parts of Amazonia:

The **Napo moist forests (fNW)**, located in northwest Amazonia, receive some of the highest amounts of annual precipitation in the biome, reaching up to 4000 mm in some parts. This highly biodiverse region has canopies in the terra firme (firm land) forests reaching 40 m.[1]

The **Guianan moist forests (fNE)** are "one of the largest continuous tracts of relatively pristine lowland tropical rainforest in the world". There are two distinct wet seasons: in December-January and May-August. The floral diversity is rich, with multi-tiered vegetation of 40 m tall trees with herbaceous plants below. The dry season (August-December) can see a substantial reduction in leaves, although the forest is evergreen.[1]

The **Southwest Amazon moist forests (fSW)** show significant variations in topography and soil characteristics, leading to extremely high biodiversity. The size of the ecoregion means that climatic conditions vary markedly – the north being wetter and less seasonal than the south. The inaccessibility of the region has aided in its conservation.[1]

The **Tapajós-Xingu moist forests (fSE)** have high levels of urbanization and deforestation, being transected by the Transamazon Highway. There are characteristic liana (woody vine) forests "with a lower (less than 25 m) and more open canopy than the typical humid terra firme forest".[1]

The **Juruá-Perez moist forests (fC)** consist of largely intact forests on the low Amazon Basin. The canopy goes to 30 m heights, with some patches of open canopy.[1]

The seasonal cycles of radiation and precipitation for these regions are shown in Figure 2.4.

[1] https://www.worldwildlife.org/biome-categories/terrestrial-ecoregions

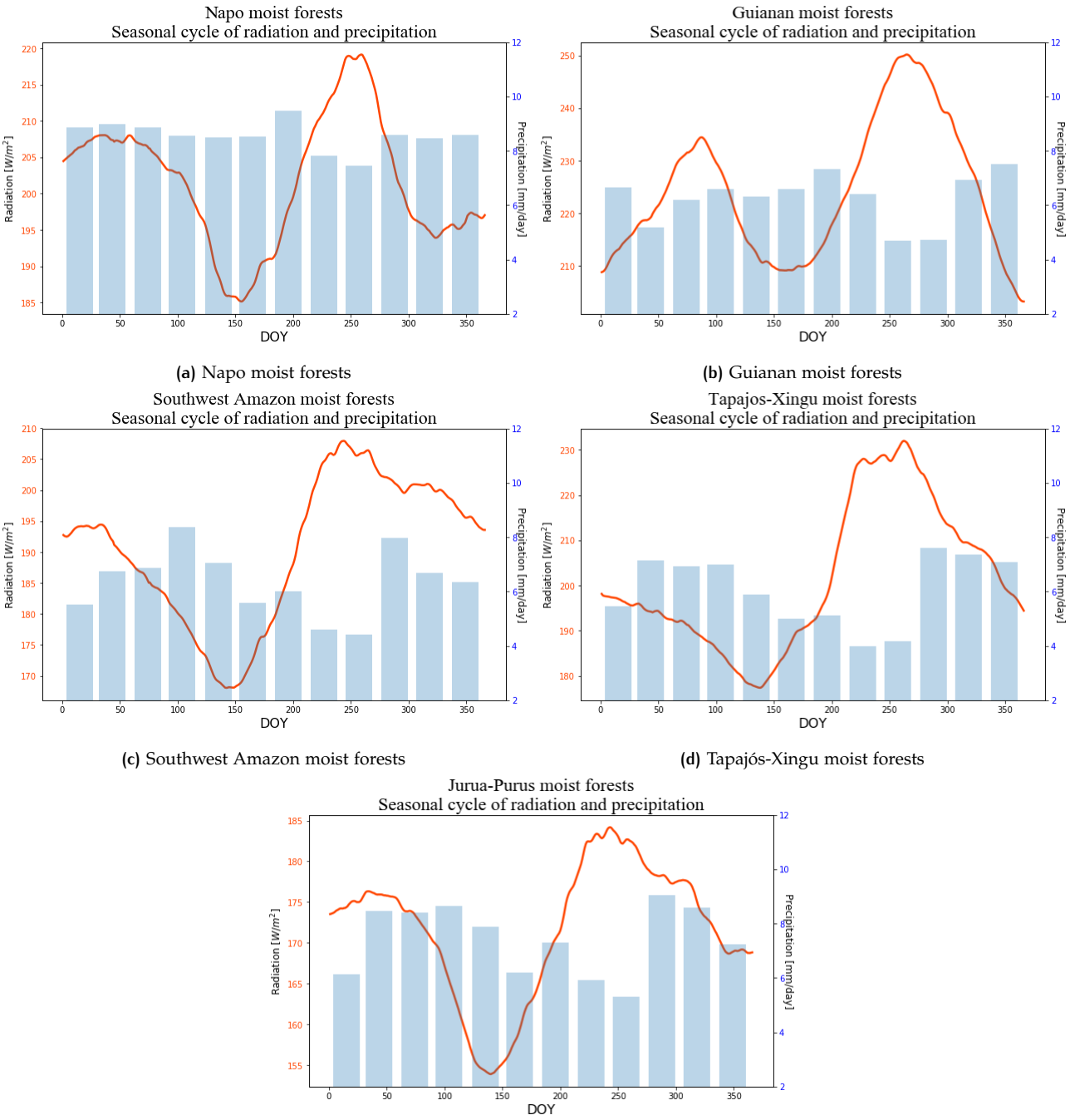

(a) Napo moist forests

(b) Guianan moist forests

(c) Southwest Amazon moist forests

(d) Tapajós-Xingu moist forests

(e) Juruá-Perez moist forests

Figure 2.4: Seasonality of radiation (red line) and precipitation (bars) for evergreen forests.

Seasonally flooded forest

Marajó várzea (ff) is located at the mouth of the Amazon River. The vegetation is dominated by palms, and shorter than surrounding forests. It has areas with tidal flows from the Atlantic Ocean, as well as seasonally and permanently inundated forests.[1] The annual seasonal flooding occurs during the peak precipitation pe-

riod between January-May [Camarão et al., 2002].

The seasonal cycles of radiation and precipitation for the regions are shown in Figure 2.5.

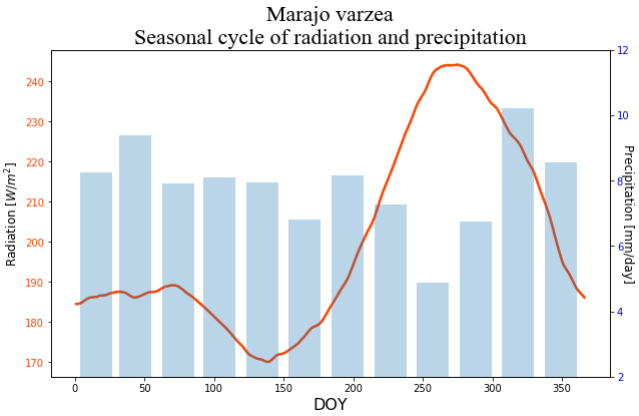

Figure 2.5: Seasonality of radiation (red line) and precipitation (bars) for Marajó várzea (seasonally flooded forest).

Savanna

Three ecoregions of interest are savannas:

The **Guianan savanna (sG)** consists of forest patches encircled by extensive grasslands and shrub formations. There is a susceptibility to vegetation fires that is not typical for humid moist forest environments. These can create "local greenhouse effect during the hottest time of the year". The dry season lasts from December-March.[1]

The **Beni savanna (sB)** is a wetland region with riverine gallery forests and small forest islands.[1] The landscape is dominated by the palm species Attalea princeps [Hordijk et al., 2019]. Seasonal flooding occurs in up to half the region for 4 to 9 months, peaking in March-April [Hamilton et al., 2004].

The **Cerrado (sC)** borders the Amazon biome to the southeast. It occupies an area of 2 million km^2 in the Brazilian Central Plateau. The vegetation cover varies from closed tree canopy to grasslands with low shrubs only.[Eiten, 1972] It is the second largest biome in South America, and faces deforestation rates higher than that in the Amazon forest [Oliveira et al., 2005].

The seasonal cycles of radiation and precipitation for these regions are shown in Figure 2.6.

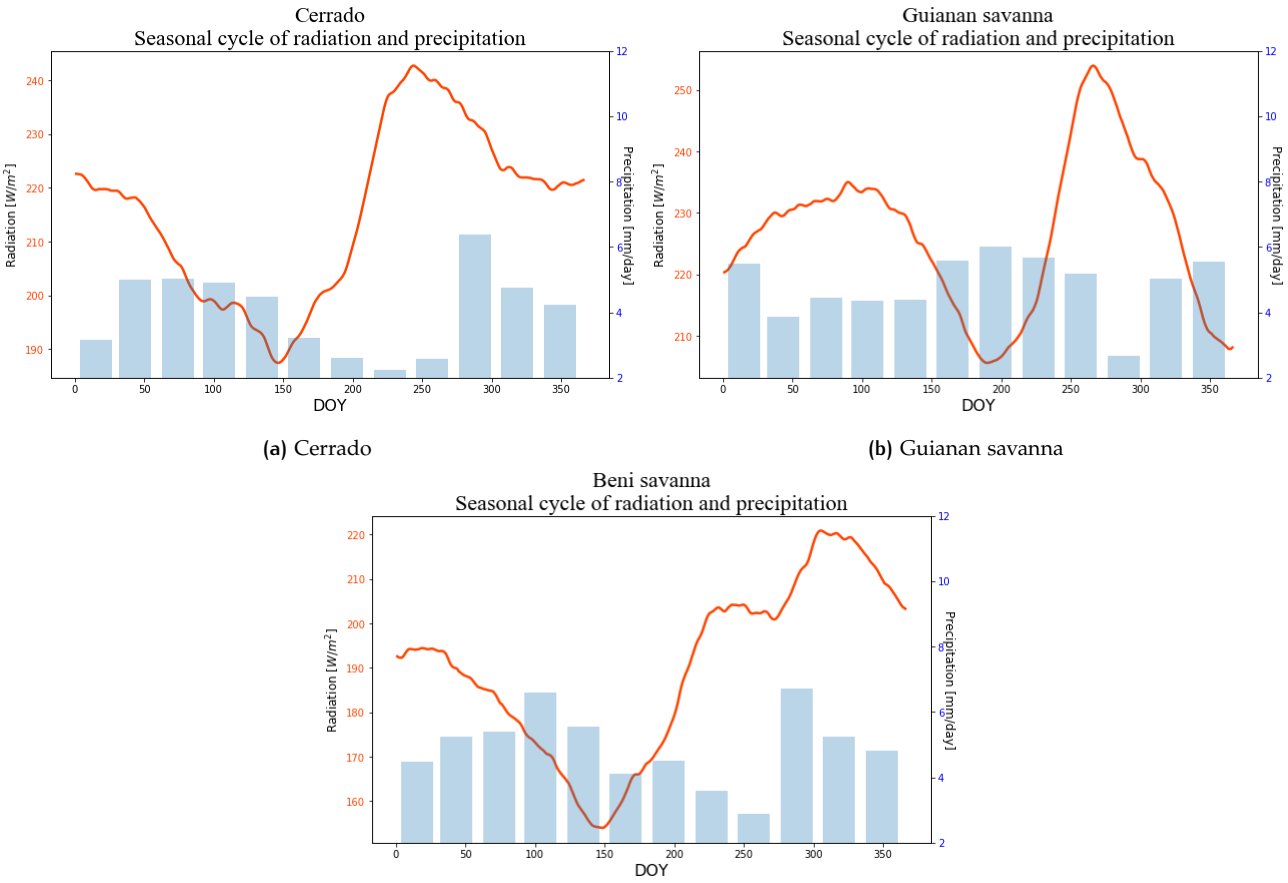

(a) Cerrado

(b) Guianan savanna

(c) Beni savanna

Figure 2.6: Seasonality of radiation (red line) and precipitation (bars) for savannas.

2.2 DATASETS

The datasets used for the study are described below. All datasets use grid-points within the extent of the study area coordinates, and extend over the duration of the study period (2007-16).

2.2.1 ASCAT backscatter

The Advanced SCATterometer (ASCAT) backscatter data at 12.5km grid sampling resolution was obtained from the EUMETSAT Data Centre. The overpass times for the descending and ascending overpasses over the study area are around 10 am and 10 pm, respectively. However, "the revisit time dictates that observations from the descending and ascending overpasses are unlikely to occur on the same day, and that a limited number of values are available for a given day of the year." [Steele-Dunne et al., 2019] Hence, the σ_{40} data was aggregated into 10-day intervals (dekads).

2.2.2 Terrestrial ecoregions

The regions of interest (detailed in section 2.1.3) used in the study were based on WWF Terrestrial Ecoregions of the World (TEOW) [Olson et al., 2001].

2.2.3 Precipitation

The dataset "GPCPMON: GPCP Precipitation Level 3 Monthly 0.5-Degree V3.0 beta" was used, accessed from NASA Earthdata. The data is at 0.5°x0.5° monthly resolution.[2]

The precipitation data has been used for relating seasonal cycles and diurnal differences in backscatter, slope, and curvature to the dynamics of moisture availability. It was also used for indicating the severity of the 2010 and 2015 droughts in different parts of Amazonia, and the temporal development of the droughts.

2.2.4 Princeton meteorological dataset

The Princeton meteorological dataset was developed "to drive models of land surface hydrology" [Sheffield et al., 2006]. The parameters used in this study are downwelling shortwave radiation at the surface and specific humidity. The data is at 0.5°x0.5° daily resolution.[3]

The radiation and humidity data have been used for relating the seasonal cycles and diurnal differences in slope and curvature to the dynamics of moisture demand in Amazonia.

2.2.5 Equivalent water thickness (EWT)

The Gravity Recovery and Climate Experiment (GRACE) mission by NASA observes monthly variations in the Earth's gravitational potential caused by changes in mass. Most of these changes are caused by variations in water storage in hydrologic reservoirs, the vertical extent of which is measured in centimetres of EWT. [Landerer and Swenson, 2012]

The equivalent water thickness (EWT) from the GRACE Tellus dataset is available at 1°x1°, monthly resolution from the NASA JPL Physical Oceanography Distributed Active Archive Center (PO.DAAC).[4] This data gives the changes in EWT relative to a time-mean baseline, the method of calculation for which is explained in Wahr et al. [1998]. On monthly to inter-annual timescales, it is mainly related to fluctuations in the terrestrial water storage (TWS) [Landerer and Swenson, 2012; Swenson and Wahr, 2006].

This dataset has been used for relating seasonal cycles and diurnal differences in backscatter, slope, and curvature to the cycles of moisture availability in the Amazon.

2.3 METHODOLOGY

The following section gives a detailed description of the methodologies for the different types of analyses performed in the study.

2.3.1 Spatial patterns

For an exploratory look, maps of mean and range of backscatter, slope, and curvature in the study area were prepared. The mean and range (difference between maximum and minimum values) were calculated over the study period (2007-16) for all grid points and then plotted. Shapefiles of the regions of interest overlie the maps to facilitate exploration of variations between the land cover types. Analysis was focussed on the

[2] Accessed on 05/06/2019 from: https://disc.gsfc.nasa.gov/datasets/GPCPMON_3.0/summary
[3] Accessed on 19/06/2019 from: http://hydrology.princeton.edu/data.pgf.php
[4] Accessed on 28/06/2019 from: https://podaac.jpl.nasa.gov/dataset/TELLUS_LAND_NC_RL05

observations from the descending overpass for the sake of uniformity. The difference between the overpasses is considered separately in the section on diurnal differences.

Since the maps indicated clear spatial patterns matching cover types, the major cover types (evergreen forests, savannas, and seasonally flooded forests) were analysed separately. Scatter plots of mean vs. range were generated for each cover type, with each dot representing individual grid points. To consider a relation between backscatter and curvature values in the region, scatter plots of mean curvature against mean backscatter were also made.

2.3.2 Seasonal variations

To look for seasonal cycles in the backscatter, slope, and curvature, climatologies of the parameters were calculated. For slope and curvature, this was done using the pytesmo package for Python. Since the backscatter data does not have daily resolution, the climatology calculation was manually coded in Python.[5] To find the factors driving these seasonal cycles, climatologies were also obtained for precipitation, radiation, humidity, and EWT.

To make comparison between different datasets (with different grid points) easier, mean climatologies were calculated for the different regions of interest. First, using QGIS, the grid-points in each dataset that fell within the boundaries of each region of interest were delineated. Then the climatologies within each region were averaged.

For studying how climatic variables such as radiation and humidity affect the backscatter and dynamic vegetation parameters, phase differences were analysed between their seasonal cycles. These phase differences were calculated as follows:

$$PD_{AB} = DOY_{max/min_A} - DOY_{max/min_B} \tag{2.1}$$

where PD_{AB} is the phase difference between parameters A and B, $DOY_{max/minA}$ is the day of the year when the parameter A peaks/troughs, and $DOY_{max/minB}$ is the same for parameter B. If the value exceeded 186 (half a year), a wrap-around was performed as follows:

$$PD^f_{AB} = \begin{cases} PD_{AB} + 366 & \text{if } PD_{AB} < -186 \\ PD_{AB} - 366 & \text{if } PD_{AB} > 186 \\ PD_{AB} & \text{otherwise} \end{cases} \tag{2.2}$$

where PD^f_{AB} is the final phase difference after wrap-around.

To quantify the effect of a climatic variable (such as radiation) on the backscatter and vegetation parameters, cross-correlation analysis was performed. For this, the variables were resampled into monthly averages, and then correlated for different values of (monthly) lag, ranging between -6 and +6 months. This analysis was not possible with the EWT dataset because of gaps in data.

A flooding effect was observed in the seasonal cycles for the regions Marajó várzea and Beni savanna, observed as a change in the backscatter-incidence angle relationship. To elucidate this effect, the extrapolated backscatter values over a range of incidence angles (20°-70°) were calculated, using Equation 1.3, from the mean climatologies of backscatter, slope, and curvature at the reference angle (40°). The climatologies of

[5] https://pytesmo.readthedocs.io/en/latest/

backscatter at incidence angles of 20°, 40°, and 60° were compared to see a change during flooding season. Then the backscatter curves on flooded and non-flooded days were plotted for comparison.

2.3.3 Diurnal differences

Diurnal differences are calculated as the difference between the two satellite overpasses in a day: the descending overpass (in the morning around 10 am) and ascending overpass (in the evening around 10 pm). Thus:

$$\text{Diurnal difference} = \text{Descending overpass value} - \text{Ascending overpass value} \tag{2.3}$$

Accordingly, the diurnal difference is positive when the morning backscatter (or slope/curvature) value is higher than the corresponding evening value, and negative when the evening value is higher.

Maps of monthly means (over the study period 2007-16) were generated for diurnal differences in backscatter, slope, and curvature. Since differences were observed between the values for different months, climatologies of diurnal differences were calculated as per the method described in 2.3.2. Since slope and curvature showed less consistent patterns within the regions of interest, further analysis in the section was focussed on diurnal differences in backscatter.

To compare the seasonality of diurnal differences in backscatter to the dynamics of moisture demand and availability in the region, the phase differences between the seasonal cycles of backscatter, and those of radiation and EWT were calculated as in section 2.3.2.

2.3.4 Drought effect

The Amazon droughts of 2010 and 2015 were included in the study. The backscatter at 60° incidence angle, calculated using the methodology described in section 2.3.2, was chosen since the effect of vegetation is more at bigger incidence angles. The σ°_{60} values were calculated for the full study period 2007-16, and then mean climatologies were calculated for the regions of interest, using the method used in section 2.3.2. The values of σ°_{60} for the drought years were subtracted by the mean climatologies to obtain drought year anomalies.

For the regions that showed significant anomalies, time series of σ°_{60} values for the respective drought years were plotted along with the mean climatologies to see the temporal evolution of the droughts. To see if the deviations from the climatologies during the drought years were significant, standard deviations of σ°_{60} values (over the study period) were calculated for each day (that had backscatter observations available). Anomalies in precipitation during the drought years were also calculated (as drought year values – climatology) and the negative anomalies were plotted alongside the backscatter time series to see effect of water stress on backscatter.

3 RESULTS

3.1 SPATIAL PATTERNS

This section looks at spatial patterns in the mean and range of backscatter, slope, and curvature over the study period (2007-16). All analysis was done with the observations from the descending overpass for uniformity. The difference between the overpasses is considered separately in section 3.3.

3.1.1 Backscatter

Figure 3.1 shows the mean and range of backscatter for the study period (2007-16). A first look suggests that there are significant variations in both. A visual comparison with the map of land cover types (Figure 2.1) indicates that the patterns in the backscatter match the distribution of vegetation types in the region. This is in agreement with the findings of Wagner et al. [1999] that the ERS scatterometer can be used for differentiating between regions of major vegetation types (such as forests and grasslands).

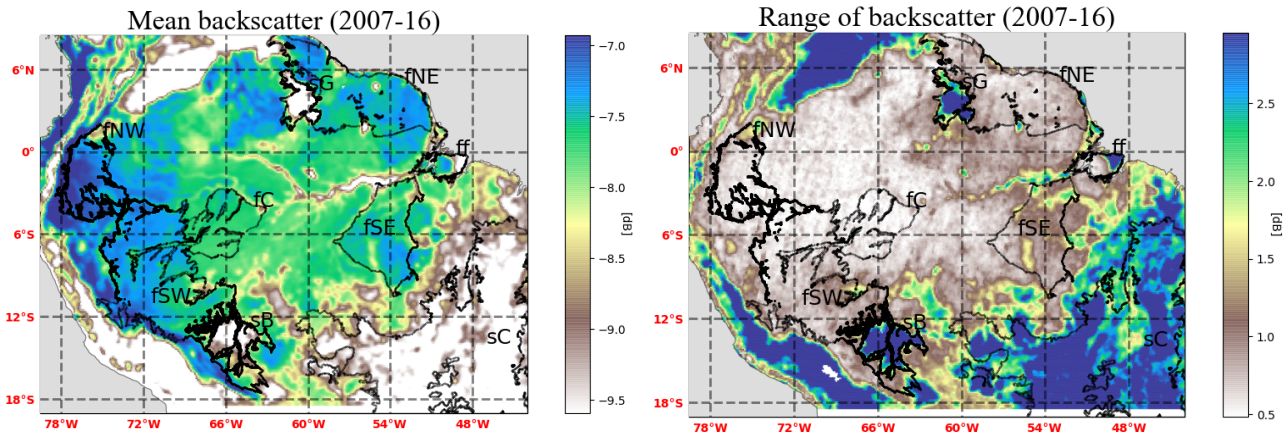

(a) Mean backscatter

(b) Range of backscatter

Figure 3.1: Mean and range of backscatter in the study area for the study period (2007-16). The regions of interest are marked in black outline.

From Figure 3.1a, the forest regions seem to have a higher mean backscatter than other regions. Figure 3.1b shows that forests also have a lower range in backscatter.

This is confirmed by the scatter plots (Figure 3.2) of mean and range of backscatter for the different vegetation types. The forest points (Figure 3.2a) are fairly homogenous, with most having mean values between -7dB and -9dB. The dense vegetation, with high moisture content drives high values of backscatter. The evergreen nature of the forests, with no distinct part of the year when the trees shed leaves, is seen in the low

ranges (mostly less than 1.5dB).

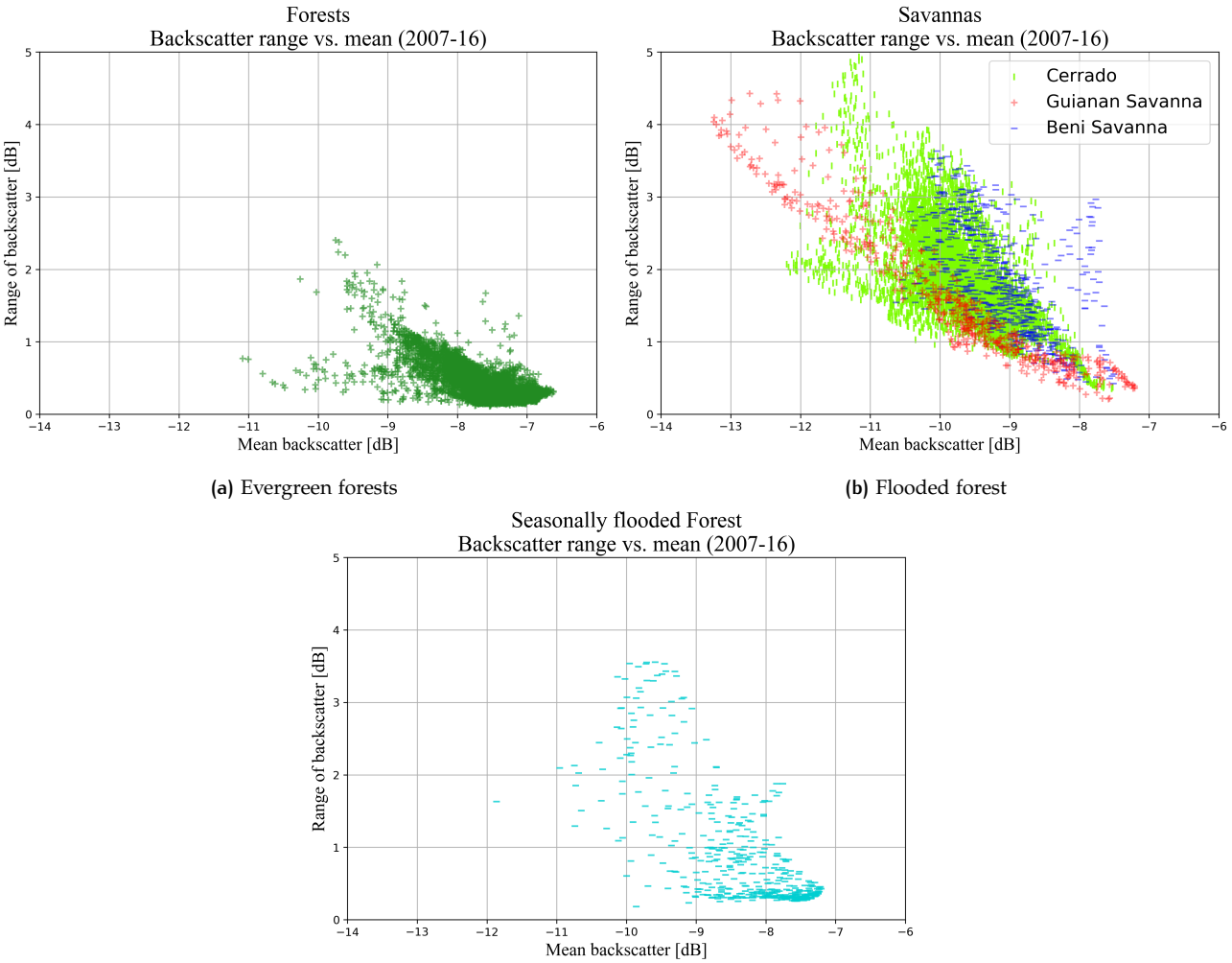

(a) Evergreen forests

(b) Flooded forest

(c) Savannas

Figure 3.2: Scatter plots of backscatter range vs. mean (by cover type). Each dot corresponds to an individual grid point belonging to the corresponding land cover type.

The savannas on the other hand (Figure 3.2b) have sparser vegetation with stronger seasonal trends and dry periods. This results in lower means and higher ranges. There is variation between the three savannas as well. Beni savanna (seen in dark blue) being a wetland, shows higher means than the sparser and drier Guianan savanna (seen in red). The Cerrado (seen in light green), being a diverse region with varied cover types within [Eiten, 1972], shows a wide spread of mean and range values.

The seasonally flooded forest (Figure 3.2c) shows mean values between that of the forests and savannas, with a high degree of variation. The high degree of seasonality in this cover type is seen in the large range in backscatter. The changes associated with the flooded and non-flooded seasons are explored further in section 3.2.4.

3.1.2 Slope

Figure 3.3 shows that, as with the backscatter, the spatial variations in the slope can be explained by differences in land cover types seen in Figure 3.3. The forests, again, show lower ranges than other regions (Figure 3.3b) due to their evergreen nature. The seasonally flooded forest (as seen in the scatter plot in Figure 3.4c), again, shows a high degree of variation, with large range value due to its strong seasonality.

This is the case with Beni savannas (dark blue dots in Figure 3.4b) as well, which being a wetland with seasonal flooding, has high ranges and variation similar to the seasonally flooded forest. The other two savannas, with lower seasonality, show range values more comparable to the evergreen forest (Figure 3.4a).

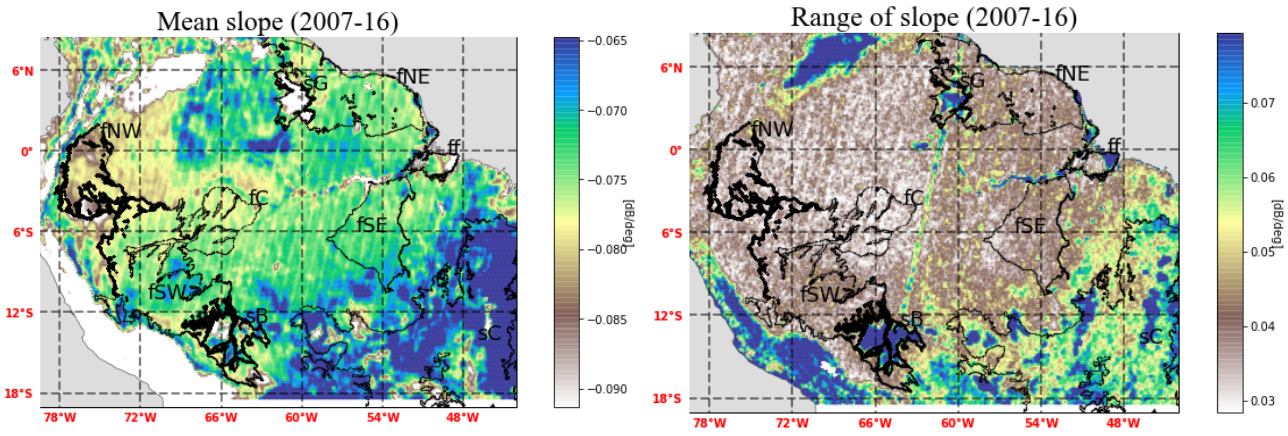

(a) Mean slope

(b) Range of slope

Figure 3.3: Mean and range of slope in the study area for the study period (2007-16). The regions of interest are marked in black outline.

The distribution of mean values (shown in 3.3a) is less straightforward. Beni savanna and Marajó várzea (the seasonally flooded forest), being wetlands contained within the Amazon forest, have mean slopes comparable to the evergreen forest (visible in 3.4). The Guianan savanna (red dots in Figure 3.4b), with sparse vegetation, has low mean slope values. The Cerrda (green dots in Figure 3.4b), on the other hand, shows mean values higher than the evergreen forests. This is unexpected since slope is considered a measure of "vegetation density", and the evergreen forests are much denser than savannas.

A possible explanation for this could be soil volume scattering, since the Cerrado is a savanna region with an intense dry season [Oliveira et al., 2005]. In places with low soil moisture, there is a possibility of soil volume scattering that can result in an increased backscatter [Vreugdenhil et al., 2016]. While the mean backscatter in the Cerrado seems low (Figure 3.1a), soil volume scattering would increase backscatter across all incidence angles, including at bigger angles where a region of sparse vegetation would typically show low values. This increase of backscatter at bigger angles could explain the high slope values since the incidence angle-backscatter curve becomes less steep.

The striations visible in Figure 3.3b have been addressed in section 3.1.4.

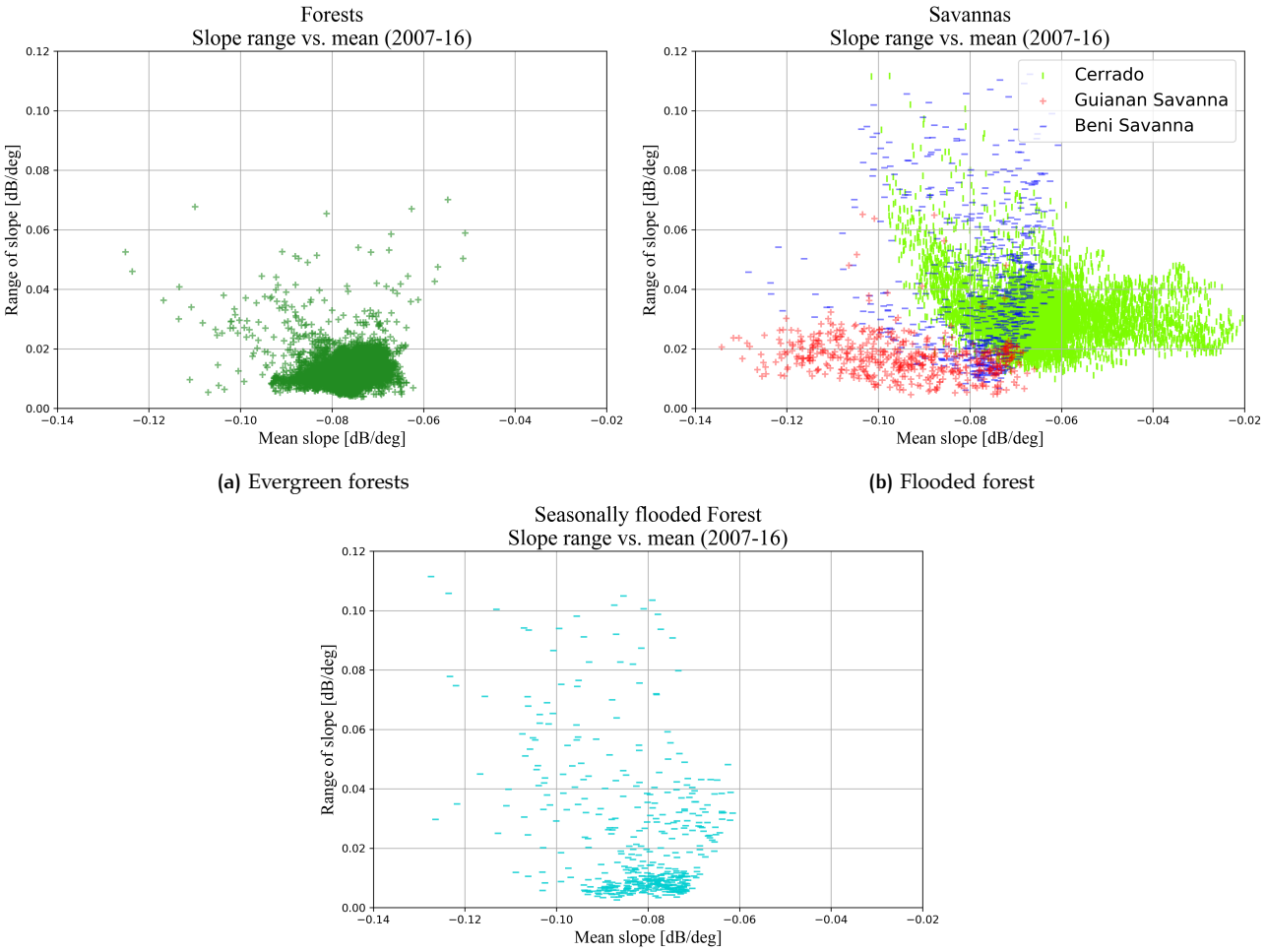

(a) Evergreen forests

(b) Flooded forest

(c) Savannas

Figure 3.4: Scatter plots of slope range vs. mean (by cover type). Each dot corresponds to an individual grid point belonging to the corresponding land cover type.

3.1.3 Curvature

Like backscatter and slope, the spatial distribution of the mean and range of curvature (Figure 3.5) matches land cover types in the study area (Figure 2.1). Again, the forests have lower ranges (Figure 3.5b) than the other types. Here, the mean values are higher for non-forests, compared to the forests (Figure 3.5a).

The scatter plots (Figure 3.6) confirm this, with the majority of the grid points in the evergreen forest regions (Figure 3.6a) having negative mean curvature less than -0.001 dB/deg^2. The dense canopy of the Amazon with high tree cover is less sensitive to incidence angles. Hence, it doesn't show the increase in backscatter at bigger incidence angles as in the case of vegetation that has more vertical structures. This results in low curvature values. Evergreen forests also have low range in curvature since they don't have a specific shedding season.

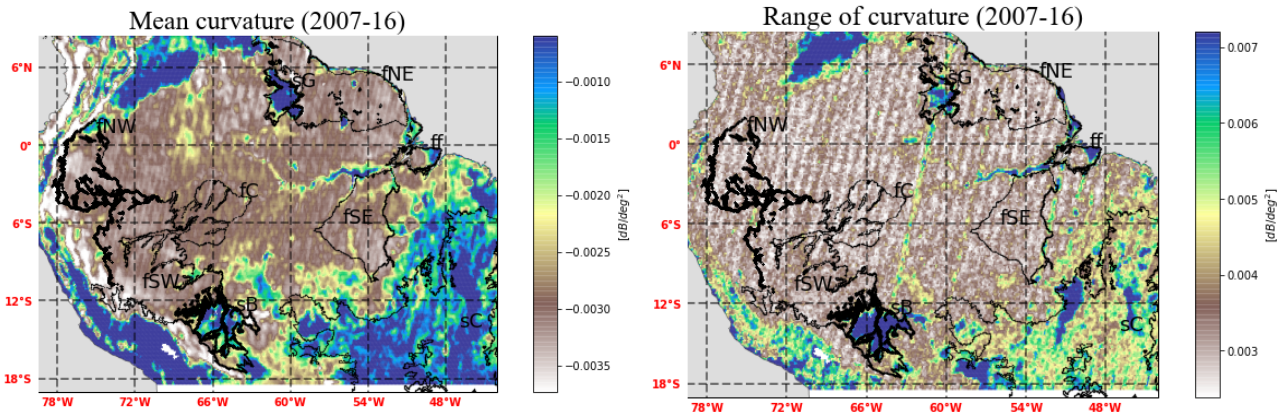

(a) Mean curvature

(b) Range of curvature

Figure 3.5: Mean and range of curvature in the study area for the study period (2007-16). The regions of interest are marked in black outline.

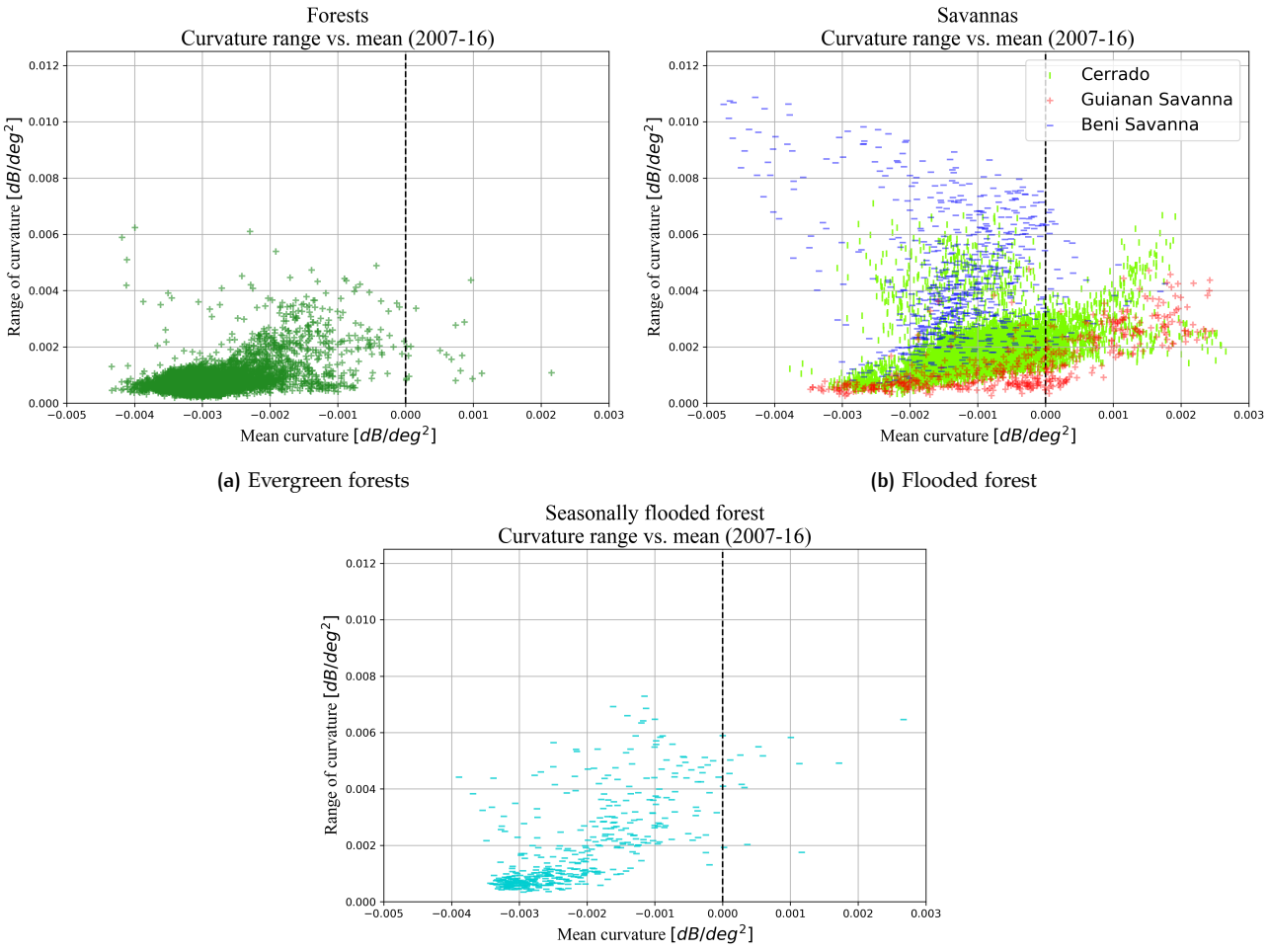

(a) Evergreen forests

(b) Flooded forest

(c) Savannas

Figure 3.6: Scatter plots of curvature range vs. mean (by cover type). Each dot corresponds to an individual grid point belonging to the corresponding land cover type.

Among the non-forest regions, Marajó várzea (Figure 3.6c) and Beni savanna (seen in dark blue in Figure 3.6b) are wetland regions contained within the Amazon. Consequently, they have higher tree cover, which is seen in the mostly negative mean curvature values. The high seasonality in these regions with seasonal flooding also results in high ranges in curvature.

The other two savannas: Cerrado and Guianan savanna (seen in green and red colour, respectively, in Figure 3.6b) have sparser vegetation with less tree cover, resulting in more grid points with positive mean curvature values. These regions also, in general, have lower seasonality than the wetlands (which see seasonal flooding). This is evident in the comparatively lower range values.

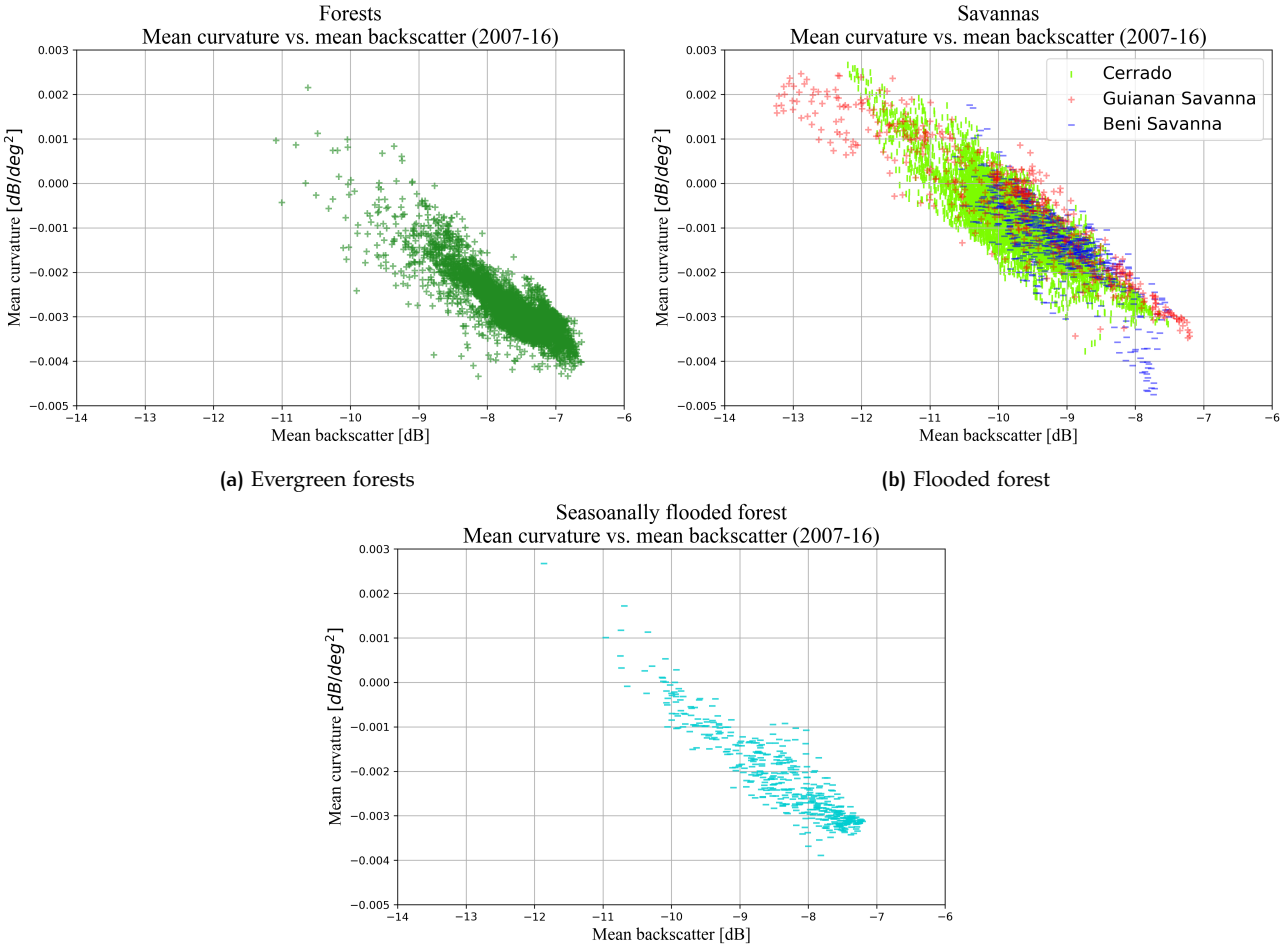

(a) Evergreen forests

(b) Flooded forest

(c) Savannas

Figure 3.7: Scatter plots of curvature mean vs. backscatter mean (by cover type). Each dot corresponds to an individual grid point belonging to the corresponding land cover type.

Looking at means of backscatter and curvature together in Figure 3.7, there seems to be a general trend of decreasing curvature with increasing backscatter. The regions of dense wet canopy (high backscatter) have high tree cover and, consequently, highly negative curvature values. Conversely, drier regions with sparse vegetation (low backscatter) have lower tree cover, and hence, higher mean curvatures.

3.1.4 Artifact in data

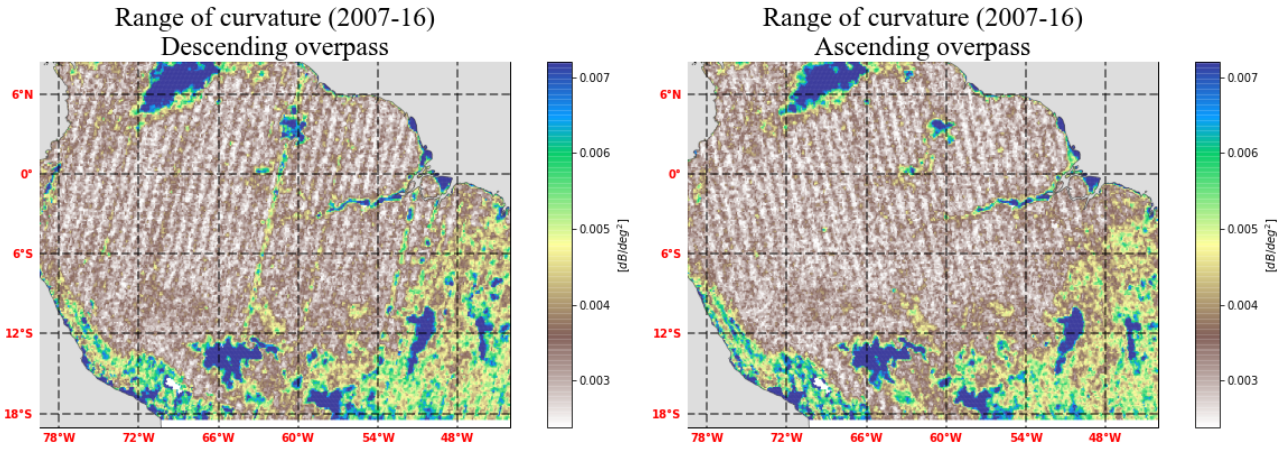

(a) Descending overpass

(b) Ascending overpass

Figure 3.8: Range of curvature in the study area for both overpasses, showing an artifact in data.

The maps of range of curvature for both overpasses (Figure 3.8) shows striations of points with much lower ranges than their surroundings. The regular spacing and straight lines point to a non-natural cause. The different angles of striations suggest an effect of satellite swaths.

At the swath edges, backscatter observations are available only at very high or very low incidence angles, skewing the calculations of the dynamic vegetation parameters. The effect is more visible over the forest regions since they have otherwise low values. Since these grid points are spread throughout the study area, and are different for the overpasses, they could not be excluded from the analysis.

3.2 SEASONAL VARIATIONS

This section looks at the seasonal cycles in backscatter, slope, and curvature over the study period (2007-16). Region-wise mean climatologies were calculated (as mentioned in 2.3.2) for the ASCAT parameters, as well as climatic variables such as radiation and precipitation. All analysis was done with the observations from the descending overpass for uniformity.

3.2.1 Backscatter

Figure 3.9 summarizes the mean seasonal cycles in backscatter for the regions of interest. It is evident that there is seasonality in all regions, however the amplitudes of variation differ. The evergreen forest regions all show similar cycles with very limited amplitudes of variation. The other regions show much stronger changes, and show differences in their seasonality. The Guianan savanna, for instance, peaks around the middle of the year, when most other seasons are in receding phase.

To discern the reason for these differences in seasonality, the relation between moisture availability and backscatter was explored. Figures 3.10 and 3.11 show the backscatter seasonal variation in the regions of interest, along with climatologies of precipitation and equivalent water thickness (EWT).

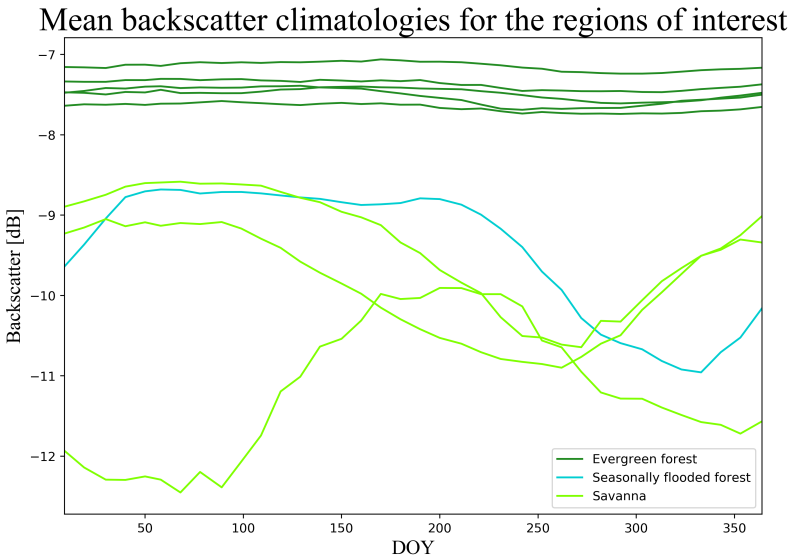

Figure 3.9: Mean backscatter climatologies for the regions of interest.

There is a clear correlation between the trends in EWT and backscatter. In all the regions, the backscatter peaks in the wet season, and decrease with the onset of the dry season. The EWT especially corresponds well with the backscatter seasonality. In all the regions, the peak and trough of the cycles coincide for backscatter and EWT. The different seasonality of the Guianan savanna (see Figure 3.11c), since like the other regions, the backscatter cycle follows the wet and dry seasons.

This is also visible in the phase relationship between the two parameters over the study area (Figure 3.12). In most of Amazonia, the backscatter is either in phase or lags the EWT by less than 100 days. Backscatter in Amazonia, thus, seems to be driven by moisture availability.

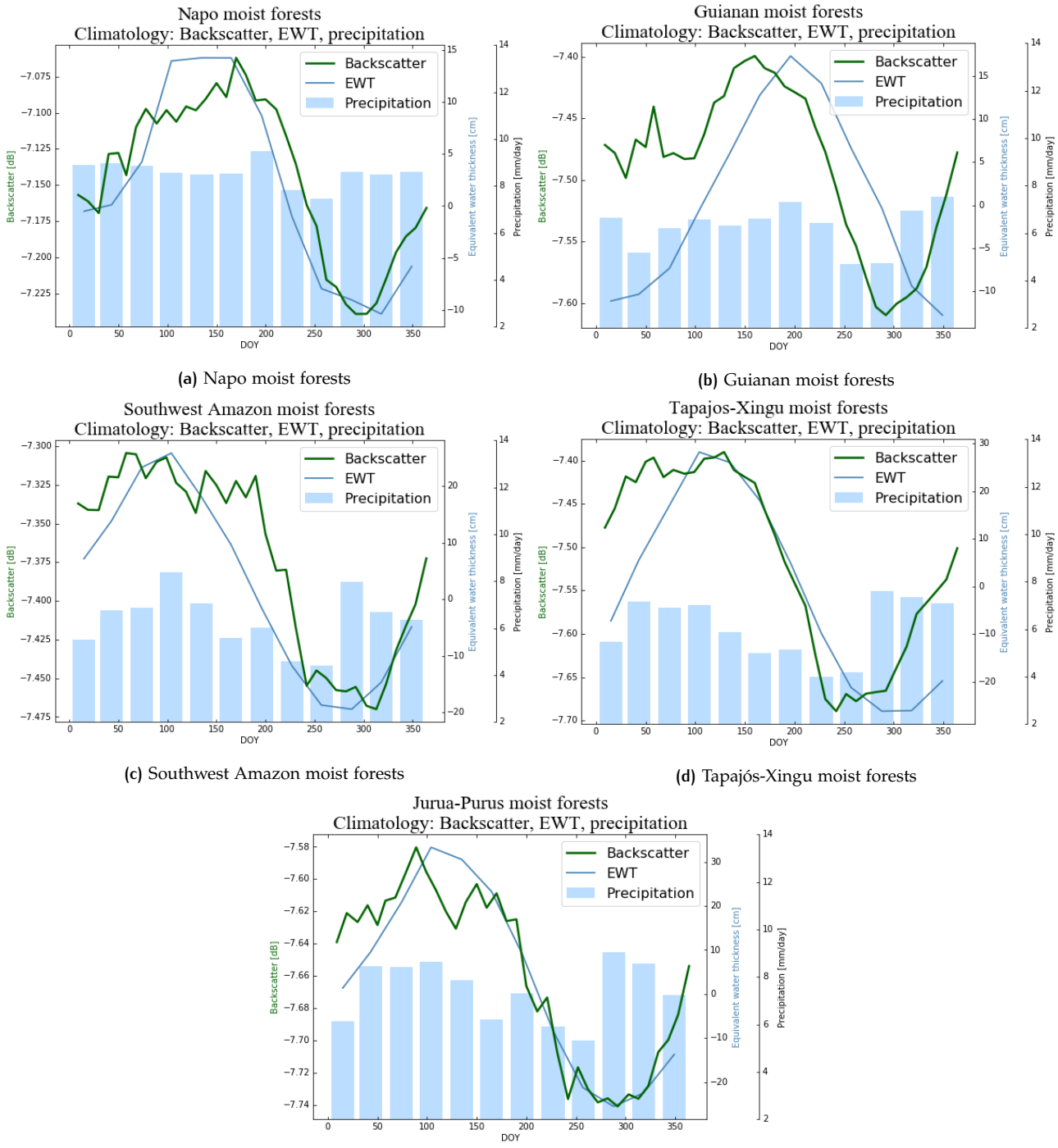

(a) Napo moist forests

(b) Guianan moist forests

(c) Southwest Amazon moist forests

(d) Tapajós-Xingu moist forests

(e) Juruá-Perez moist forests

Figure 3.10: Climatology of backscatter (green line), precipitation (bars), and EWT (blue line) for evergreen forests.

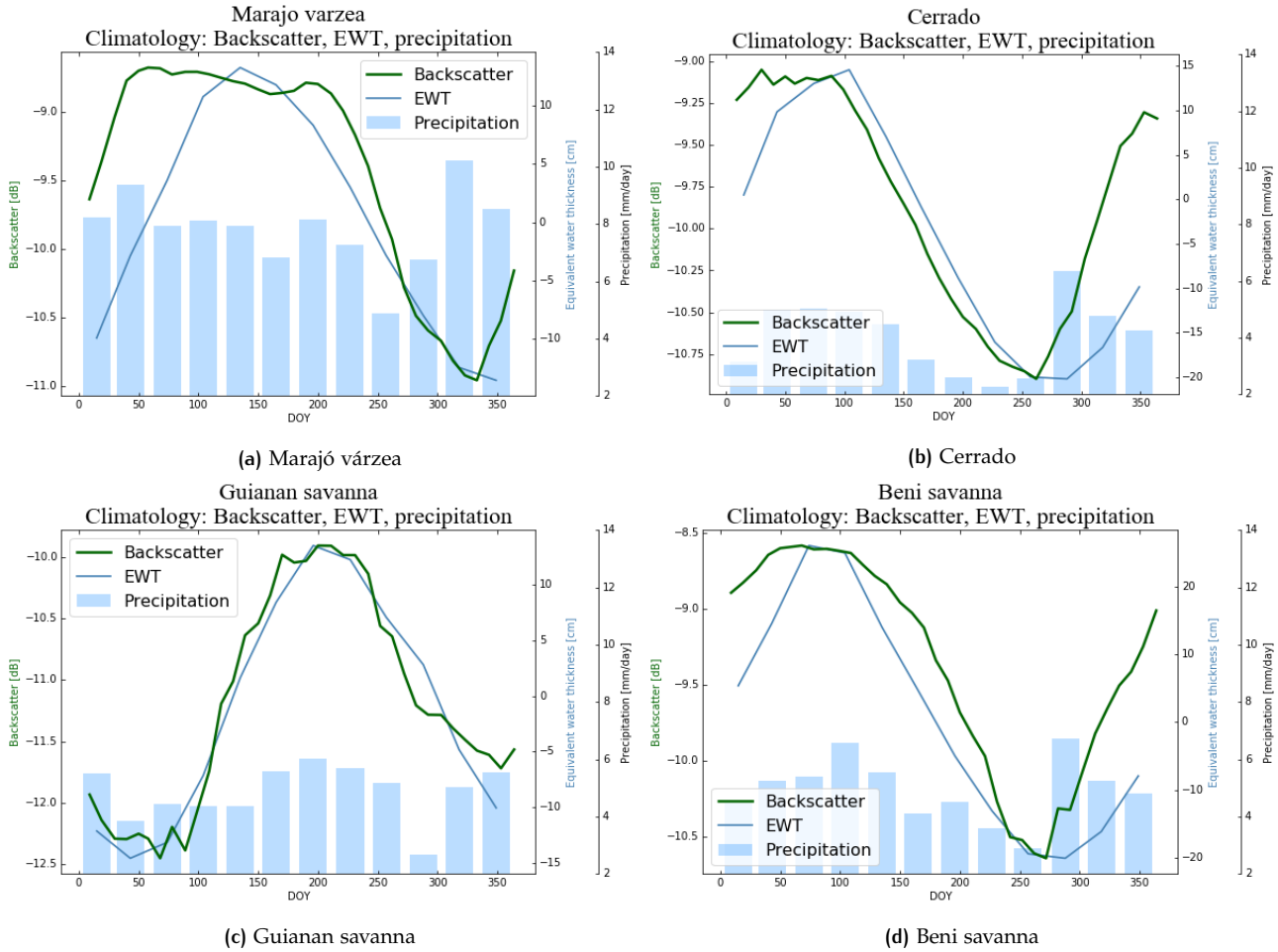

(a) Marajó várzea

(b) Cerrado

(c) Guianan savanna

(d) Beni savanna

Figure 3.11: Climatology of backscatter (green line), precipitation (bars), and EWT (blue line) for savannas and seasonally flooded forest.

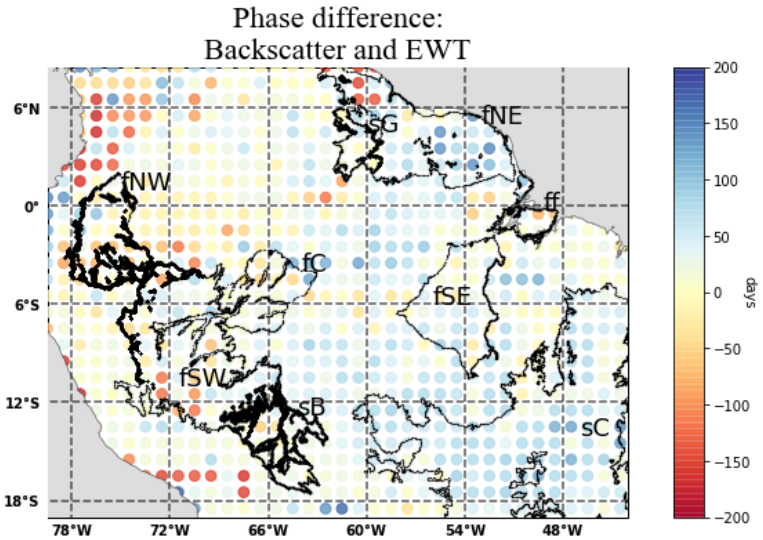

Figure 3.12: Map of study area showing the phase difference (in days of year) between backscatter and EWT. Positive values indicate that backscatter leads EWT, while negative values indicate that EWT leads backscatter. The regions of interest are marked in black outline.

3.2.2 Slope

Figure 3.13 summarizes the mean seasonal trends in slope for the regions of interest. As with backscatter, there are seasonal trends in all regions; however the amplitudes of variation differ – the evergreen forests (dark green lines) show much smaller changes, with differences among themselves. Beni savanna and Marajó várzea (seasonally flooded forest) show significantly different seasonality compared to the other regions, peaking in the early part of the year.

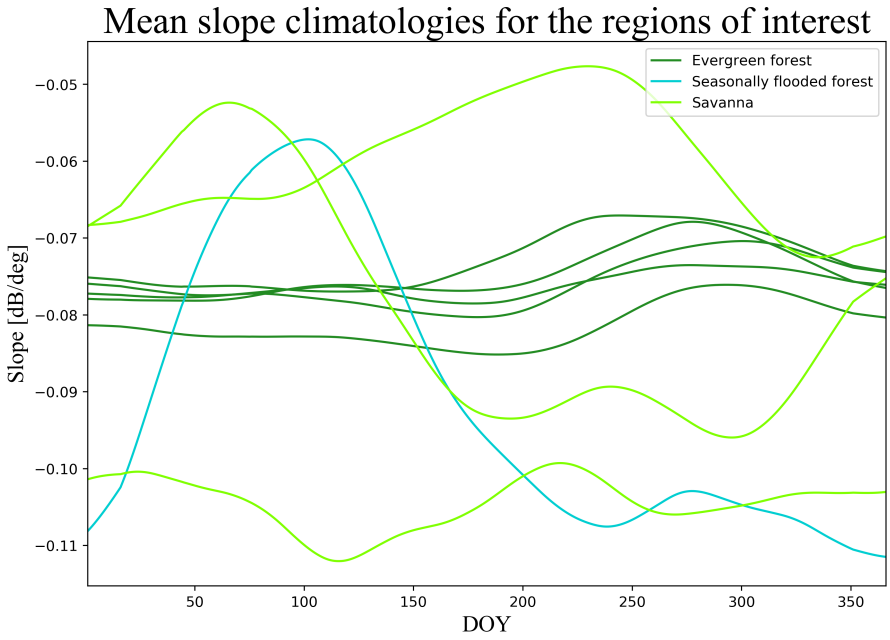

Figure 3.13: Mean slope climatologies for the regions of interest.

The slope is said to be related to vegetation dynamics [Vreugdenhil et al., 2016]. In evergreen forests like the Amazon that are not water-limited, the vegetation phenology is driven by radiation [Romatschke and Houze Jr, 2013]. The photosynthetic capacity depends on the available solar energy [Borchert et al., 2015]. This means that the photosynthetic activity, and consequently the transpiration rates would increase when radiation peaks.

The climatology of slope in the evergreen forests of Amazonia clearly follow the trend of radiation, as is visible in Figure 3.14. The cycles are correlated, and the peaks of slope coincide with or follow that of radiation. This is also observed in the map of phase difference between slope and radiation (Figure 3.16a). The evergreen forest regions have slope in phase with radiation or lagging by less than 100 days. Since the phenology in the forest is synced with radiation, the transpiration rates are linked to the radiation cycle, thus peaking in the dry season when the incoming radiation is maximum. The increased water flowing through the dense canopy due to the transpiration would increase the backscatter less sensitive to incidence angle, hence increasing the slope. There is a difference in the magnitude of lag between the slope and radiation seasonalities among the regions, which could be a matter of difference in vegetation species.

Slope shows an inverse relation to humidity since the evaporative demand, and therefore the transpiration rate, and consequently the slope increases as humidity decreases. The plots in Figures 3.14 and 3.15 show

humidity values on a reversed axis to make the relation between the cycles clearer to see. For Figure 3.16b), the day of year (DOY) corresponding to the minimum in humidity is considered for calculating the phase difference with the peak in slope, in consideration to the inverse relationship. The evergreen forests again, show a strong correlation between slope and humidity, with the peak in slope closely following the minimum in humidity, although with a greater lag than with radiation.

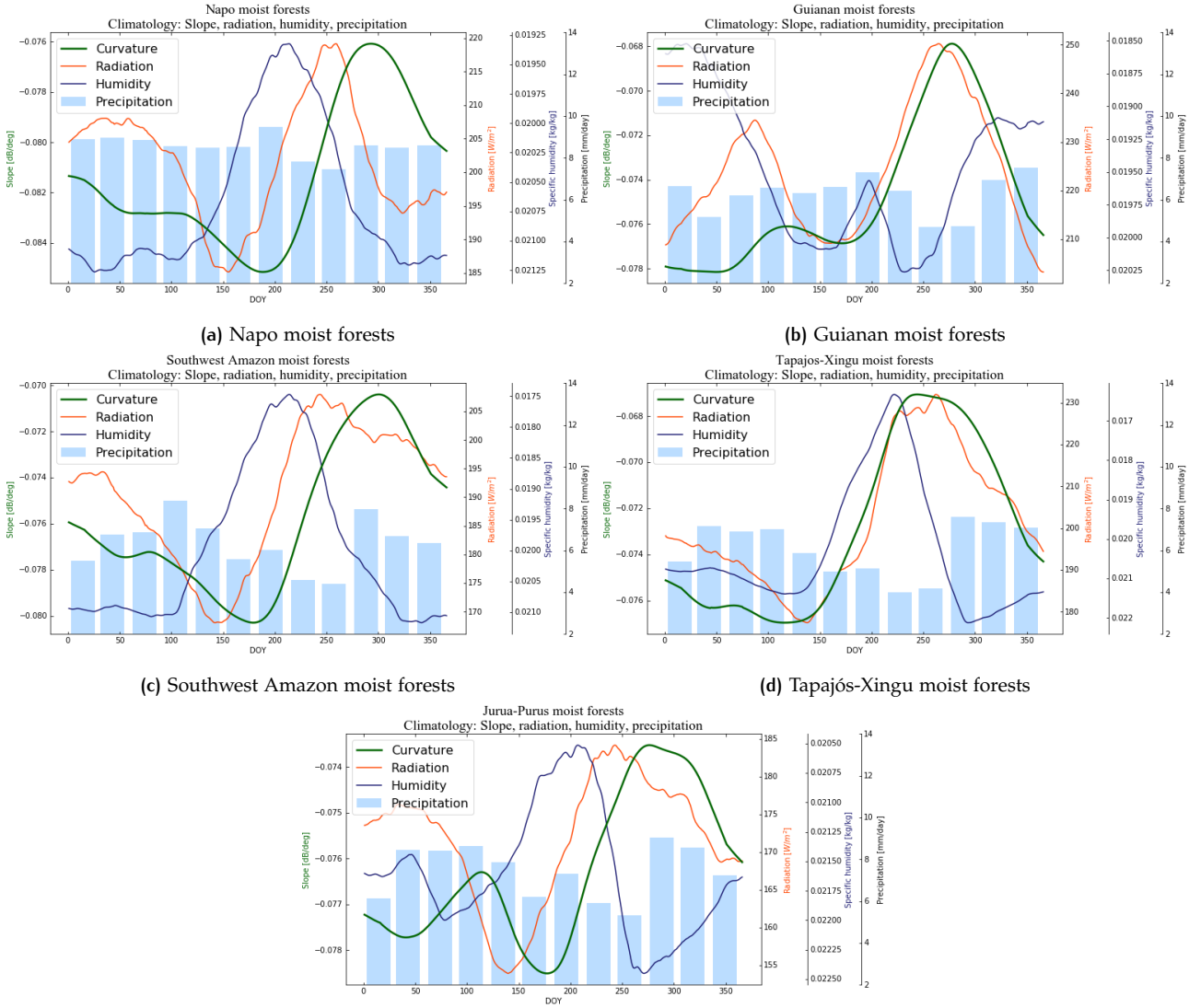

(a) Napo moist forests

(b) Guianan moist forests

(c) Southwest Amazon moist forests

(d) Tapajós-Xingu moist forests

(e) Juruá-Perez moist forests

Figure 3.14: Climatology of slope (green line), radiation (red line), humidity (blue line) and precipitation (bars) for evergreen forests. Note that the axis for humidity is flipped.

The non-evergreen forest regions (see Figure 3.15) show more variations in their relation to radiation and humidity. Beni savanna (sB) (Figure 3.15d) and Marajó várzea (ff) (Figure 3.15a), as mentioned earlier in the section, have different seasonality compared to the other regions. This is explored further in section 3.2.4. The Guianan savanna (sG) (Figure 3.15c) shows disparities in the phase relationship, as does the Guianan moist forest region (Figure 3.14b). The humidity cycle in these two adjacent regions is distinct with a minimum in the begining of the year unlike other regions where the humidity minimum closely preceded the radiation

peak. This increasing the phase differences between slope and humidity for the regions.

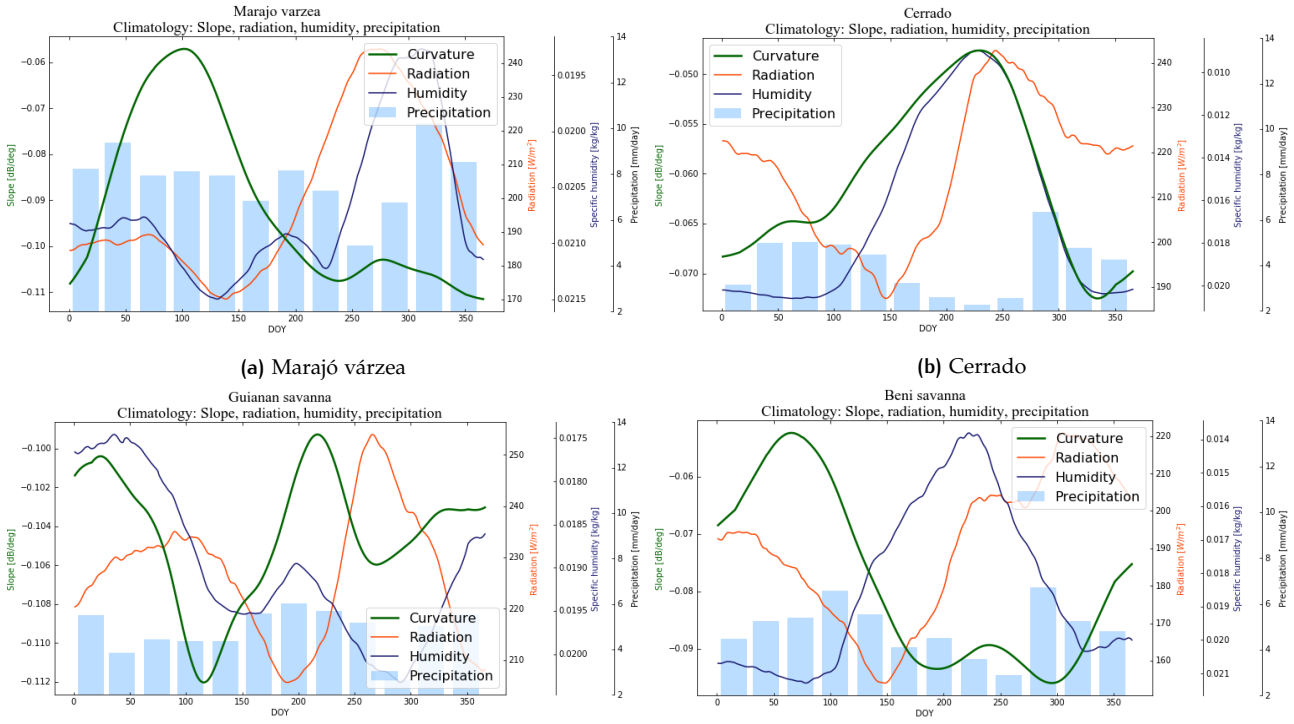

(a) Marajó várzea

(b) Cerrado

(c) Guianan savanna

(d) Beni savanna

Figure 3.15: Climatology of slope (green line), radiation (red line), humidity (blue line) and precipitation (bars) for savannas and seasonally forests. Note that the axis for humidity is flipped.

The cross-correlation analysis between slope and radiation confirms the observations from the climatologies and phase differences. The evergreen forests (Figure 3.16a) show high correlation between slope and radiation with maximum correlations for less than 2 months of lag (slope follows radiation). In the case of humidity (Figure 3.16b), the inverse relationship is visible in the higher magnitude of negative correlations. Overall, when compared to humidity, the slope in evergreen forests shows greater correlation with smaller lags.

The non-evergreen forest regions show more varies results. The Guianan savanna (sG) shows a weak correlation with both radiation and humidity. It could be that the sparse vegetation in the dry savanna region is moisture-limited and less radiation-driven than the evergreen forests. The region shows a different phase relationship with humidity compared to other regions, and more similar to Guianan moist forests. As mentioned before, this is because of the disparity in the humidity seasonality in the regions. Marajó várzea (ff) and Beni savanna (sB) show differences due to a possible flooding effect, explored further in section 3.2.4.

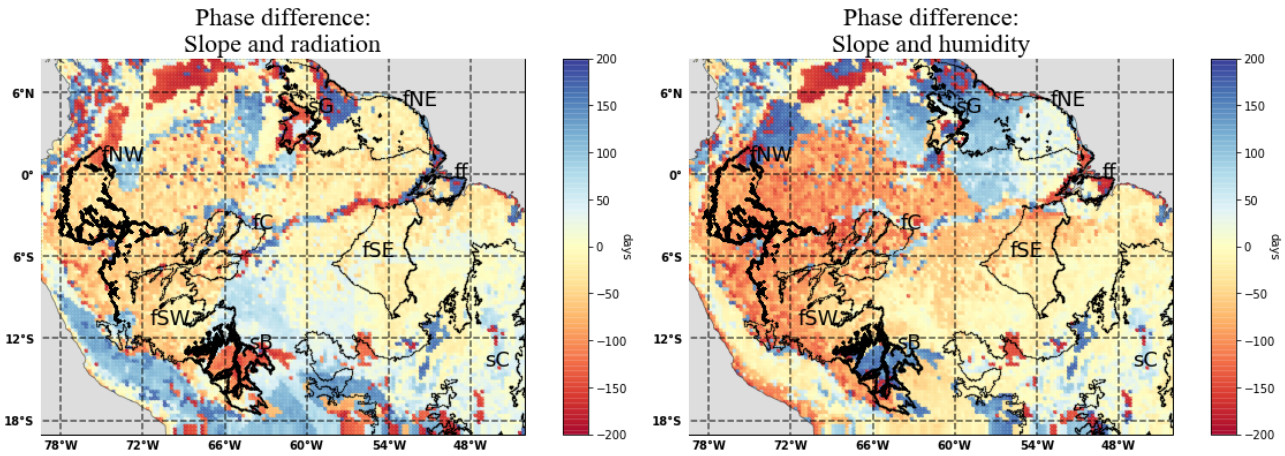

(a) Slope and radiation

(b) Slope and humidity

Figure 3.16: Map of study area showing the phase difference (in days of year) between slope and variables of evaporative demand. Positive values indicate that slope leads, while negative values indicate that slope lags. The regions of interest are marked in black outline.

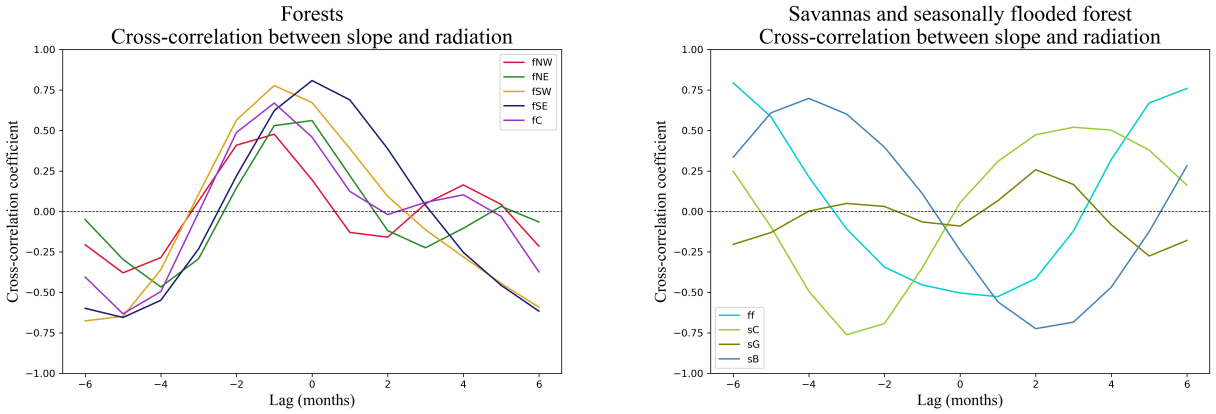

(a) Evergreen forests

(b) Savannas and seasonally flooded forest

Figure 3.17: Region-wise cross-correlation coefficients between slope and radiation for different (monthly) values of lag. Positive lag indicates that slope leads.

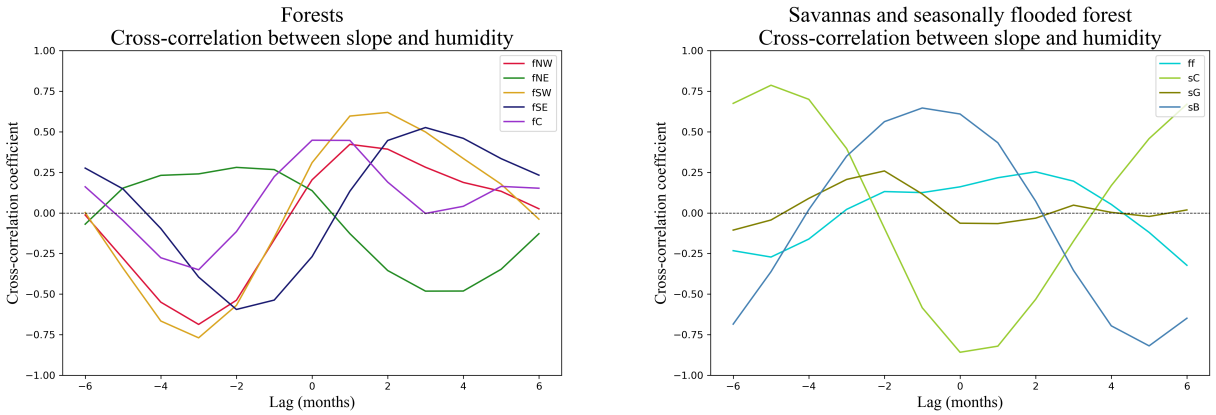

(a) Evergreen forests

(b) Savannas and seasonally flooded forest

Figure 3.18: Region-wise cross-correlation coefficients between slope and humidity for different (monthly) values of lag. Positive lag indicates that slope leads.

3.2.3 Curvature

Figure 3.19 presents the mean seasonal cycles in curvature for the regions of interest. Like backscatter and slope, there are seasonal variations in all regions. Other than the Guianan savanna, the regions peak around the same part of the year. The differences in the amplitudes of variation between the regions are, however, especially significant. While the evergreen forests vary less than 0.0005 dB/deg^2, the wetland regions (Beni savanna and Marajó várzea) show almost 0.005 dB/deg^2 variation.

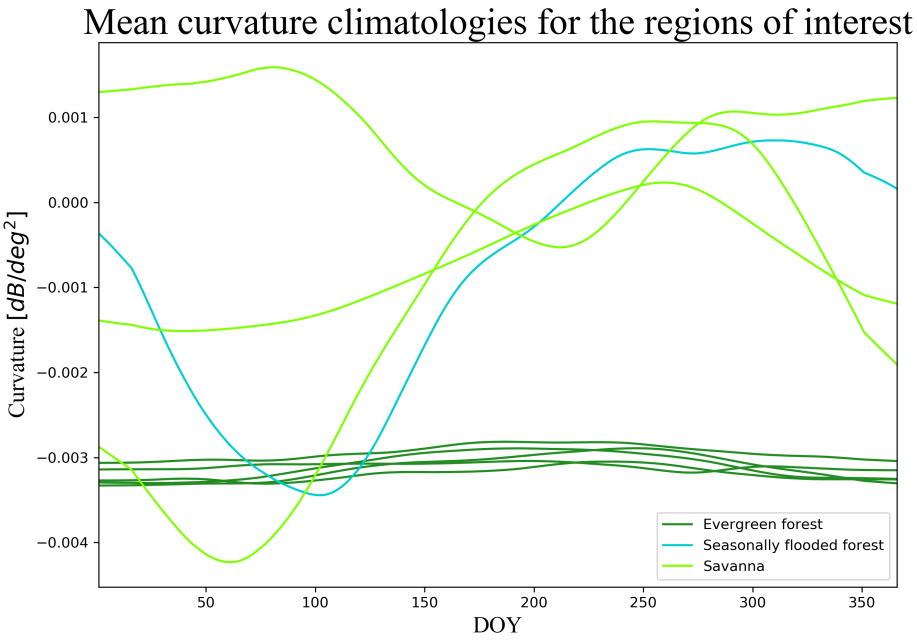

Figure 3.19: Mean curvature climatologies for the regions of interest.

Curvature has been shown to be related to vegetation phenology and structure [Steele-Dunne et al., 2019]. Since the vegetation phenology in much of the region has been seen to be radiation-driven, the curvature seasonality as well would be related to radiation and evaporative demand. Wagner et al. [2016] observed that litterfell coincides with maximum evaporative demand (which would coincide with minimum humidity). Leaf flushing, Borchert et al. [2015] found, is induced by an increase in radiation.

The climatology of curvature in Amazonia (seen in Figures 3.20 and 3.21) shows a relation to both radiation and humidity (the axis for humidity is reversed to make the inverse relation more visible), although the correlation seems to be weaker than in the case of slope. In most regions, the humidity minimum, curvature peak, and radiation peak coincide or closely follow each other. In some regions (such as in Figures 3.20d, 3.20e, and 3.21d), the curvature peak period seems to stretch across the period of steep decrease and then increase in humidity. It could be that the curvature peak phase includes both the litterfell and leaf flushing occurrences.

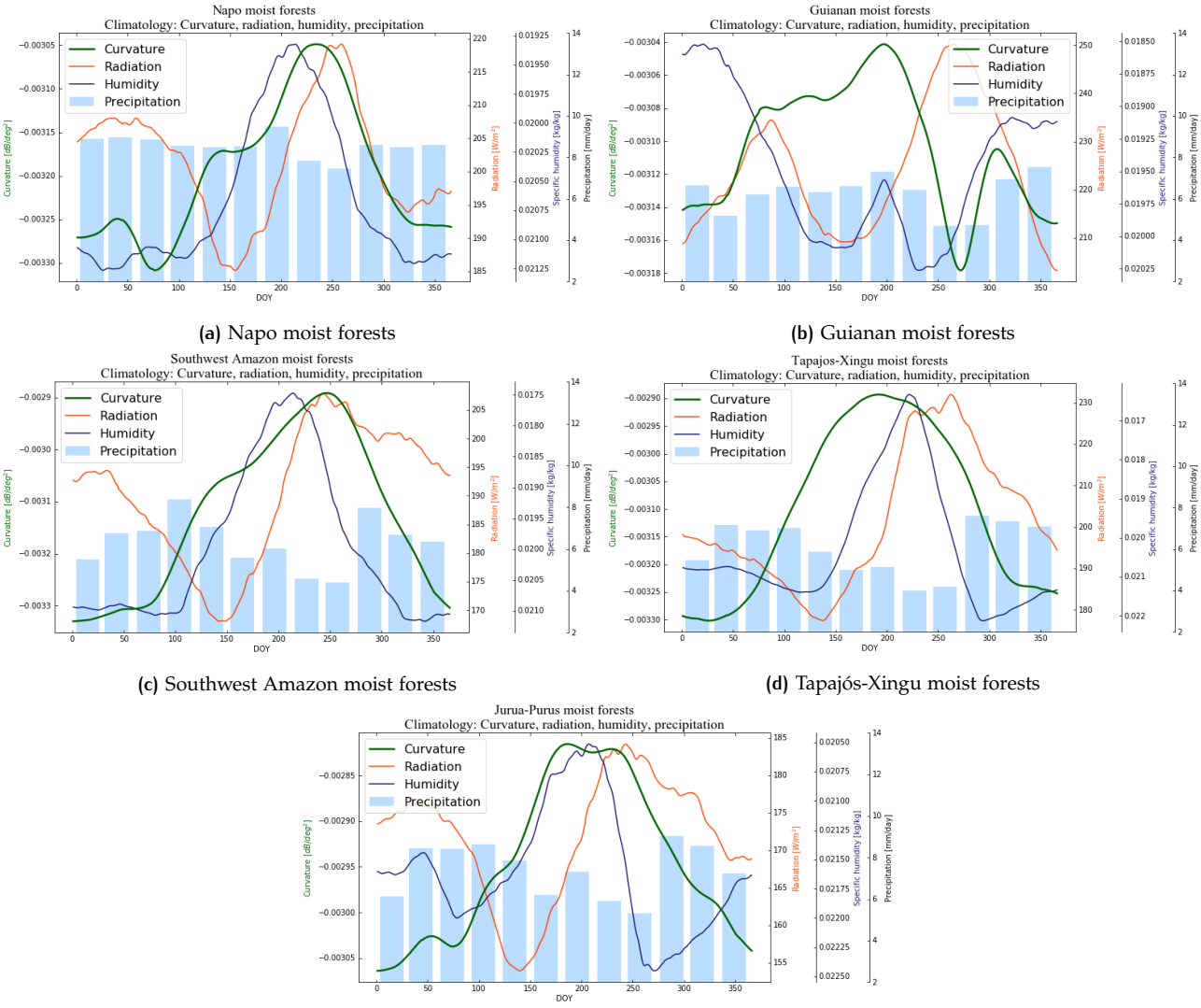

(a) Napo moist forests

(b) Guianan moist forests

(c) Southwest Amazon moist forests

(d) Tapajós-Xingu moist forests

(e) TJuruá-Perez moist forests

Figure 3.20: Climatology of curvature (green line), radiation (red line), humidity (blue line) and precipitation (bars) for evergreen forests. Note that the axis for humidity is flipped.

This variability in the length of the curvature peak phase is also visible in the more noisy spatial patterns in the phase relationships (Figure 3.22). In some regions, the curvature leads radiation, which might seem counter-intuitive. This means that the leaf flushing occurs before the radiation maximum. This makes sense if the time for leaves to mature is taken into consideration. Mature leaves have a higher photosynthetic capacity than new leaves [Maeda et al., 2017]. Hence, the vegetation phenology would be set to have maximum photosynthetic capacity when the radiation is strongest. Thus, leaf flushing would precede radiation.

The cross-correlation coefficients (Figure 3.23) show that curvature leads radiation by 2-4 months. The Guianan savanna and Guianan moist forests show weak correlations. As mentioned in the previous section, the Guianan savanna being drier region, could be more moisture limited, leading to less influence of radiation. In both these regions (which are located close to each other), the radiation cycle has another smaller peak in the beginning of the year, which seems to have affected the curvature seasonality.

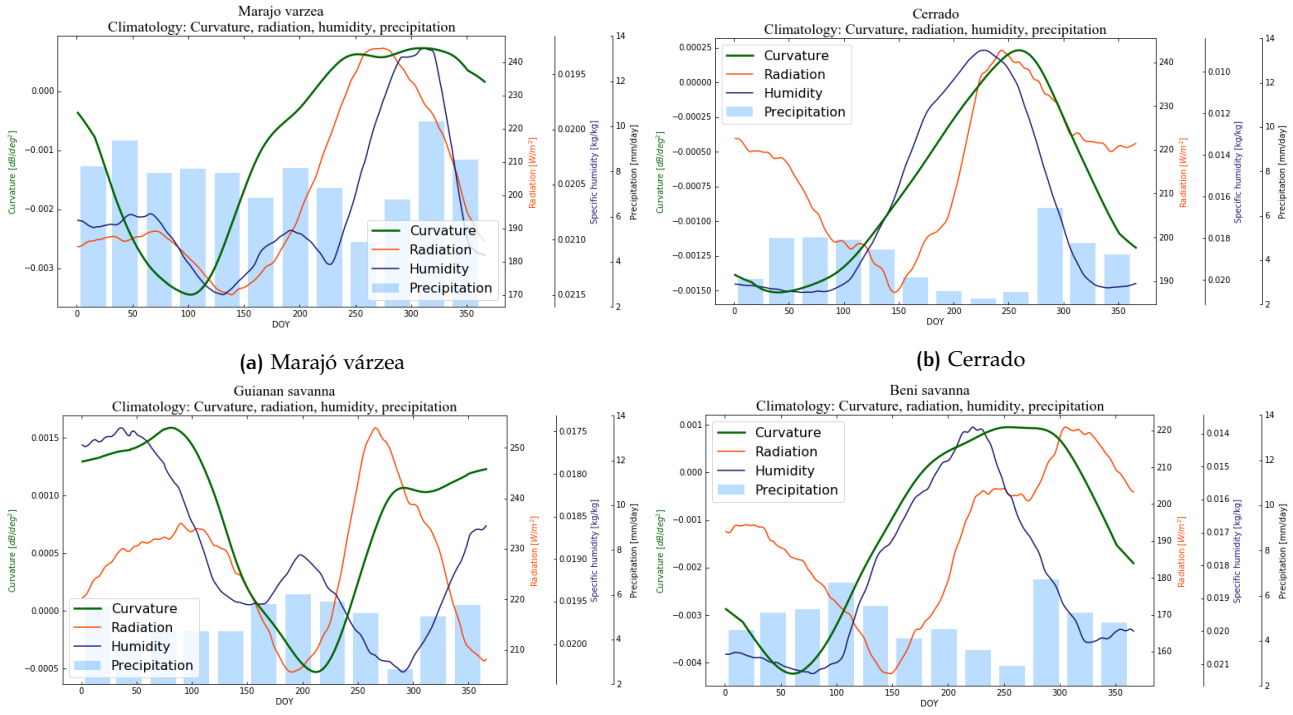

(a) Marajó várzea

(b) Cerrado

(c) Guianan savanna

(d) Beni savanna

Figure 3.21: Climatology of curvature (green line), radiation (red line), humidity (blue line) and precipitation (bars) for savannas and seasonally forests. Note that the axis for humidity is flipped.

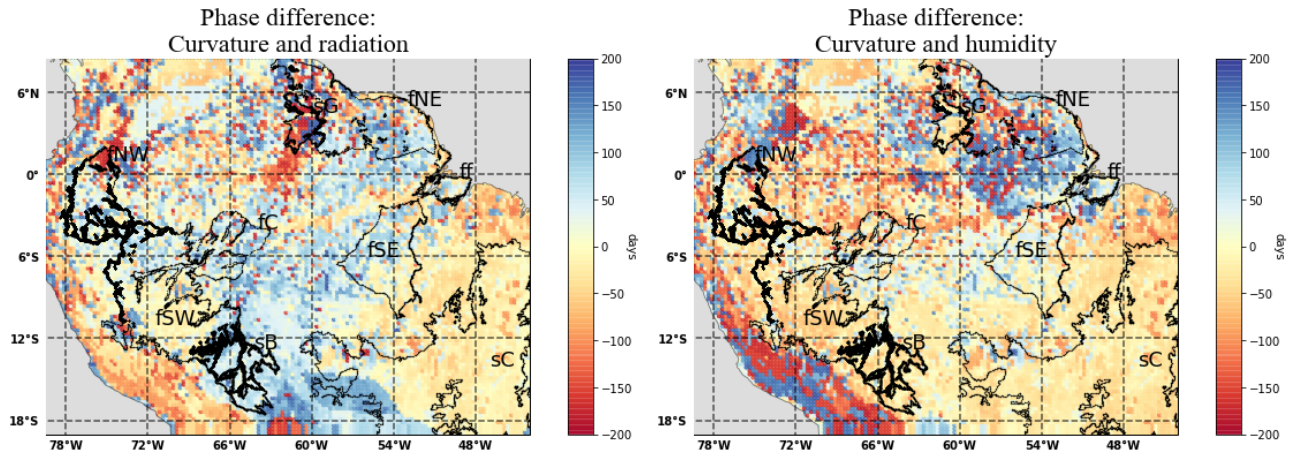

(a) Curvature and radiation

(b) Curvature and humidity

Figure 3.22: Map of study area showing the phase difference (in days of year) between curvature and variables of evaporative demand. Positive values indicate that slope leads, while negative values indicate that slope lags. The regions of interest are marked in black outline.

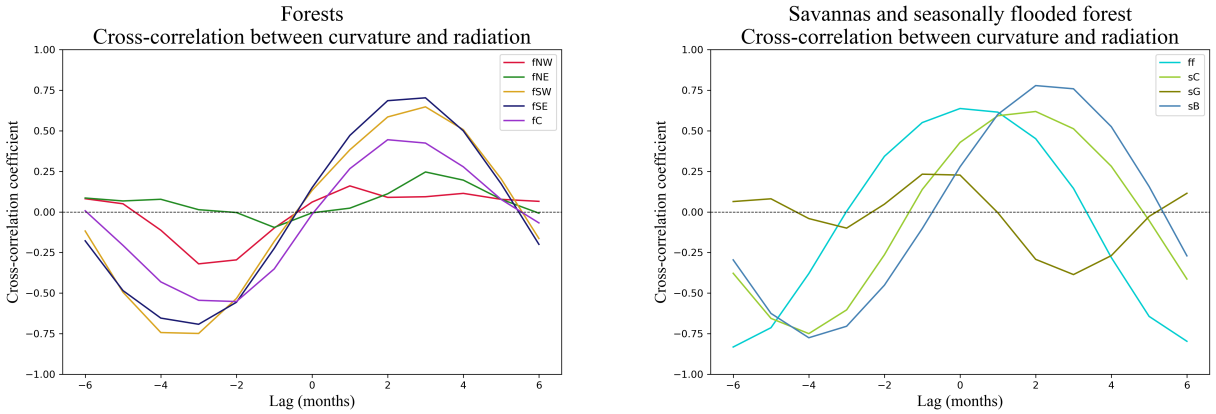

(a) Evergreen forests

(b) Savannas and seasonally flooded forest

Figure 3.23: Region-wise cross-correlation coefficients between curvature and radiation for different (monthly) values of lag. Positive lag indicates that curvature leads.

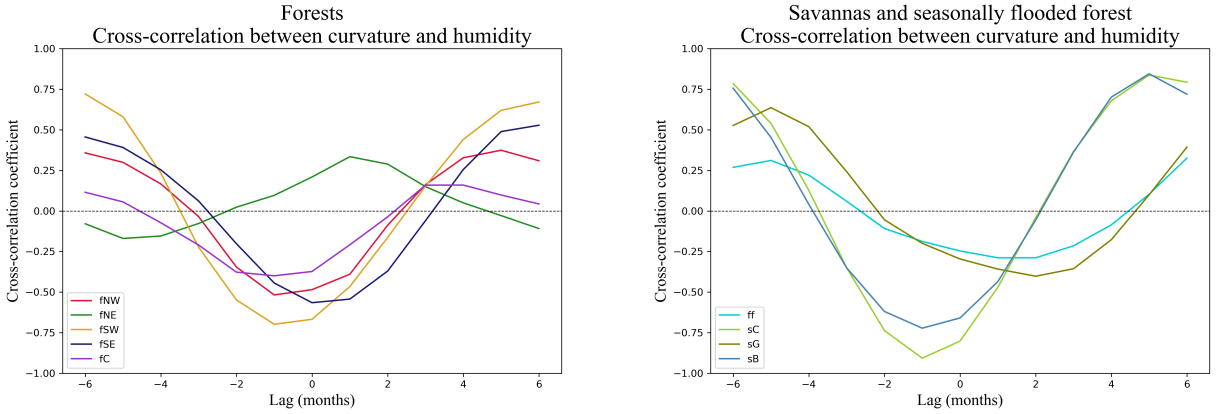

(a) Evergreen forests

(b) Savannas and seasonally flooded forest

Figure 3.24: Region-wise cross-correlation coefficients between curvature and humidity for different (monthly) values of lag. Positive lag indicates that curvature leads.

Since humidity has an inverse relationship with curvature, the negative correlations are more important (seen in Figure 3.24). For the forests (Figure 3.24a), the optimum lag is less than with radiation, since the humidity minimum generally precedes the radiation peak. Guianan moist forests show a different relation because of the humidity minimum occuring in the beginning of the year, unlike for other regions.

3.2.4 Flooding

The regions of interest Marajó várzea (seasonally flooded forest) and Beni savanna show very different seasonality of slope compared to the other regions. This is hypothesized to be due to the seasonal flooding that occurs in both regions during the peak precipitation season, which as mentioned in section 2.1.3, occurs between January-March in Marajó várzea, and March-April in Beni savanna.

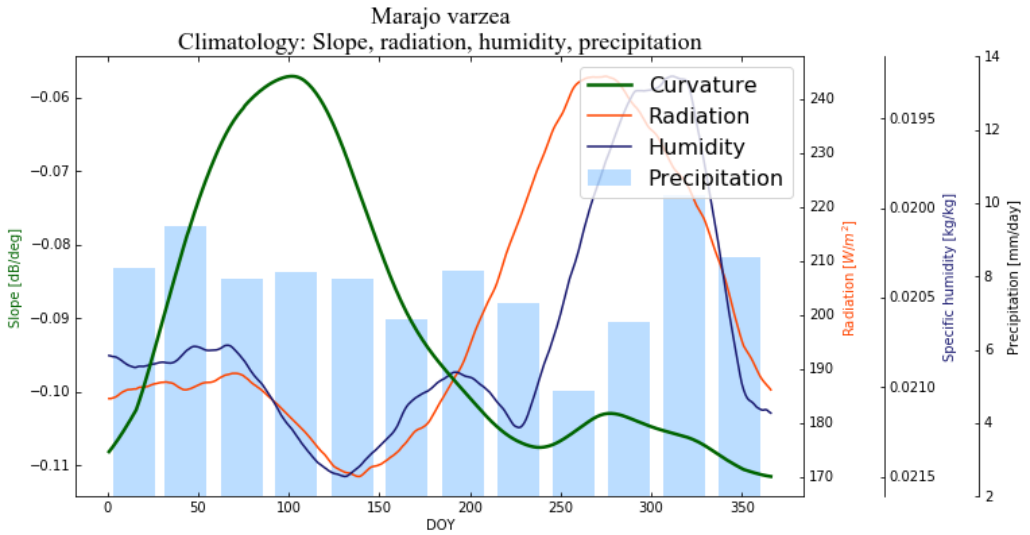

(a) Marajó várzea (ff)

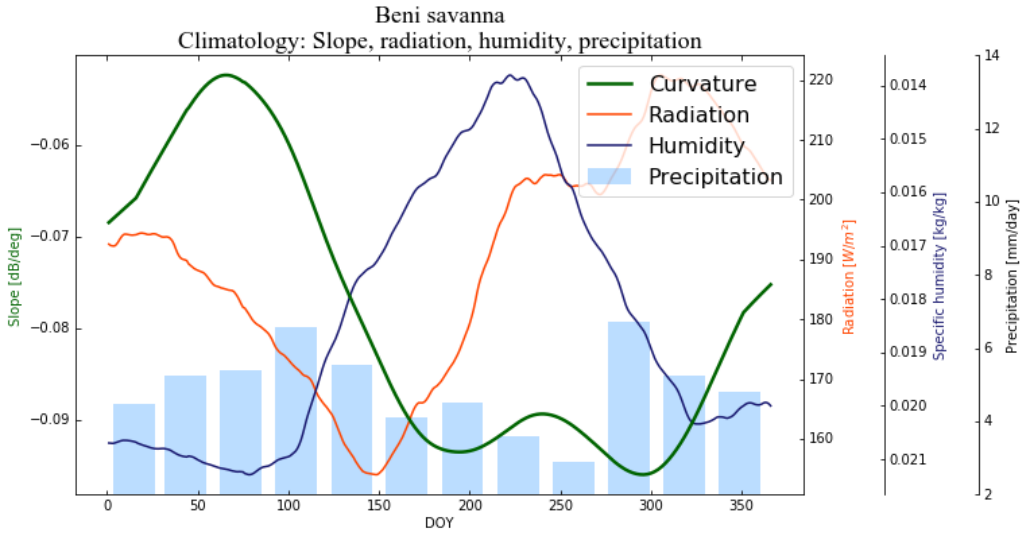

(b) Beni savanna (sB)

Figure 3.25: Climatology of slope (green line), radiation (red line), humidity (blue line) and precipitation (bars) for wetland regions.

Both regions show a steep increase in slope during the flooding season, as is visible in Figure 3.25. This can be explained by looking at their backscatter climatologies for a range of incidence angles (Figure 3.26). There is a sharp drop in the σ°_{20} values for both regions coinciding with the period of increase in slope. This drop is unaccompanied by a proportional change at the 40° and 60° incidence angles. This results, as shown in Figure 3.27, in a concave $\sigma - \theta$ curve during the flooded period, as opposed to the convex curve observed in non-flooded intervals.

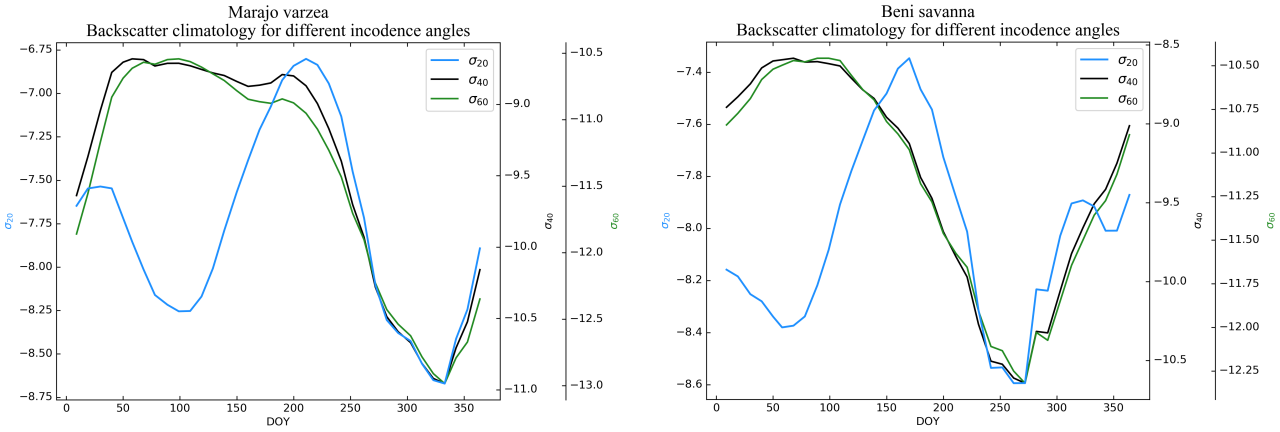

(a) Marajó várzea

(b) Beni savanna

Figure 3.26: Climatologies of backscatter at incidence angles of 20°, 40°, and 60° for regions with seasonal flooding.

Hess et al. [1990] found that flooded lands can show decreased backscatter. However, there can be "double-bounce reflections between smooth water surfaces and tree trunks or branches". This can result in an asymmetric increase/decrease of backscatter at different incidence angles. Hence, the $\sigma - \theta$ would see a change between flooded and non-flooded intervals, as is seen in Figure 3.27. The change is especially marked in the Beni savanna, where the backscatter at steep incidence angles (around 20°) is less during flooding than during non-flooded times.

This incidence-angle relationship during flooding depends on the vegetation type in a region [Wang et al., 1995]. Past studies have found that flooded varzeas (seasonally flooded forests) in the Amazon basin are distinguishable from non-flooded forests due to an increase in backscatter Hess et al. [1990]. In the case of the regions of interest in this study, the flooding seems to decrease backscatter at steep angles, but at bigger angles, multiple reflections cause an increase. The study by Hess et al. [1990] also found that the presence of palms could bring errors in forest flooding estimates. Palms dominate both Marajó várzea and Beni savanna, as mentioned in section 2.1.3. This could be reason for the unusual backscatter-incidence angle relationships.

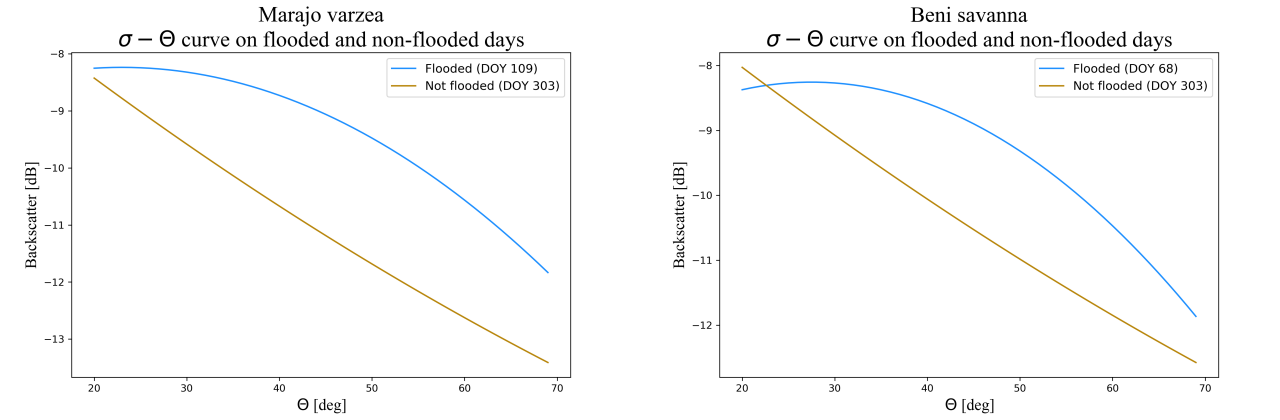

(a) Marajó várzea

(b) Beni savanna

Figure 3.27: $\sigma - \theta$ curves during flooded (blue line) and non-flooded days (golden line) for wetland regions.

3.3 DIURNAL DIFFERENCES

This section analyses the differences in the studied parameters between morning and evening values. This is measured through variations in the values for the parameters between the descending and ascending satellite overpasses, which occur around 10 am and 10 pm over the Amazon. The 10 am overpass time reduces the probability of the presence of dew droplets in the canopy.

Figure 3.28 shows the mean diurnal differences for all parameters in the study area for the months of January and July. Clearly, there are disparities between the overpasses in all regions and all parameters. The slope and curvature, however, show less consistent patterns within the regions of interest, as seen in the figure. Consequently, the subsequent discussion in the section focuses on diurnal differences in backscatter.

On comparing Figures 3.28a and 3.28b, it is clear that there are intra-annual differences in spatial distribution of diurnal differences backscatter. This indicates a seasonal cycle in the diurnal differences. Figures 3.29 and 3.30 show the climatology of diurnal differences in the regions of interest.[1] There seem to be an influence of both moisture demand (through radiation), as well as moisture availability (through precipitation and EWT).

For most regions, especially the evergreen forests, in the wet season, the backscatter is higher in the evening (diurnal difference is negative). This is consistent with the finding that precipitation in tropical South America (since it is generally produced by convective systems) predominantly occurs in the late afternoons and evenings [Romatschke and Houze Jr, 2013]. Hence, the wetter canopy in the evening would have greater backscatter.

In the dry season, the morning backscatter is generally higher (diurnal difference is positive). In a light-limited evergreen forest such as the Amazon (rather than a water-limited forest), the canopy photosynthetic capacity seasonality is driven by radiation [Wagner et al., 2016]. Accordingly, since the plants are phenologically active, they lose water in the daytime through transpiration. The evening backscatter is, thus, lower. This is in agreement with the findings of studies by Frolking et al. [2011] and Friesen et al. [2012] that found the morning backscatter over Amazonia to be on an average higher than the evening values due to higher water content in the vegetation.

Both the radiation and moisture cycles, therefore, play a key role in diurnal differences. It is hard to say which factor is more important since the radiation seasonality is, in itself, related to the precipitation seasons through the effect of cloud cover.

Figures 3.29 and 3.30 show a difference in the phase relationship of the diurnal difference in backscatter with the climatic variables. The Guianan moist forests (see Figure 3.29b), for instance, shows a much greater difference in number of days between the peaks of radiation and diurnal difference, compared to the other evergreen forest regions in Figure 3.29. This could be due to a difference in the vegetation species prevalent in the region.

Figure 3.31 looks at the phase difference of the diurnal difference climatology in the study area with radiation and EWT. The EWT minimum is used to compute the phase difference instead of the maximum, since (as seen in Figures 3.29 and 3.30), the diurnal difference is higher (more positive) when the EWT is lower.

From Figure 3.31, it is seen that the forest regions are, on an average, in phase with radiation and EWT (within a window of 50 days on either side). The Beni savanna (sB) (Figure 3.30d) shows a similar trend as that of the forests. The Cerrado (sC) (Figure 3.30b) shows large variations within, and does not show a

[1] The climatologies of diurnal differences for slope and curvature have been included in Appendix A.

consistent unified trend.

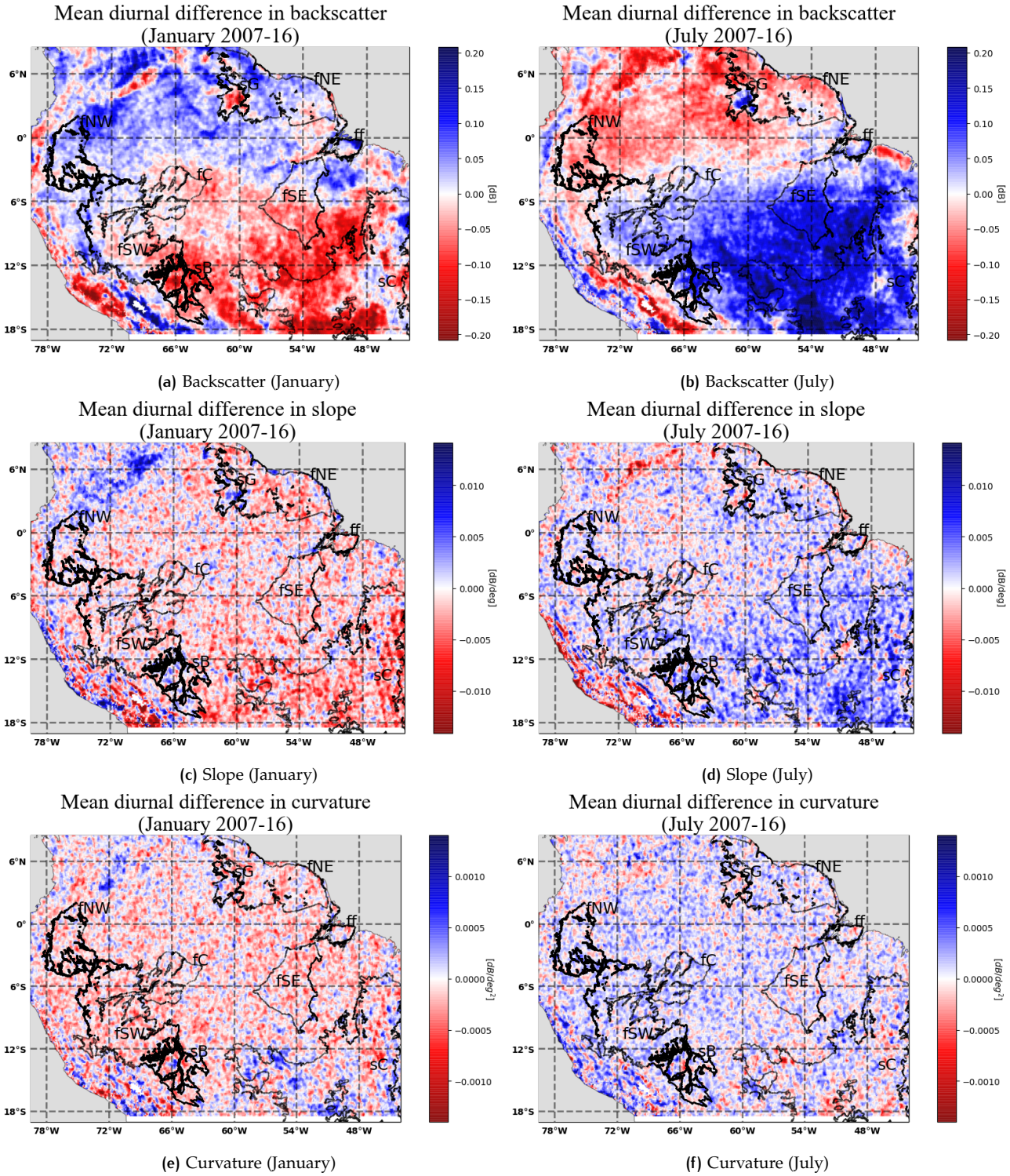

(a) Backscatter (January)

(b) Backscatter (July)

(c) Slope (January)

(d) Slope (July)

(e) Curvature (January)

(f) Curvature (July)

Figure 3.28: Map of monthly mean diurnal differences in study parameters for the months of January (left) and July (right). The regions of interest are marked in black outline.

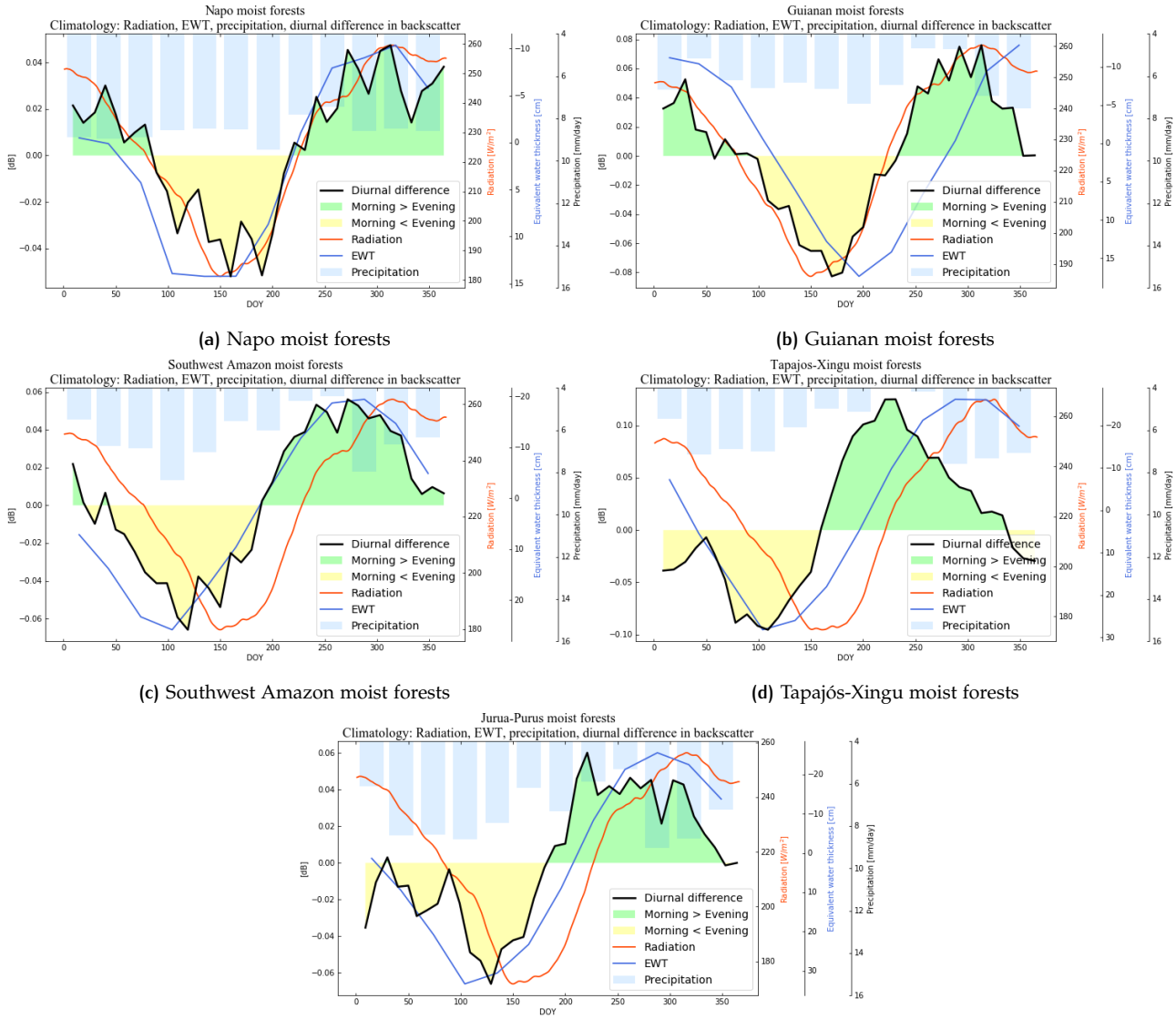

(a) Napo moist forests

(b) Guianan moist forests

(c) Southwest Amazon moist forests

(d) Tapajós-Xingu moist forests

(e) Juruá-Perez moist forests

Figure 3.29: Climatology of diurnal difference in backscatter (black line), radiation (red line), EWT (blue line), and precipitation (bars) for evergreen forests. Green fill indicates days with positive diurnal difference, while yellow fill indicates negative values.

The Guianan savanna (sG) (Figure 3.30c) shows a trend opposite to that of the forests as well as its surrounding regions in terms of both radiation and EWT (also visible in the mean values of Figure 3.28). This could be an effect of the satellite overpass times over the region.

Before the morning overpass (around 10 am), the vegetation has already lost a significant amount of moisture through transpiration (particularly important in the dry savanna region, compared to the forest). Also, before the evening overpass (around 10 pm), some of the lost water content could be regained. Steele-Dunne et al. [2019] made similar observations in the North American grasslands. The Beni savanna, being a wetland, is less dry, and hence, would be less sensitive to this overpass time effect.

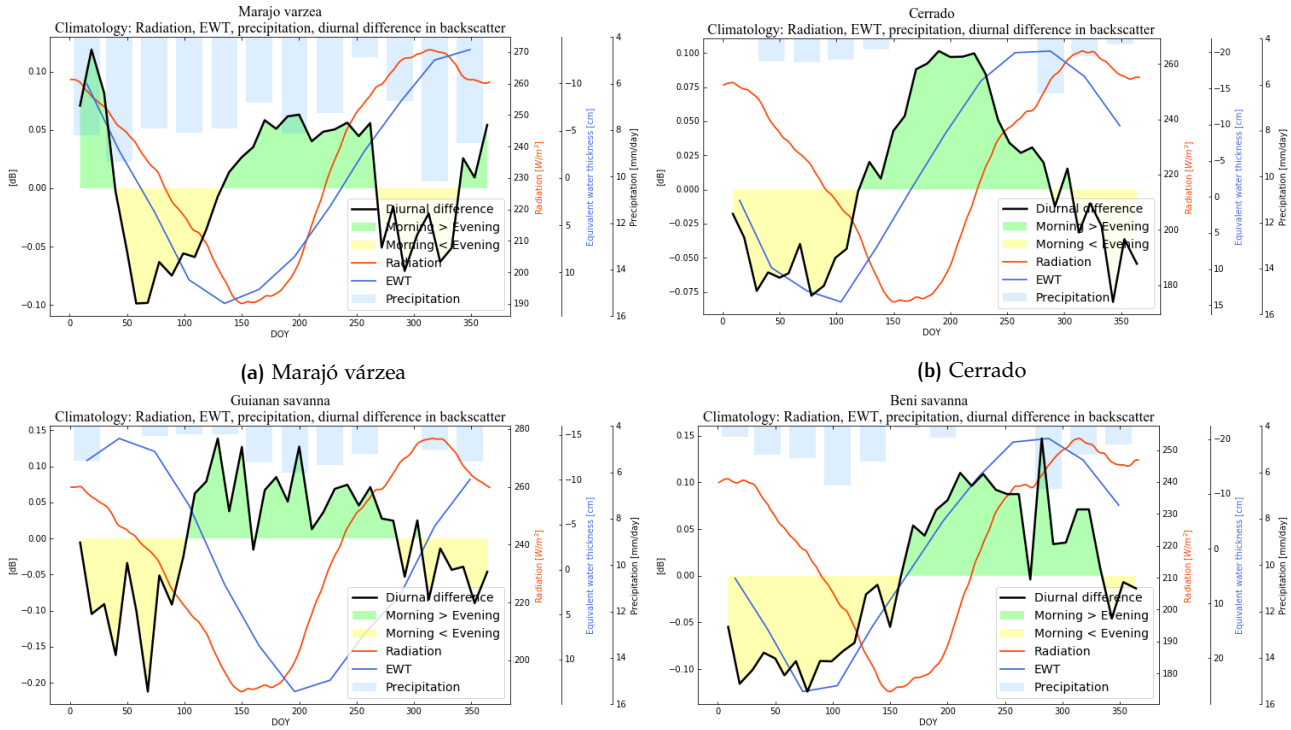

(a) Marajó várzea

(b) Cerrado

(c) Guianan savanna

(d) Beni savanna

Figure 3.30: Climatology of diurnal difference in backscatter (black line), radiation (red line), EWT (blue line), and precipitation (bars) for savannas and seasonally flooded forest. Green fill indicates days with positive diurnal difference, while yellow fill indicates negative values.

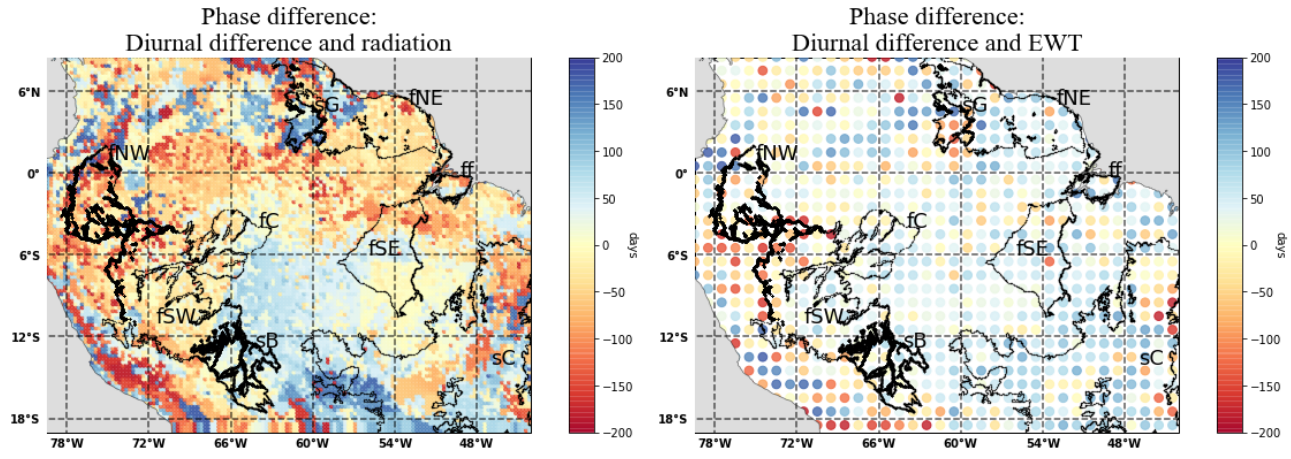

(a) Diurnal difference and radiation

(b) Diurnal difference and EWT

Figure 3.31: Map of study area showing the phase difference (in days of year) between diurnal difference in backscatter, and radiation and EWT. Positive values indicate that diurnal difference leads, while negative values indicate that it lags. The regions of interest are marked in black outline.

Another possibility, since the diurnal difference for the Guianan savanna is anti-phase with EWT (and hence, the morning backscatter values are higher in the wet season), is that the vegetation phenology in this

dry region is driven by more moisture than radiation. This has been pointed to in section 3.2.2 with respect to the anti-phase relationship seen in the region between slope and radiation. The effect of convective storms (on the time of precipitation) would also be lesser here than in the evergreen forest. The non-forest regions, in general, have greater phase differences with radiation.

3.4 DROUGHT EFFECT

During the study period (2007-16), two major droughts occurred in Amazonia: in the years 2010 and 2015. The following section looks to see whether the droughts are visible in the ASCAT parameters, which would provide a potential new method for drought monitoring in the Amazon region. The backscatter at 60° incidence angle, calculated using the methodology described in section 2.3.4, was chosen for the study. This choice was made since the effect of vegetation is more at bigger incidence angles, making it ideal for monitoring vegetation during droughts.

In addition, the extrapolated curve also contains information about slope and curvature, making it a more comprehensive parameter to study compared to the individual dynamic parameters. The analysis of slope and curvature anomalies did not yield consistent meaningful patterns. The plots have been included in Appendix B.

3.4.1 Amazon drought 2010

The 2010 drought was most severe over southern and western Amazonia. The peak drought months were July-September. Figure 3.32 shows the mean backscatter anomaly for the year in the study area. The spatial distribution of the negative anomalies is comparable to that of the negative precipitation anomalies observed over the peak drought interval by Panisset et al. [2018] (Figure 3.33), which hints that the backscatter indeed shows a drought effect. This is in accordance with the findings by Frolking et al. [2011] of similar negative anomalies in backscatter during the Amazon drought of 2005. The slope and curvature anomalies have been included in Appendix B.1.1.

The findings are further strengthened by the time series analysis in Figure 3.34 of mean backscatter and precipitation anomalies over the year for the drought-affected regions of interest. A significant backscatter anomaly compared to the standard deviation is observed in all regions, the strongest anomaly being during the peak drought interval (marked between dotted blue lines in the plots). The Cerrado (Figure 3.34d) shows weaker mean anomalies since the region of interest also includes parts of the savanna that were not affected by the drought. The time series of slope and curvature during the drought have been included in Appendix B.1.

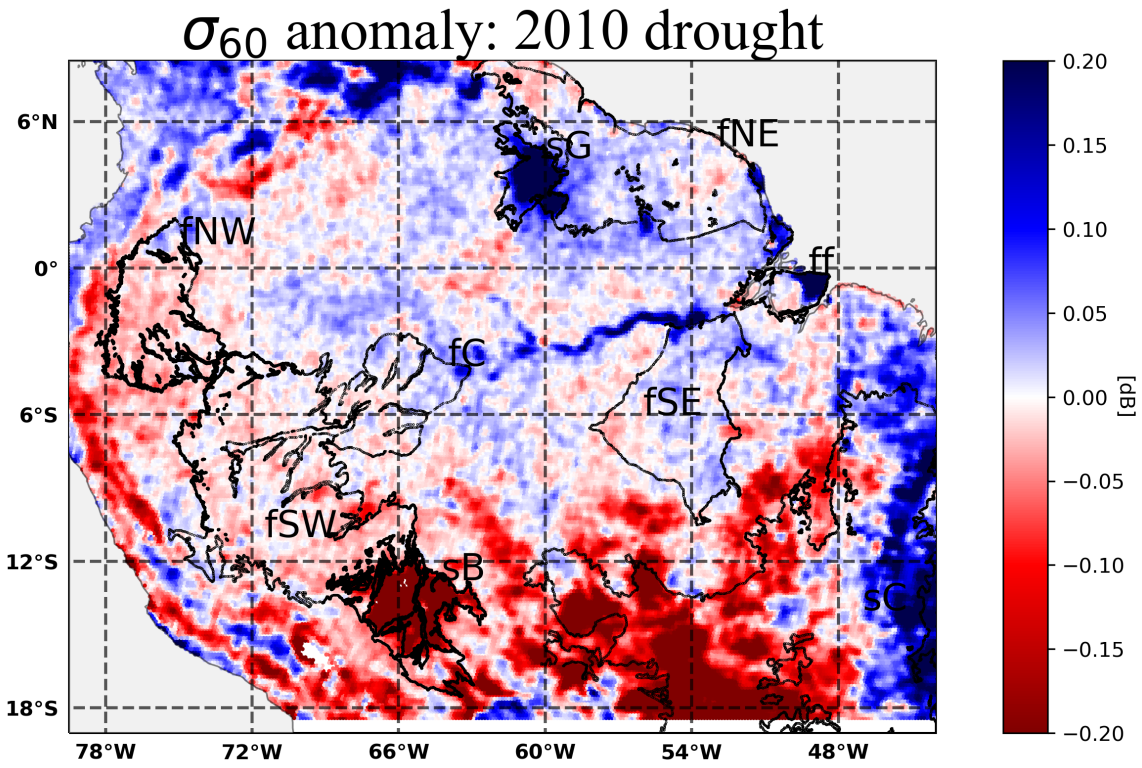

Figure 3.32: Mean backscatter anomaly for the year 2010 in the study area. The regions of interest are marked in black outline.

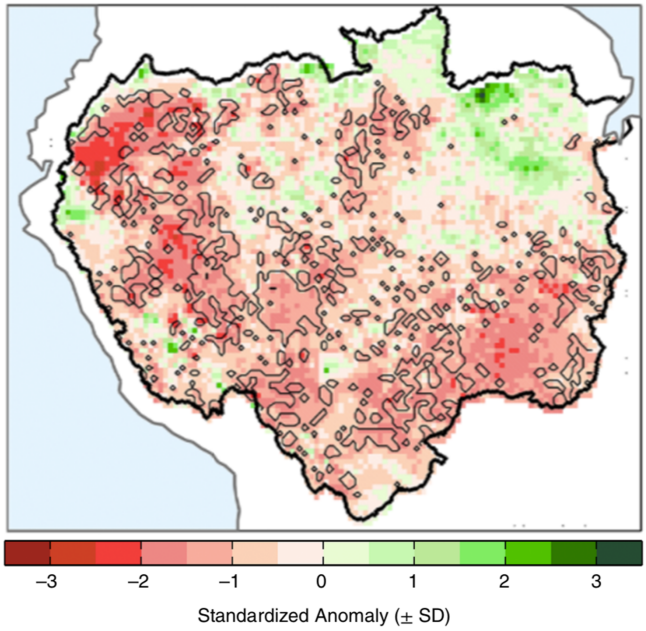

Figure 3.33: Mean precipitation anomaly during 2010 for the study area (Source: Panisset et al. [2018]).

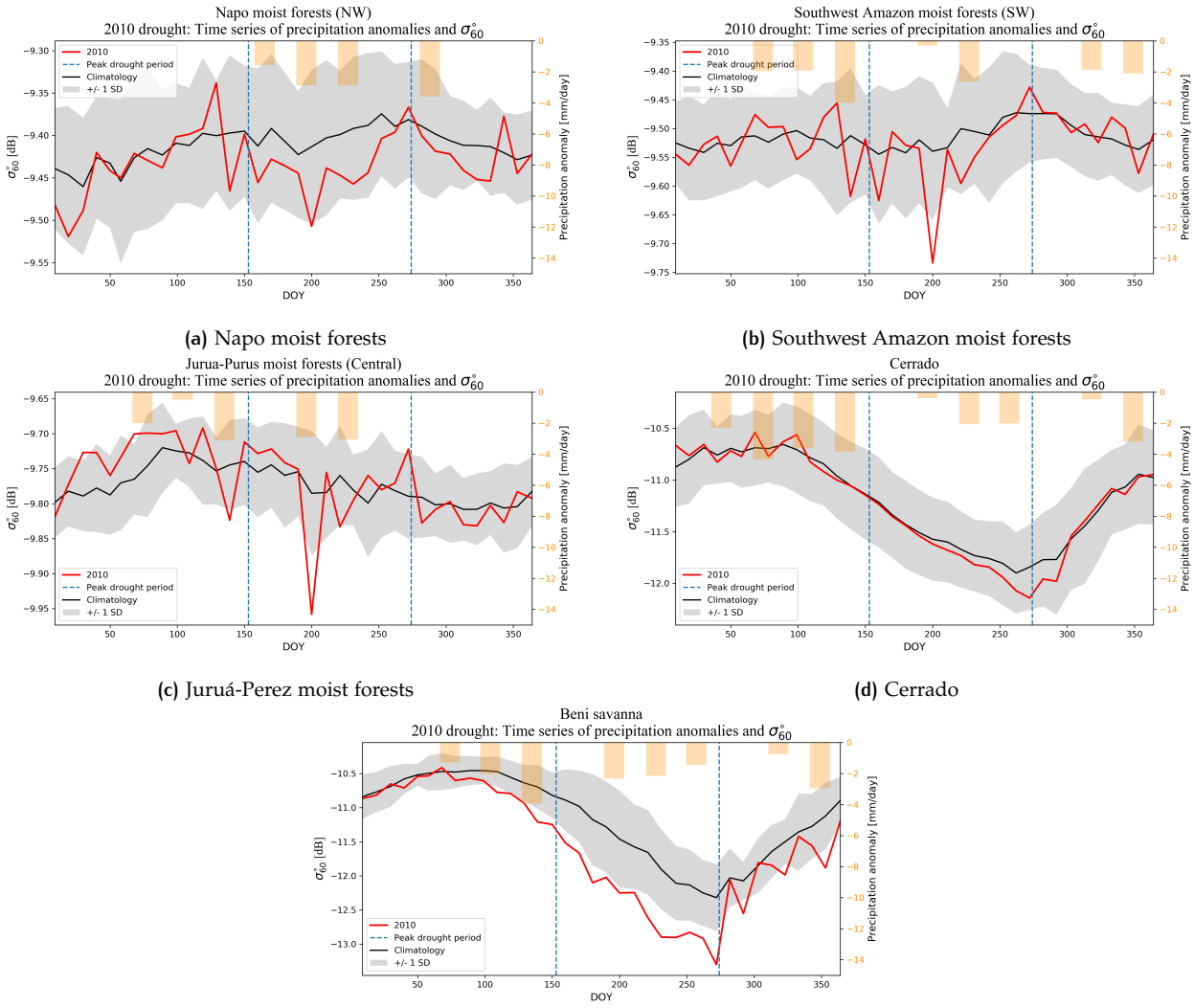

(a) Napo moist forests

(b) Southwest Amazon moist forests

(c) Juruá-Perez moist forests

(d) Cerrado

(e) Beni savanna

Figure 3.34: Time series of mean backscatter and negative precipitation anomalies for the year 2010 compared with the backscatter climatologies, for drought-affected regions of interest. The peak drought interval (June-September) is shown within dotted blue lines.

3.4.2 Amazon drought 2015

The 2015 drought was more widespread than the previous event in 2010. The drought peak started in October, and extended into January 2016. The worst affected region was eastern Amazonia. Figure 3.35 shows the mean backscatter anomaly for the year in the study area. As with the 2010 drought, the spatial distribution of the negative anomalies is comparable to that of the negative precipitation anomalies observed over the peak drought interval by Panisset et al. [2018] (Figure 3.36). The slope and curvature anomalies have been included in Appendix B.2.1.

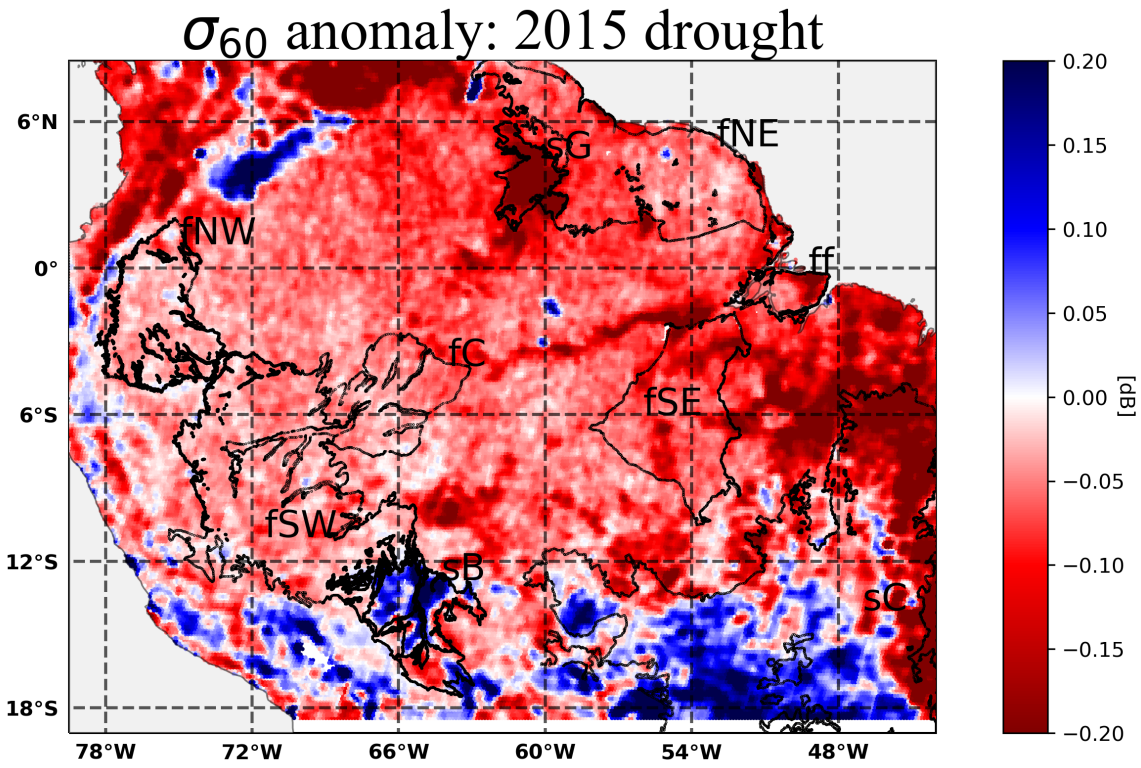

Figure 3.35: Mean backscatter anomaly for the year 2015 in the study area. The regions of interest are marked in black outline.

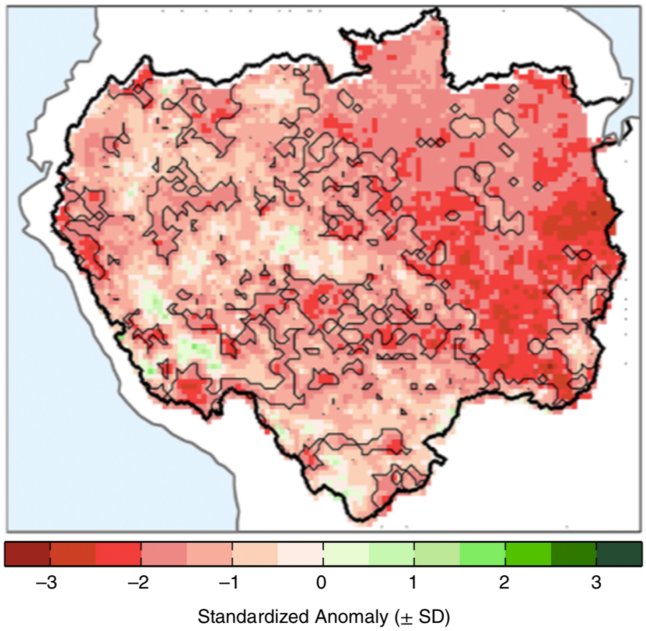

Figure 3.36: Mean precipitation anomaly during 2015 for the study area (Source: Panisset et al. [2018]).

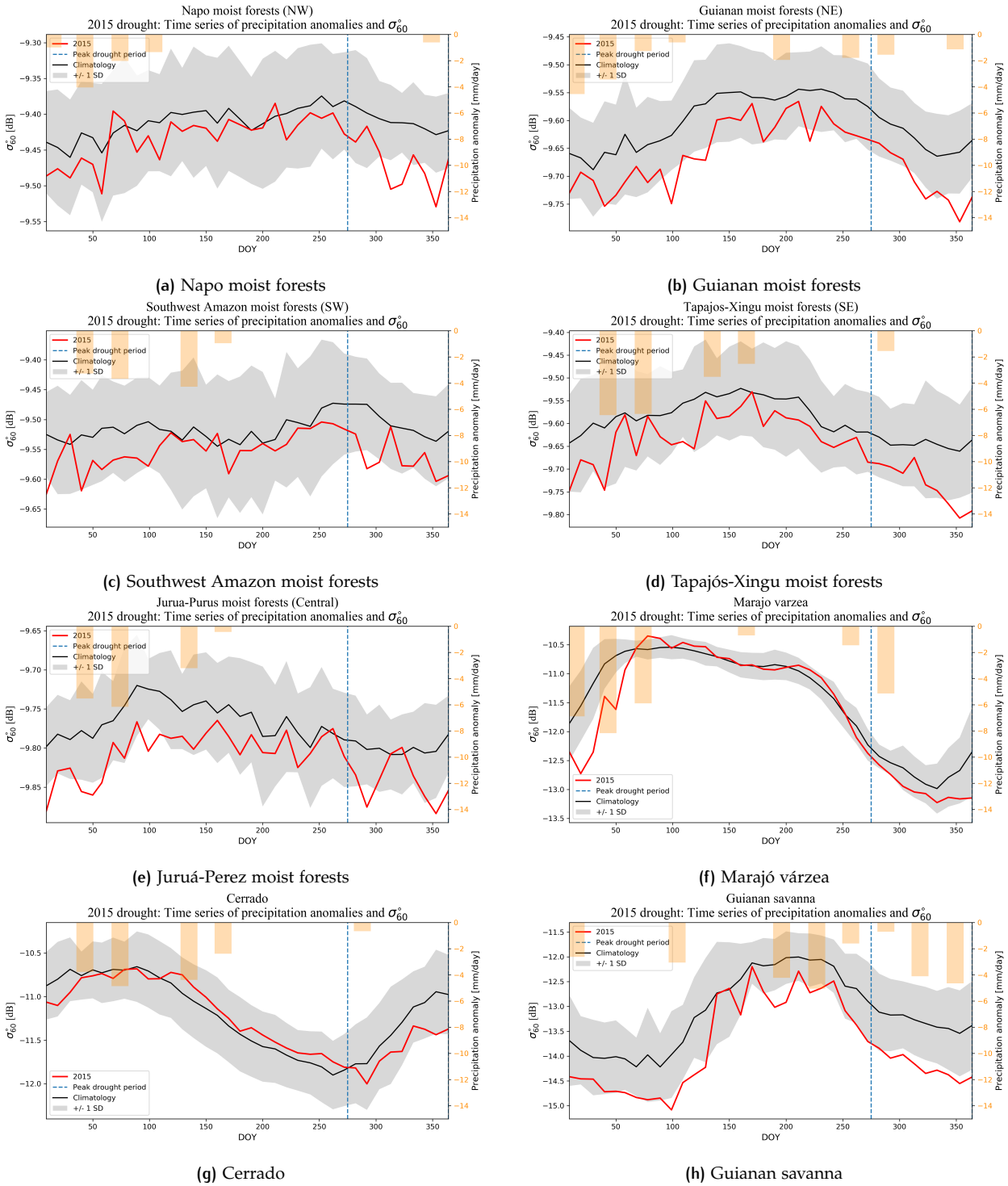

(a) Napo moist forests

(b) Guianan moist forests

(c) Southwest Amazon moist forests

(d) Tapajós-Xingu moist forests

(e) Juruá-Perez moist forests

(f) Marajó várzea

(g) Cerrado

(h) Guianan savanna

Figure 3.37: Time series of backscatter and negative precipitation anomalies for the year 2015 compared with the backscatter climatologies, for drought-affected regions of interest. The peak drought interval (October-December) is shown within dotted blue lines.

Figure 3.37 shows the time series of mean backscatter and precipitation anomalies over the year for the drought-affected regions of interest. Like the 2010 drought, significant backscatter anomaly compared to

the standard deviation is observed in all regions, strongest in the peak drought interval. This drought too, then, had an effect on the ASCAT backscatter. The Cerrado (Figure 3.37g), as before, shows weaker mean anomalies since the region also includes parts that were not affected by the drought.The time series of slope and curvature during the drought have been included in Appendix B.2.

Unlike the 2010 drought, significant anomalies are observed here in many regions throughout the year. The 2015 drought was considered a "record-breaking" event with stronger warming than that seen in previous events [Jiménez-Muñoz et al., 2016]. According to Panisset et al. [2018], there was a "pronounced lack of rainfall availability during late spring and early summer" (visible in the negative precipitation anomalies in Figure 3.37), which could explain this observation.

4 CONCLUSIONS AND RECOMMENDATIONS

4.1 CONCLUSIONS

This study aimed to improve the understanding of the ASCAT backscatter and dynamic vegetation parameters, and assess their suitability for monitoring vegetation water dynamics in the Amazon forest regions. This region was, in the past, considered a suitable calibration target. The findings from this research show significant spatial and temporal variations in the ASCAT parameters. These patterns show promise for monitoring of vegetation moisture demand and availability, and of episodic events such as droughts.

The spatial differences in the backscatter, slope, and curvature match the major land cover types in the Amazon region. The evergreen forests show high mean backscatter and low curvature, with very small amplitudes of seasonal variations. The savannas show much stronger seasonalities, with variations among themselves. The wetlands show especially high ranges, especially in curvature. While Wagner et al. [1999] found that the ERS scatterometer can be used for differentiating between regions of major vegetation types, the present study extends this conclusion to the ASCAT parameters.

The wetland regions with seasonal flooding show a spike in slope during the flooding periods. This results from a drop in the backscatter values at steep (around 20°) incidence angles, while at bigger angles, there is a compensating increase due to possible multiple reflections between the flood-water surface and the vegetation. This change in the backscatter-incidence angles dependence could be used for detecting flooding in such forests.

Consistent diurnal differences were observed between he morning and evening values of backscatter throughout the study area. In most regions, the evening values were higher in the wet season due to the canopy being wet in the aftermath of afternoon and evening precipitation. In the dry season, the morning values of backscatter were higher because of reduced vegetation water after loss through transpiration. These results indicate that the difference between the two overpasses could be used as a measure of water stress, especially in the dry season, although the observed diurnal differences can be sensitive to satellite overpass times.

Water stress in vegetation was also observed in the form of negative anomalies in backscatter during the Amazon droughts of 2010 and 2015. The spatial distribution of these anomalies matched that of precipitation deficit in the drought years. The time series of backscatter during the drought years showed strongest anomalies in the peak drought months. There is clear evidence, hence, that drought-affected regions show reduced ASCAT backscatter, which could be used for monitoring Amazon forest droughts.

For a better understanding of what drives the ASCAT backscatter and dynamic vegetation parameters, the seasonality of the parameters were matched to that of climatic variables. While backscatter was found to follow moisture availability in all the cover types, the slope and curvature were influenced by phenological activity and changes, in turn driven by variables of evaporative demand (mainly radiation and humidity). In the largely radiation-limited Amazonia region, the phenology is synced with the radiation cycle [Wagner et al., 2016]. The slope and curvature, consequently, show high correlation with the radiation and humidity

cycles. The ASCAT backscatter and dynamic vegetation parameters, thus, show relation to canopy water dynamics in a range of land cover types in the Amazon forest region.

These findings show a marked improvement over the state-of-the-art understanding of slope as "vegetation density" and curvature to be related to vegetation properties. This is especially significant since the findings are in the Amazon forest region where the parameters were once thought to be static. The ASCAT backscatter and dynamic vegetation parameters have been shown to contain patterns and variations driven by land cover types and climatic parameters. This has enhanced the value of the ASCAT instruments and dataset through demonstrated potential for monitoring of canopy water dynamics and and the health of the forest in the face of calamities like droughts.

4.2 FUTURE RESEARCH

The study found significant spatial and temporal patterns in the ASCAT backscatter and dynamic vegetation parameters over Amazonia, and related it to vegetation type, and to variables of canopy moisture demand and availability. This shows potential ASCAT data to be used for monitoring applications in the Amazon forest.

ASCAT parameters have been shown to be successful in differentiating between the major land cover types in Amazonia. While the focus of this research was mainly on nine regions of interest, the next step would be to extend the study to other regions and cover types in the forest. The Caatinga, a xeric shrubland close to the Amazonia could provide further insights into the contrast between forests and other regions. The effect of soil volume scattering in the Cerrado, could also occur in this desert-like landscape. The Cerrado itself is an important ecosystem with diverse vegetation covers. It would be worthwhile to zoom into the variations in backscatter and vegetation parameters juxtaposed with the distinct vegetation covers in the region. Such an expansive study would beget a deeper understanding of the distinction between the cover types, and perhaps yield quantitative estimates for classification.

The disparities between forests and savannas could be useful for applications in detecting and monitoring deforestation in the Amazon, and potentially other rainforests across the world. The Amazon has also seen major windthrow events during storms, such as one in January 2005 that lead to an estimated tree mortality upwards of 500 million [Negrón-Juárez et al., 2010]. These episodic events could possibly be visible as an anomaly or a trend in the parameters. With the likelihood of future intensification of these events due to climate change and escalating deforestation, these findings could be crucial.

A prospect for water stress detection was seen in two parts of the study: diurnal differences in backscatter, and as negative anomalies in backscatter during droughts. More research is needed for attributing these backscatter differences to actual levels of water stress. The study also found an initial indication into the possibility of forest flood detection. Further studies could take a concentrated look on the distinction between flooded and non-flooded times at seasonally flooded sites. Major floods in the Beni Savanna, such as those in the years 2007, 2008, and 2014 [Ovando et al., 2016] could be a possible focus of research.

The major highlight of the study was the relation of the ASCAT backscatter and dynamic vegetation parameters to the canopy dynamics of moisture demand and availability. While backscatter has been shown to follow the cycle of EWT (and TWS), a more quantitative analysis for backscatter to be used as a measure of canopy water availability. This study found that slope follows the seasonality in evapotranspiration, and curvature is influenced by leaf flushing events. Fieldwork in Amazonia could verify these hypotheses through observations, and provide basis for monitoring applications in the future: slope for transpiration levels, and curvature for detection of structural changes in the vegetation. This would pave the way for ASCAT backscat-

ter and vegetation parameters to be used for monitoring canopy water dynamics in the Amazon forest region.

...

BIBLIOGRAPHY

Aragao, L. E., Poulter, B., Barlow, J. B., Anderson, L. O., Malhi, Y., Saatchi, S., Phillips, O. L., and Gloor, E. (2014). Environmental change and the carbon balance of Amazonian forests. *Biological Reviews*, 89(4):913–931.

Asner, G. P. (2001). Cloud cover in Landsat observations of the Brazilian Amazon. *International Journal of Remote Sensing*, 22(18):3855–3862.

Bagley, J. E., Desai, A. R., Harding, K. J., Snyder, P. K., and Foley, J. A. (2014). Drought and deforestation: Has land cover change influenced recent precipitation extremes in the Amazon? *Journal of Climate*, 27(1):345–361.

Birrer, I., Bracalente, E., Dome, G., Sweet, J., and Berthold, G. (1982). σ signature of the Amazon rain forest obtained from the SeaSat scatterometer. *IEEE Transactions on geoscience and remote sensing*, (1):11–17.

Borchert, R., Calle, Z., Strahler, A. H., Baertschi, A., Magill, R. E., Broadhead, J. S., Kamau, J., Njoroge, J., and Muthuri, C. (2015). Insolation and photoperiodic control of tree development near the equator. *New Phytologist*, 205(1):7–13.

Bradley, A. V., Gerard, F. F., Barbier, N., Weedon, G. P., Anderson, L. O., Huntingford, C., Aragão, L. E., Zelazowski, P., and Arai, E. (2011). Relationships between phenology, radiation and precipitation in the Amazon region. *Global Change Biology*, 17(6):2245–2260.

Brienen, R. J., Phillips, O. L., Feldpausch, T. R., Gloor, E., Baker, T. R., Lloyd, J., Lopez-Gonzalez, G., Monteagudo-Mendoza, A., Malhi, Y., Lewis, S. L., et al. (2015). Long-term decline of the Amazon carbon sink. *Nature*, 519(7543):344.

Buainain, A. M., Lanna, R., and Navarro, Z. (2019). *Agricultural Development in Brazil: The Rise of a Global Agro-food Power*. Routledge.

Camarão, A., Júnior, L., Dutra, S., et al. (2002). Flooded pasture production for grazing buffalo in the brazilian Amazon region. In *Embrapa Amazônia Oriental-Artigo em anais de congresso (ALICE)*. In: Buffalo Symposium Of Americas, 1., 2002, Belém. Proceedings of the ....

Doughty, C. E., Metcalfe, D., Girardin, C., Amézquita, F. F., Cabrera, D. G., Huasco, W. H., Silva-Espejo, J., Araujo-Murakami, A., Da Costa, M., Rocha, W., et al. (2015). Drought impact on forest carbon dynamics and fluxes in Amazonia. *Nature*, 519(7541):78.

Eiten, G. (1972). The cerrado vegetation of Brazil. *The Botanical Review*, 38(2):201–341.

Friesen, J., Steele-Dunne, S. C., and van de Giesen, N. (2012). Diurnal differences in global ERS scatterometer backscatter observations of the land surface. *IEEE Transactions on Geoscience and Remote Sensing*, 50(7):2595–2602.

Frison, P.-L., Jarlan, L., and Mougin, E. (2016). Using Satellite Scatterometers to Monitor Continental Surfaces. In *Land Surface Remote Sensing in Continental Hydrology*, pages 79–113. Elsevier.

Frolking, S., Hagen, S., Braswell, B., Milliman, T., Herrick, C., Peterson, S., Roberts, D., Keller, M., and Palace, M. (2017). Evaluating multiple causes of persistent low microwave backscatter from Amazon forests after the 2005 drought. *PloS one*, 12(9):e0183308.

Frolking, S., Milliman, T., Palace, M., Wisser, D., Lammers, R., and Fahnestock, M. (2011). Tropical forest backscatter anomaly evident in SeaWinds scatterometer morning overpass data during 2005 drought in Amazonia. *Remote Sensing of Environment*, 115(3):897–907.

Hahn, S., Reimer, C., Vreugdenhil, M., Melzer, T., and Wagner, W. (2017). Dynamic characterization of the incidence angle dependence of backscatter using metop ASCAT. *IEEE Journal of Selected Topics in Applied Earth Observations and Remote Sensing*, 10(5):2348–2359.

Hamilton, S. K., Sippel, S. J., and Melack, J. M. (2004). Seasonal inundation patterns in two large savanna floodplains of South America: the Llanos de Moxos (Bolivia) and the Llanos del Orinoco (Venezuela and Colombia). *Hydrological Processes*, 18(11):2103–2116.

Hess, L. L., Melack, J. M., and Simonett, D. S. (1990). Radar detection of flooding beneath the forest canopy: a review. *International Journal of Remote Sensing*, 11(7):1313–1325.

Hordijk, I., Meijer, F., Nissen, E., Boorsma, T., and Poorter, L. (2019). Cattle affect regeneration of the palm species Attalea princeps in a Bolivian forest–savanna mosaic. *Biotropica*, 51(1):28–38.

Jiménez-Muñoz, J. C., Mattar, C., Barichivich, J., Santamaría-Artigas, A., Takahashi, K., Malhi, Y., Sobrino, J. A., and Van Der Schrier, G. (2016). Record-breaking warming and extreme drought in the Amazon rainforest during the course of El Niño 2015–2016. *Scientific reports*, 6:33130.

Landerer, F. W. and Swenson, S. (2012). Accuracy of scaled GRACE terrestrial water storage estimates. *Water resources research*, 48(4).

Liu, Y. Y., van Dijk, A. I., Miralles, D. G., McCabe, M. F., Evans, J. P., de Jeu, R. A., Gentine, P., Huete, A., Parinussa, R. M., Wang, L., et al. (2018). Enhanced canopy growth precedes senescence in 2005 and 2010 Amazonian droughts. *Remote sensing of environment*, 211:26–37.

Maeda, E. E., Ma, X., Wagner, F. H., Kim, H., Oki, T., Eamus, D., Huete, A., et al. (2017). Evapotranspiration seasonality across the Amazon Basin. *Earth System Dynamics*.

Marengo, J. A., Tomasella, J., Alves, L. M., Soares, W. R., and Rodriguez, D. A. (2011). The drought of 2010 in the context of historical droughts in the Amazon region. *Geophysical Research Letters*, 38(12).

Morton, D., Le Page, Y., DeFries, R., Collatz, G., and Hurtt, G. (2013). Understorey fire frequency and the fate of burned forests in southern Amazonia. *Philosophical Transactions of the Royal Society B: Biological Sciences*, 368(1619):20120163.

Negrón-Juárez, R. I., Chambers, J. Q., Guimaraes, G., Zeng, H., Raupp, C. F., Marra, D. M., Ribeiro, G. H., Saatchi, S. S., Nelson, B. W., and Higuchi, N. (2010). Widespread Amazon forest tree mortality from a single cross-basin squall line event. *Geophysical Research Letters*, 37(16).

Oliveira, R., Bezerra, L., Davidson, E., Pinto, F., Klink, C., Nepstad, D., and Moreira, A. (2005). Deep root function in soil water dynamics in cerrado savannas of central Brazil. *Functional Ecology*, 19(4):574–581.

Olson, D. M., Dinerstein, E., Wikramanayake, E. D., Burgess, N. D., Powell, G. V., Underwood, E. C., D'amico, J. A., Itoua, I., Strand, H. E., Morrison, J. C., et al. (2001). Terrestrial Ecoregions of the World: A New Map of Life on EarthA new global map of terrestrial ecoregions provides an innovative tool for conserving biodiversity. *BioScience*, 51(11):933–938.

Ovando, A., Tomasella, J., Rodriguez, D., Martinez, J., Siqueira-Junior, J., Pinto, G., Passy, P., Vauchel, P., Noriega, L., and Von Randow, C. (2016). Extreme flood events in the Bolivian Amazon wetlands. *Journal of Hydrology: Regional Studies*, 5:293–308.

Panisset, J. S., Libonati, R., Gouveia, C. M. P., Machado-Silva, F., França, D. A., França, J. R. A., and Peres, L. F. (2018). Contrasting patterns of the extreme drought episodes of 2005, 2010 and 2015 in the Amazon Basin. *International Journal of Climatology*, 38(2):1096–1104.

Peel, M. C., Finlayson, B. L., and McMahon, T. A. (2007). Updated world map of the Köppen-Geiger climate classification. *Hydrology and earth system sciences discussions*, 4(2):439–473.

Romatschke, U. and Houze Jr, R. A. (2013). Characteristics of precipitating convective systems accounting for the summer rainfall of tropical and subtropical South America. *Journal of Hydrometeorology*, 14(1):25–46.

Saatchi, S., Asefi-Najafabady, S., Malhi, Y., Aragão, L. E., Anderson, L. O., Myneni, R. B., and Nemani, R. (2013). Persistent effects of a severe drought on Amazonian forest canopy. *Proceedings of the National Academy of Sciences*, 110(2):565–570.

Scipal, K. (2002). *Global soil moisture retrieval from ERS scatterometer data*. na.

Sheffield, J., Goteti, G., and Wood, E. F. (2006). Development of a 50-year high-resolution global dataset of meteorological forcings for land surface modeling. *Journal of climate*, 19(13):3088–3111.

Soares, B. S., Nepstad, D. C., Curran, L. M., Cerqueira, G. C., Garcia, R. A., Ramos, C. A., Voll, E., McDonald, A., Lefebvre, P., and Schlesinger, P. (2006). Modelling conservation in the Amazon basin. *Nature*, 440(7083):520–523.

Steele-Dunne, S. C., Friesen, J., and van de Giesen, N. (2012). Using diurnal variation in backscatter to detect vegetation water stress. *IEEE Transactions on Geoscience and Remote Sensing*, 50(7):2618–2629.

Steele-Dunne, S. C., Hahn, S., Wagner, W., and Vreugdenhil, M. (2019). Investigating vegetation water dynamics and drought using Metop ASCAT over the North American Grasslands. *Remote Sensing of Environment*, 224:219–235.

Stoffelen, A., Aaboe, S., Calvet, J.-C., Cotton, J., De Chiara, G., Saldana, J. F., Mouche, A. A., Portabella, M., Scipal, K., and Wagner, W. (2017). Scientific developments and the EPS-SG scatterometer. *IEEE Journal of Selected Topics in Applied Earth Observations and Remote Sensing*, 10(5):2086–2097.

Swenson, S. and Wahr, J. (2006). Post-processing removal of correlated errors in GRACE data. *Geophysical research letters*, 33(8).

van Emmerik, T., Steele-Dunne, S., Paget, A., Oliveira, R. S., Bittencourt, P. R., Barros, F. d. V., and van de Giesen, N. (2017). Water stress detection in the Amazon using radar. *Geophysical Research Letters*, 44(13):6841–6849.

Vreugdenhil, M., Dorigo, W. A., Wagner, W., De Jeu, R. A., Hahn, S., and Van Marle, M. J. (2016). Analyzing the vegetation parameterization in the TU-Wien ASCAT soil moisture retrieval. *IEEE Transactions on Geoscience and Remote Sensing*, 54(6):3513–3531.

Wagner, F. H., Hérault, B., Bonal, D., Stahl, C., Anderson, L. O., Baker, T. R., Sebastian Becker, G., Beeckman, H., D Souza, B., Cesar Botosso, P., et al. (2016). Climate seasonality limits leaf carbon assimilation and wood productivity in tropical forests. *Biogeosciences*, 13(8):2537–2562.

Wagner, W., Lemoine, G., Borgeaud, M., and Rott, H. (1999). A study of vegetation cover effects on ERS scatterometer data. *IEEE Transactions on Geoscience and Remote Sensing*, 37(2):938–948.

Wahr, J., Molenaar, M., and Bryan, F. (1998). Time variability of the Earth's gravity field: Hydrological and oceanic effects and their possible detection using GRACE. *Journal of Geophysical Research: Solid Earth*, 103(B12):30205–30229.

Wang, Y., Hess, L. L., Filoso, S., and Melack, J. M. (1995). Understanding the radar backscattering from flooded and nonflooded Amazonian forests: Results from canopy backscatter modeling. *Remote Sensing of Environment*, 54(3):324–332.

Yang, J., Tian, H., Pan, S., Chen, G., Zhang, B., and Dangal, S. (2018a). Amazon drought and forest response: Largely reduced forest photosynthesis but slightly increased canopy greenness during the extreme drought of 2015/2016. *Global change biology*, 24(5):1919–1934.

Yang, Y., Saatchi, S. S., Xu, L., Yu, Y., Choi, S., Phillips, N., Kennedy, R., Keller, M., Knyazikhin, Y., and Myneni, R. B. (2018b). Post-drought decline of the Amazon carbon sink. *Nature communications*, 9(1):3172.

Zuleta, D., Duque, A., Cardenas, D., Muller-Landau, H. C., and Davies, S. J. (2017). Drought-induced mortality patterns and rapid biomass recovery in a terra firme forest in the Colombian Amazon. *Ecology*, 98(10):2538–2546.

Appendices

A DIURNAL DIFFERENCE PLOTS

A.1 SLOPE

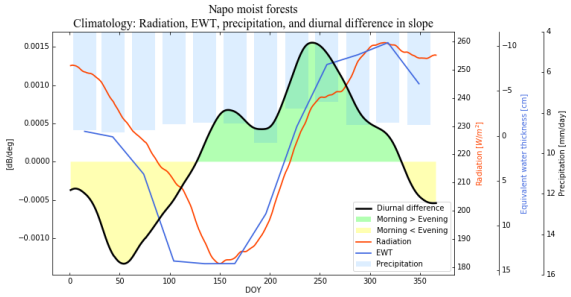

(a) Napo moist forests

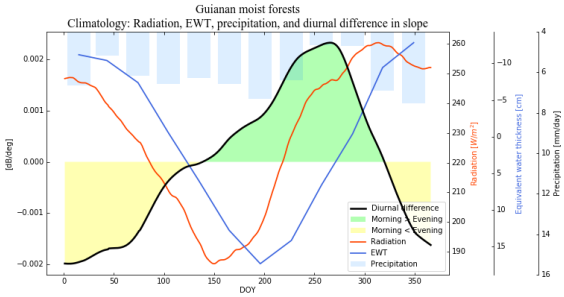

(b) Guianan moist forests

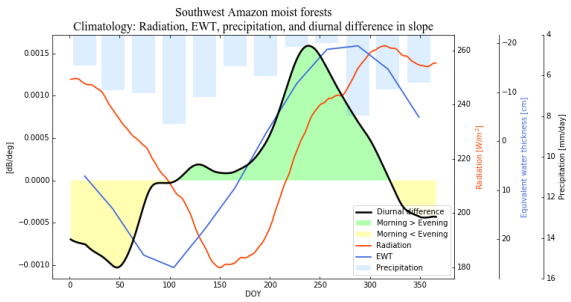

(c) Southwest Amazon moist forests

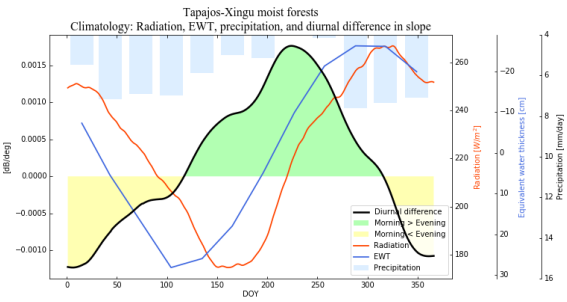

(d) Tapajós-Xingu moist forests

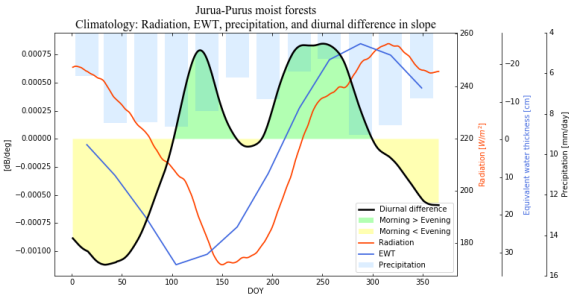

(e) Juruá-Perez moist forests

Figure A.1: Climatology of diurnal difference in slope (black line), radiation (red line), EWT (blue line), and precipitation (bars) for evergreen forests. Green fill indicates days with positive diurnal difference, while yellow fill indicates negative values.

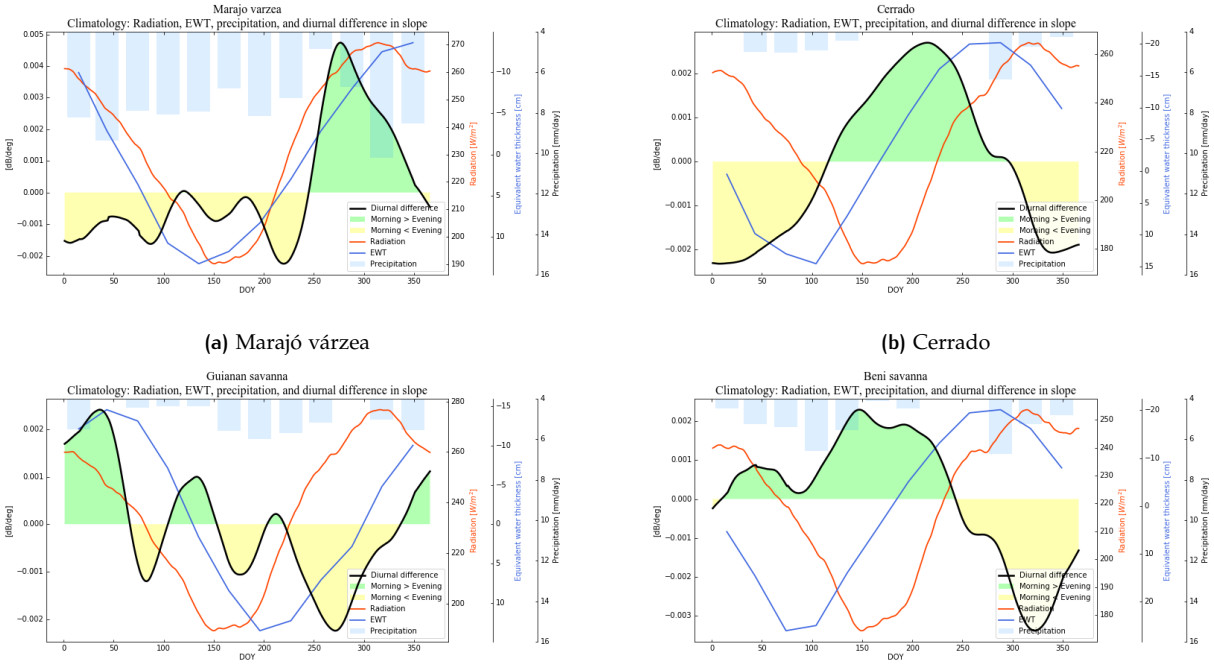

(a) Marajó várzea

(b) Cerrado

(c) Guianan savanna

(d) Beni savanna

Figure A.2: Climatology of diurnal difference in slope (black line), radiation (red line), EWT (blue line), and precipitation (bars) for savannas and seasonally flooded forest. Green fill indicates days with positive diurnal difference, while yellow fill indicates negative values.

A.2 CURVATURE

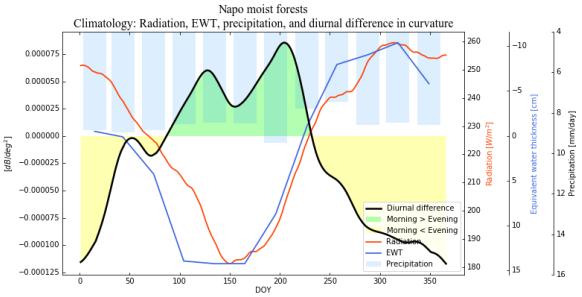

(a) Napo moist forests

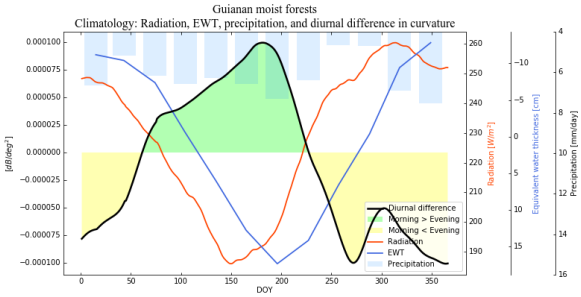

(b) Guianan moist forests

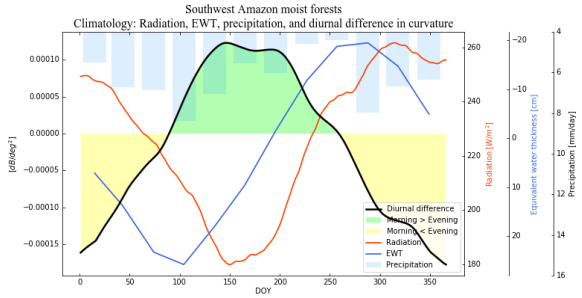

(c) Southwest Amazon moist forests

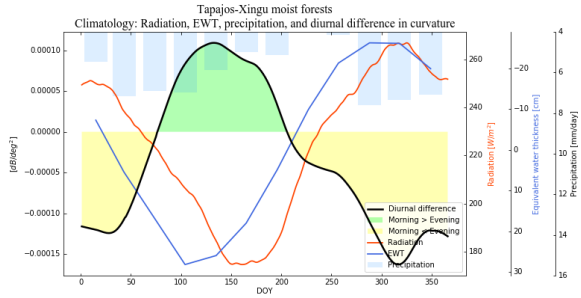

(d) Tapajós-Xingu moist forests

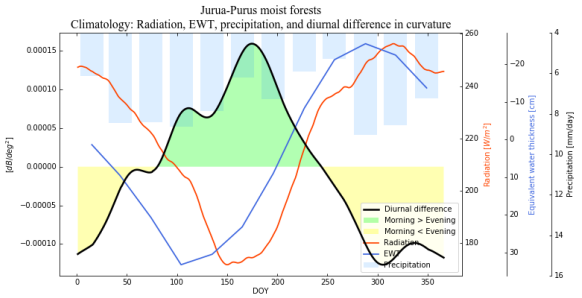

(e) Juruá-Perez moist forests

Figure A.3: Climatology of diurnal difference in curvature (black line), radiation (red line), EWT (blue line), and precipitation (bars) for evergreen forests. Green fill indicates days with positive diurnal difference, while yellow fill indicates negative values.

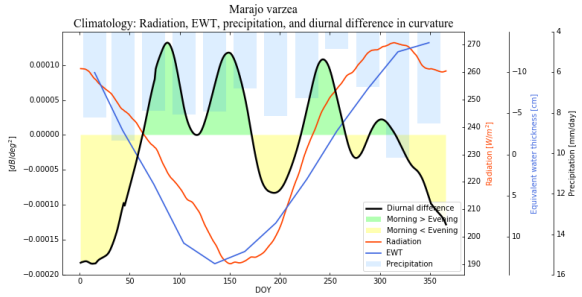

(a) Marajó várzea

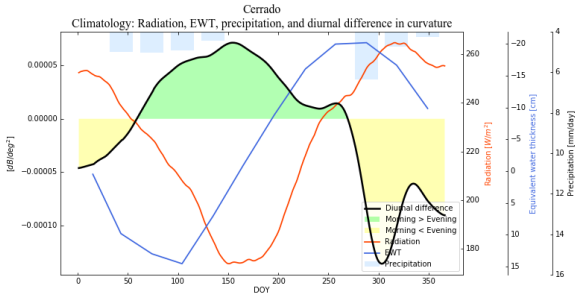

(b) Cerrado

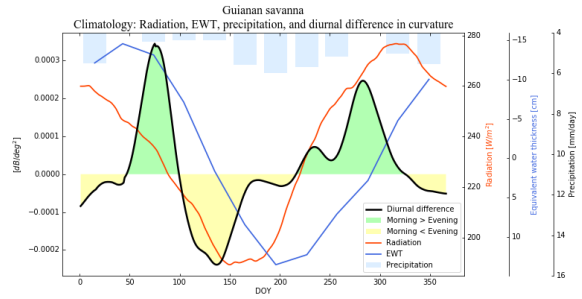

(c) Guianan savanna

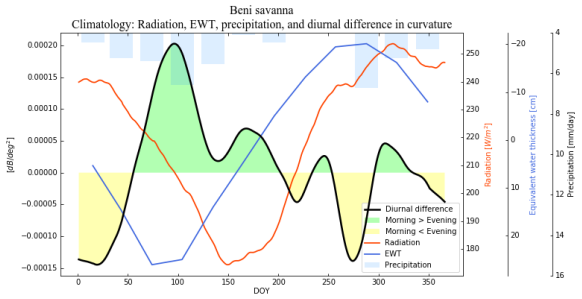

(d) Beni savanna

Figure A.4: Climatology of diurnal difference in curvature (black line), radiation (red line), EWT (blue line), and precipitation (bars) for savannas and seasonally flooded forest. Green fill indicates days with positive diurnal difference, while yellow fill indicates negative values.

B DROUGHT PLOTS

B.1 AMAZON DROUGHT 2010

B.1.1 Maps of anomalies

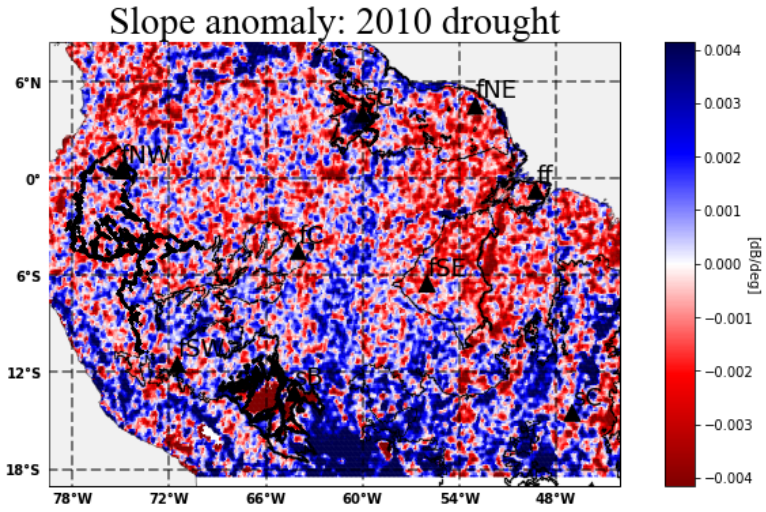

(a) Slope

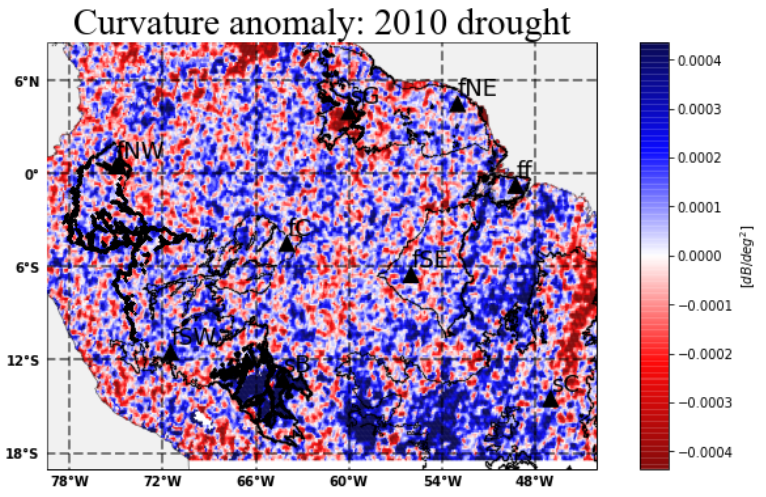

(b) Curvature

Figure B.1: Mean slope and curvature anomalies in the study area for the year 2010. The regions of interest are marked in black outline.

B.1.2 Slope time series

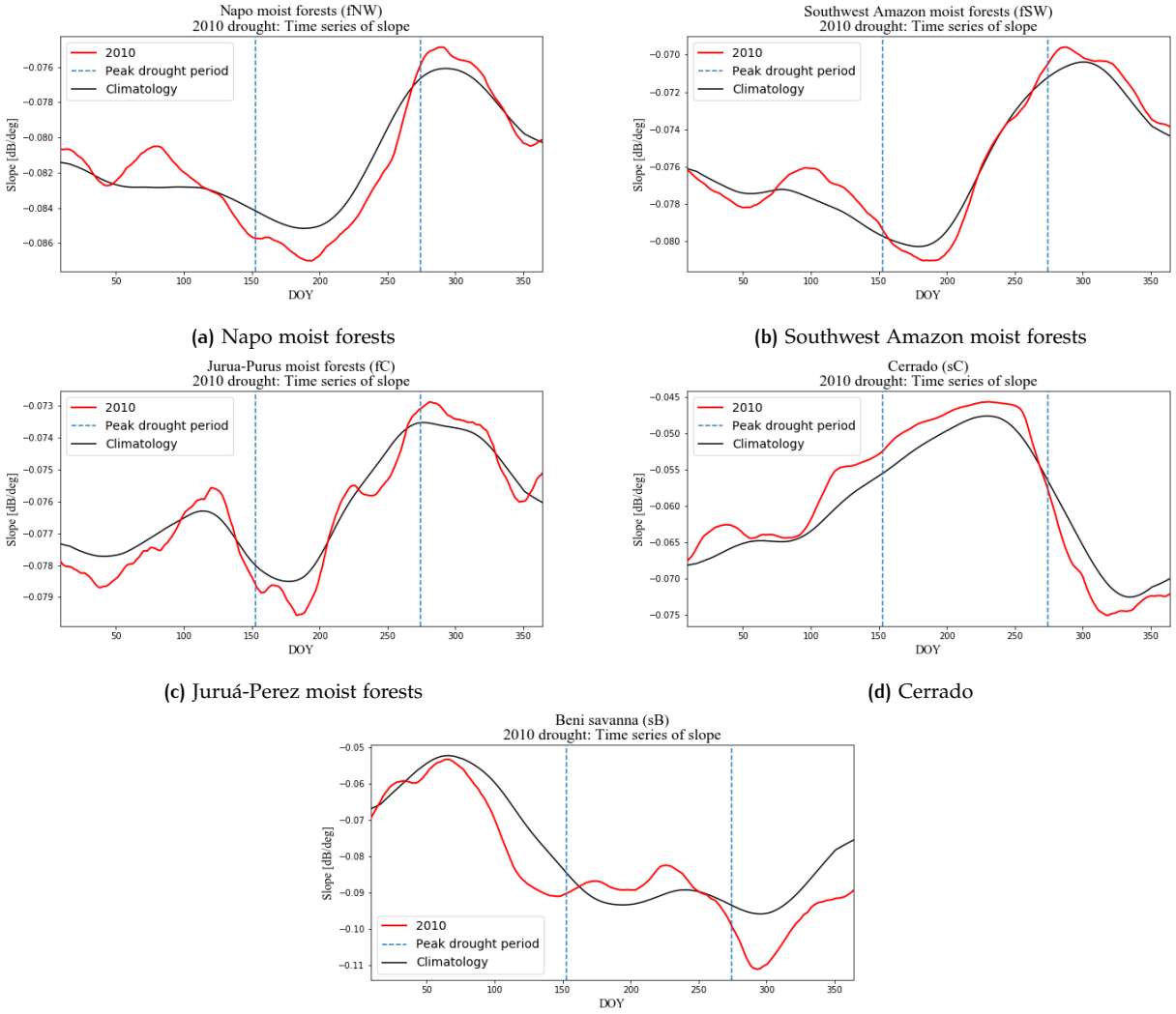

(a) Napo moist forests

(b) Southwest Amazon moist forests

(c) Juruá-Perez moist forests

(d) Cerrado

(e) Beni savanna

Figure B.2: Time series of mean slope for the year 2010 compared with the climatologies, for drought-affected regions of interest. The peak drought interval (June-September) is shown within dotted blue lines.

B.1.3 Curvature time series

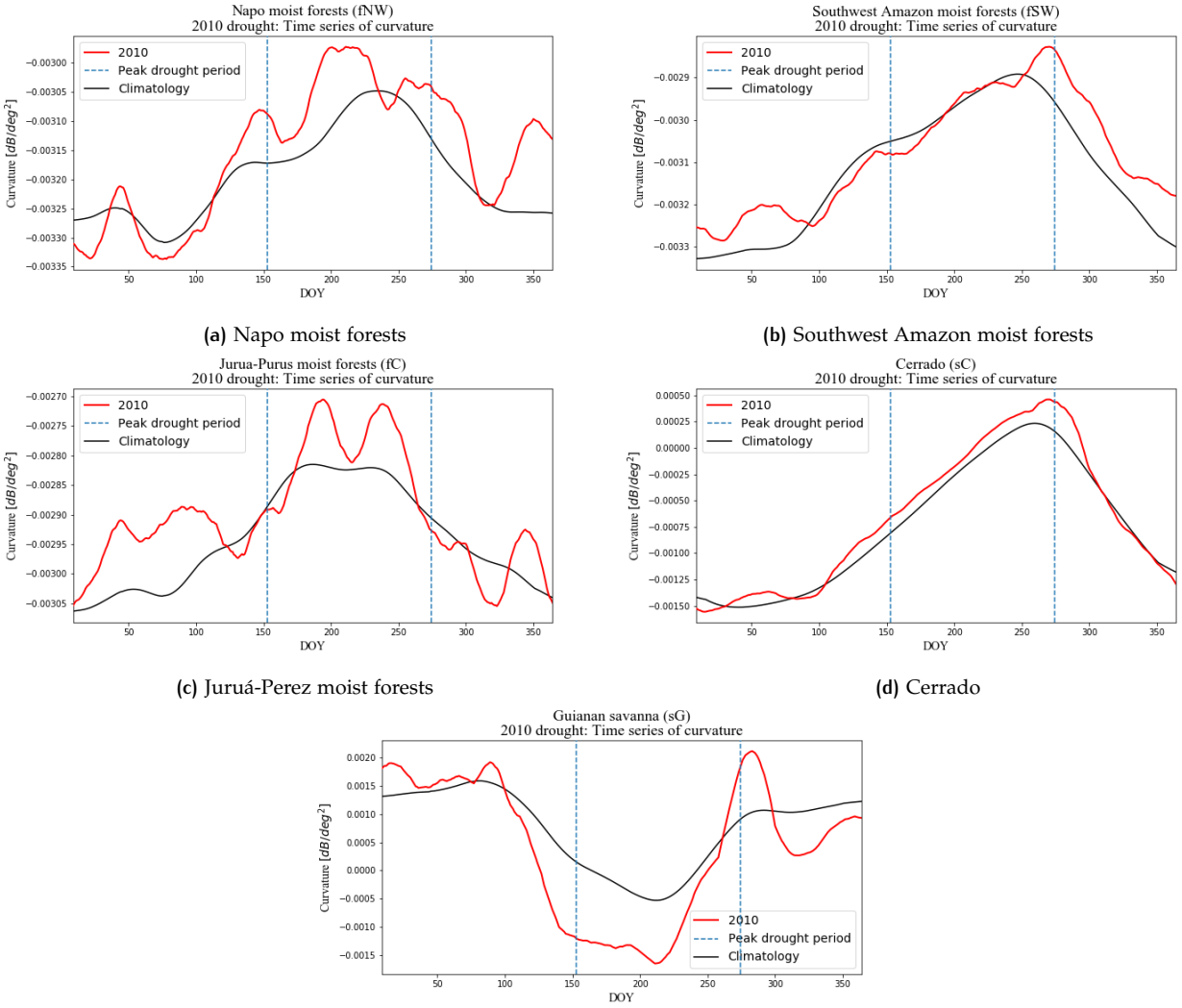

(a) Napo moist forests

(b) Southwest Amazon moist forests

(c) Juruá-Perez moist forests

(d) Cerrado

(e) Beni savanna

Figure B.3: Time series of mean curvature for the year 2010 compared with the climatologies, for drought-affected regions of interest. The peak drought interval (June-September) is shown within dotted blue lines.

B.2 AMAZON DROUGHT 2015

B.2.1 Maps of anomalies

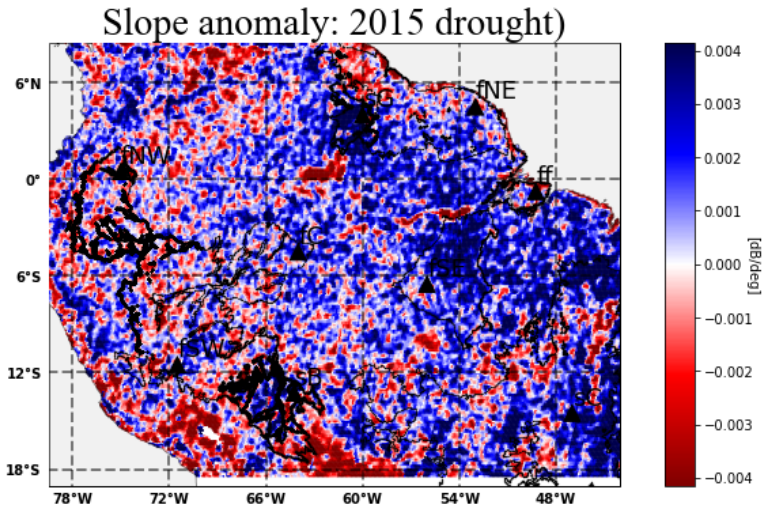

(a) Slope

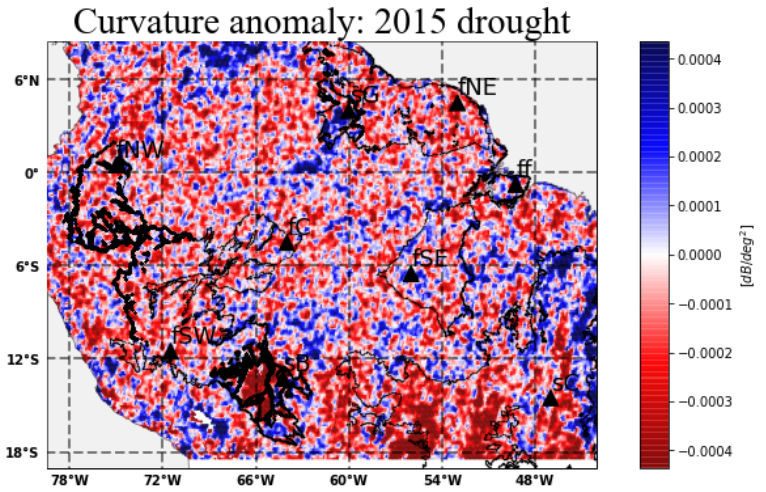

(b) Curvature

Figure B.4: Mean slope and curvature anomalies in the study area for the year 2015. The regions of interest are marked in black outline.

B.2.2 Slope time series

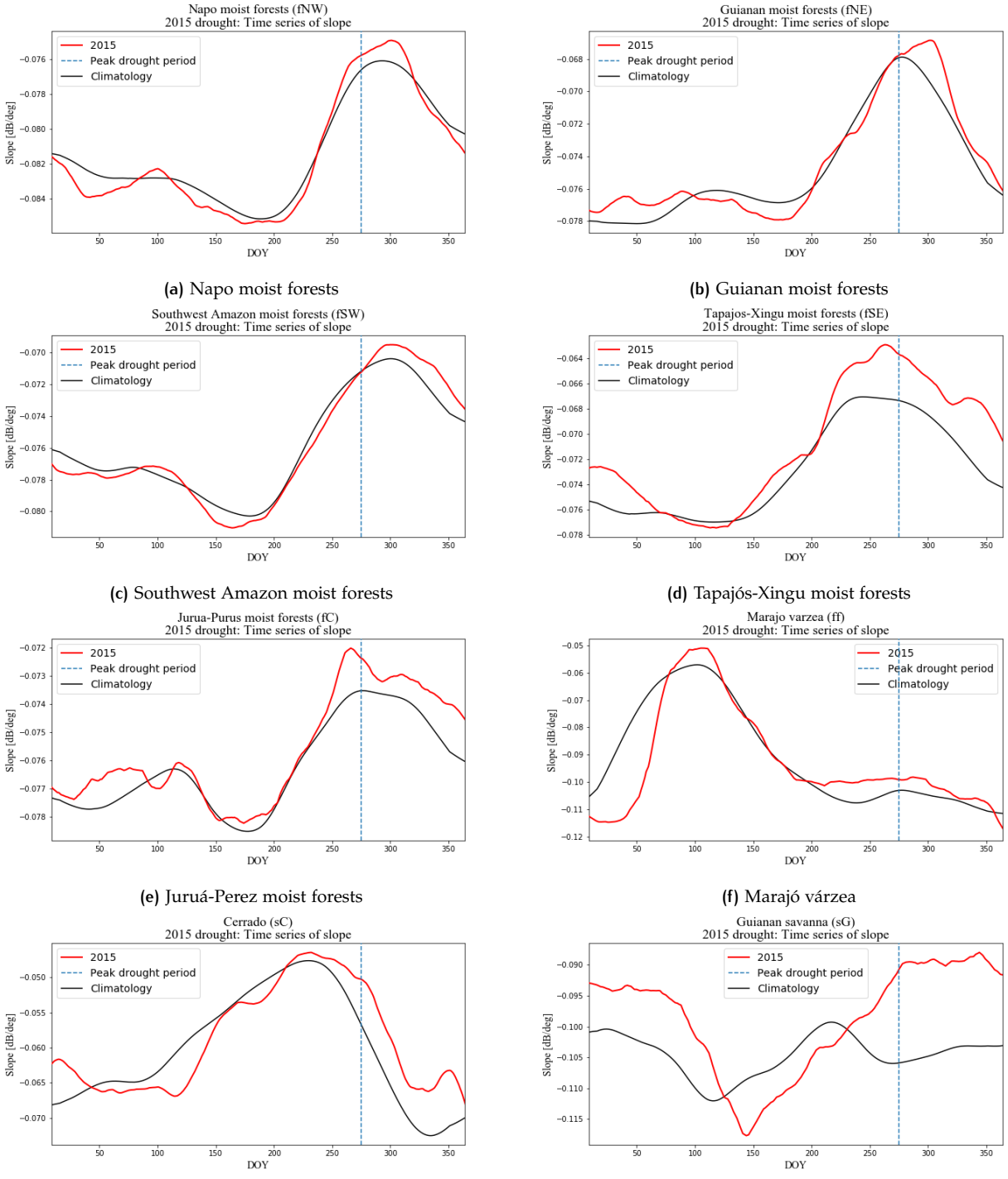

(a) Napo moist forests

(b) Guianan moist forests

(c) Southwest Amazon moist forests

(d) Tapajós-Xingu moist forests

(e) Juruá-Perez moist forests

(f) Marajó várzea

(g) Cerrado

(h) Guianan savanna

Figure B.5: Time series of mean slope for the year 2015 compared with the climatologies, for drought-affected regions of interest. The peak drought interval (October-December) is shown within dotted blue lines.

B.2.3 Curvature time series

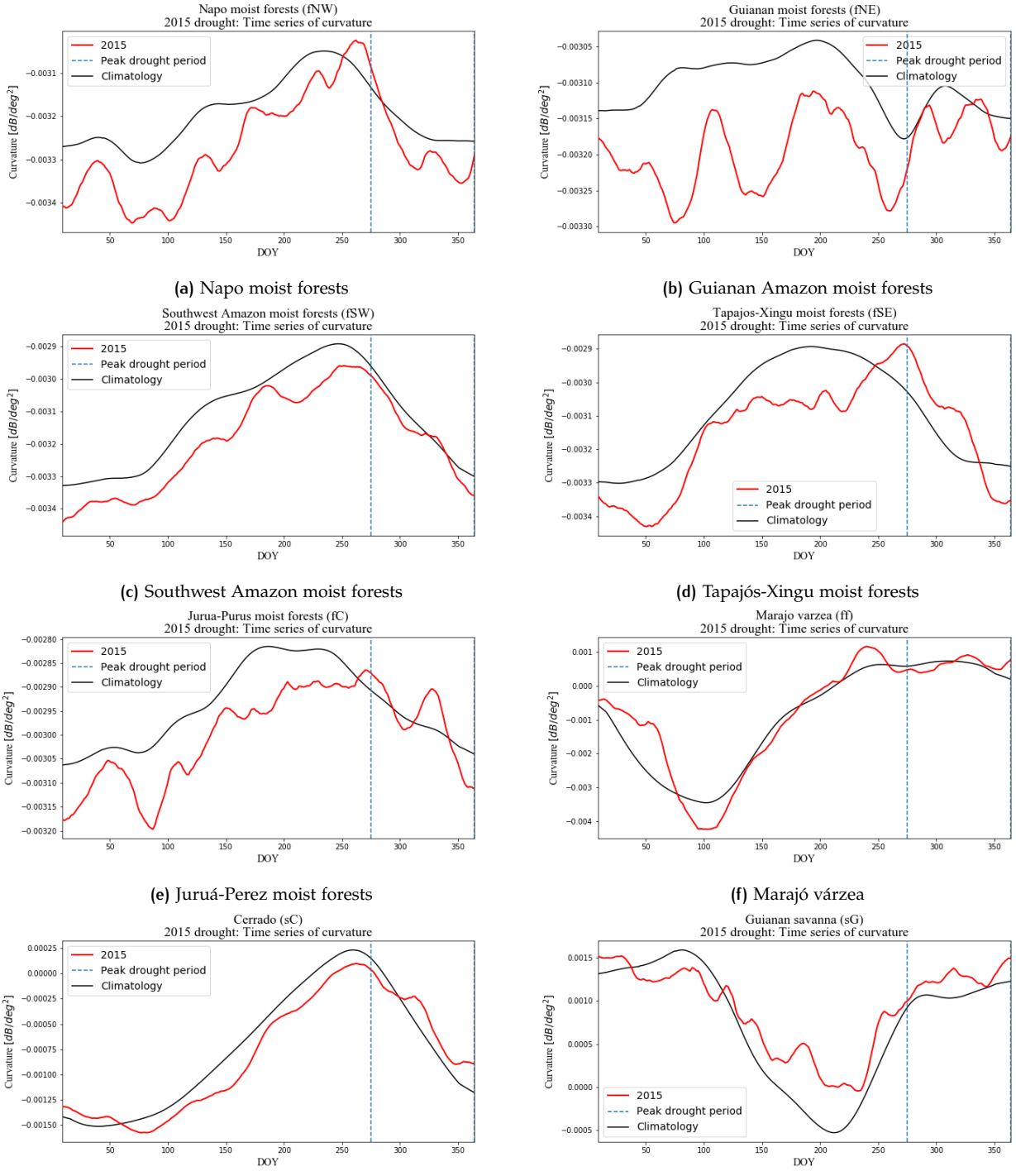

(a) Napo moist forests

(b) Guianan Amazon moist forests

(c) Southwest Amazon moist forests

(d) Tapajós-Xingu moist forests

(e) Juruá-Perez moist forests

(f) Marajó várzea

(g) Cerrado

(h) Guianan savanna

Figure B.6: Time series of mean curvature for the year 2015 compared with the climatologies, for drought-affected regions of interest. The peak drought interval (October-December) is shown within dotted blue lines.

C KÖPPEN-GEIGER CLIMATE CLASSES (KGCC)

Table C.1: List of Köppen-Geiger Climate Classes (KGCC)

KGCC symbol	Climate Type
Af	Tropical rainforest
Am	Tropical monsoon
Aw	Tropical savanna
BWh	Arid desert hot
BWk	Arid desert cold
BSh	Arid steppe hot
BSk	Arid steppe cold
Csa	Temperate hot dry summer
Csb	Temperate warm dry summer
Csc	Temperate cold dry summer
Cwa	Temperate dry winter hot summer
Cwb	Temperate dry winter warm summer
Cwc	Temperate dry winter cold summer
Cfa	Temperate hot summer without dry season
Cfb	Temperate warm summer without dry season
Cfc	Temperate cold summer without dry season
Dsa	Cold hot dry summer
Dsb	Cold warm dry summer
Dsc	Cold cold dry summer
Dsd	Cold dry summer very cold winter
Dwa	Cold dry winter hot summer
Dwb	Cold dry winter warm summer
Dwc	Cold dry winter cold summer
Dwd	Cold dry very cold winter
Dfa	Cold hot summer without dry season
Dfb	Cold warm summer without dry season
Dfc	Cold cold summer without dry season
Dfd	Cold very cold winter without dry season
E	Tundra
F	Frost

COLOPHON

This document was typeset using LaTeX. The document layout was generated using the `arsclassica` package by Lorenzo Pantieri, which is an adaption of the original `classicthesis` package from André Miede.